UNIVERSIDADE FEDERAL DE MINAS GERAIS
INSTITUTO DE GEOCIÊNCIAS
PROGRAMA DE PÓS-GRADUAÇÃO EM GEOLOGIA

TESE DE DOUTORADO

Isotopic and geothermobarometric characterisation of metasedimentary rocks from the central Araçuaí-Ribeira orogenic system and its eastern basement: Geotectonic implications

AUTOR: Reik Degler

ORIENTAÇÃO: Antônio Carlos Pedrosa-Soares

Nº da tese 36

BELO HORIZONTE
DATA (10/10/2017)

Tese de Doutorado

Isotopic and geothermobarometric characterisation of metasedimentary rocks from the central Araçuaí-Ribeira orogenic system and its basement: Geotectonic implications

Tese de doutoramento apresentada ao
Programa de Pós-Graduação em Geologia
do Instituto de Geociências da Universidade
Federal de Minas Gerais.

Autor: Reik Degler

Orientador: Prof. Antônio Carlos Pedrosa-Soares
Co-orientador: Prof. Ivo Antônio Dussin

Belo Horizonte, Outubro 2017

FOLHA DE APROVAÇÃO

Isotopic (U-Pb and Lu-Hf) and geothermobarometric characterisation of metasedimentary rocks from the central Araçuaí-Ribeira orogenic system and its basement: Geotectonic implications
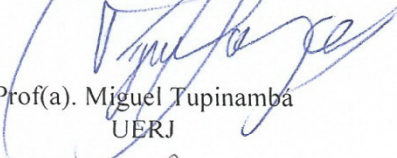
REIK DEGLER

Tese submetida à Banca Examinadora designada pelo Colegiado do Programa de Pós-Graduação em GEOLOGIA, como requisito para obtenção do grau de Doutor em GEOLOGIA, área de concentração GEOLOGIA REGIONAL.

Aprovada em 10 de outubro de 2017, pela banca constituída pelos membros:

Prof(a). Antonio Carlos Pedrosa Soares - Orientador
UFMG

Prof(a). Monica da Costa Pereira Lavalle Heilbron
UERJ

Prof(a). Miguel Tupinambá
UERJ

Prof(a). Leonardo Eustáquio da Silva Gonçalves
UFOP

Prof(a). Stefano Albino Zincone
UFOP

Belo Horizonte, 10 de outubro de 2017.

ACKNOWLEDGMENT

ABSTRACT

The Araçuaí-Ribeira orogenic system (AROS) located in south eastern Brazil comprises a wealth of lithologies, which reflect the geotectonic evolution of the region since the Precambrian. Demonstrably two large-scale orogenic events had a lasting influence on the regional geology and allow certain correlations withinthe AROS and with further stratiform rock units in SE Brazil and Africa. The extensive magmatic arc activity during the Rhyacian-Orosirian orogenic event originated the basement of this orogenic system (ROOS) and can be subdivided in relation to its evolution in a continental or oceanic magmatic arc setting. Remnants of the juvenile arc setting are the ortho-derived Juiz de Fora and Pocrane complexes. They comprise rock units representing the juvenile AROS basement. U-Pb ages of Juiz de Fora and Pocrane complexes samples point out an age interval of c. 2250 to c. 1800 Ma and show best concordance between 2184 ± 9 and 2080 ± 19 Ma for the protoliths crystallisation. The Hf in zircon data disclose juvenile to moderately juvenile signatures for both the Pocrane and Juiz de Fora complexes, which form a quite primitive magmatic arc similar to a modern intra-oceanic island arc system.(Hf T_{DM} c. 2.2 Ga) between 2196 and 1864 Ma ($\varepsilon Hf_{(t)}$ +8.2 to -3.5). Our data together with a thorough compilation from the literature allows us to envisage a complex system of orogens developed in Rhyacian-Orosirian time (ROOS). This system would include: a Western-ROOS, and Juvenile-ROOS and an Eastern-ROOS.

Large parts of the AROS are covered by metasedimentary rocks. Detrital zircons from samples of the western AROS contain grains of 2158-830 Ma ($\varepsilon Hf_{(t)}$ from -2.2 to -22.7) and suggest sediment sources located in the Rhyacian basement to the Tonian rift magmatism. Samples from the southwestern AROS have a more complex assemblage of detrital grains (987-592 Ma, $\varepsilon Hf_{(t)}$ from +14.9 to -2.9) and indicate provenance from mainly juvenile sources of distinct ages. Samples from the eastern section dated between 650-552 Ma show negative $\varepsilon Hf_{(t)}$ (-25.3 to -16.5) and suggest main sediment sources in the Rio Doce arc formed in the Brasiliano orogeny. A retrograde metamorphic path in high amphibolite facies between 621-480 Ma is typical of collisional orogens and also records a late thermal event. The studied paragneisses represent distinct Neoproterozoic basin stages, shifting from passive to active margin settings. Further, the detrital and metamorphic chronometers imply constrains in relation to the West Gondwana assembly in the final stages of the AROS geotectonic evolution.

RESUMO

O Sistema Orogênico Araçuaí-Ribeira (AROS) localizada no sudeste do Brasil compreende uma grande quantidade de litologias, que refletem a evolução geotectônica na região desde o Pré-cambriano. Demonstravelmente, dois eventos orogênicos principais tiveram uma influência duradoura na geologia regional e permitiram certas correlações com o AROS e com outras unidades de rochas estratiformes no sudeste do Brasil e na África. A extensa atividade magmática durante o evento orogênico Rhyaciano-Orosiriano originou o embasamento desse sistema orogênico (ROOS) e pode ser subdividido em relação à sua evolução em um cenário de arco magmático continental ou oceânico. Remanescentes desse ambiente juvenil são os complexos orto-derivados Juiz de Fora e Pocrane. Compreendem unidades que representam o embasamento oriental do AROS. As idades U-Pb dos complexos Juiz de Fora e Pocrane indicam um intervalo de idade de c. 2250 a c. 1800 Ma e mostram melhor concordância entre 2184 ± 9 e 2080 ± 19 Ma para a cristalização dos protólitos. No sistema Lu-Hf as amostras descrevem uma recristalização continuada de crosta juvenil entre 2196-1864 Ma $\varepsilon Hf_{(t)}$ +8.2 a -3.5). Juntando o nossos dados com compilações profundas da literatura, os dados permitem a visualização de um sistema complexo evoluído no Rhyaciano-Orosiriano (ROOS). Este sistema include: um Ocidental-Continental-ROOS, um Juvenile-ROOS e um Oriental-Continental-ROOS.

Grandes partes do AROS são cobertas pelas rochas metassedimentares. Zircões detríticos do AROS ocidental contém grãos de 2158-830 Ma ($\varepsilon Hf_{(t)}$ de -2.2 a -22.7) a e sugerem fontes sedimentais localizadas no embasamento Rhyaciano-Orosiriano. Amostras do SW AROS tem um conjunto mais complexo de grãos detríticos (987-592 Ma, $\varepsilon Hf_{(t)}$ de +14.9 a -2.9) e indicam proveniências juvenis com idades distintas. Amostras da parte oriental datados entre 650-552 Ma mostram $\varepsilon Hf_{(t)}$ negativo (-25.3 a -16.5) e sugerem fontes sedimentares no arco Rio Doce, remanescente do secundo evento orogênico principal, a orogenia Brasiliano-Pan Africano. Metamorfismo retrograde chegando em fácies anfibolito entre 621-480 Ma é principalmente relacionado ao instruções Neoproterozoicas. Dados U-Pb e Lu-Hf do embasamento juvenil orto-derivado e da cobertura para-derivada do AROS fornecem informações no intervalo de ~2.3 Ga e sugerem: Oscomplexos Juiz de Fora e Pocrane representam remanescentes do um ambiente de arco oceânico, ativo por ~330 Ma, mas parece limitado a região do AROS entre as faixas do sistema Rhyaciano-Orosiriano. O vulcanismo regional bimodal dentro do arco precursor do JF-Po parece provável. Os paragnaisses estudados representam estágios distintas de bacias, mudando de um ambiente de margem passiva para ativa e entre outros indica fontes sedimentares distantes. Adicional, os cronometres detríticos e metamórficos implicam

restrinjas em relação a assembleia do Western Gondwana como um estagio final da evolução geotectônica do AROS.

Palavras-chave: análises de U-Pb e Lu-Hf, proveniência de rochas metassedimentares, arcos magmáticos juvenis, sistema orogênico Araçuaí-Ribeira, ligações geotectônicas

CONTENT

LIST OF ABBREVIANTIONS

Abbreviation	Meaning
ACsz	Abre Campo shear zone
AROS	Araçuaí-Ribeira orogenic system
BPAO	Brasiliano-Pan-African orogenesis
Bt	Biotite
CL	Cathodoluminescence
CSFP	Congo-São Francisco palaeocontinent
E	East
E- ROOS	East-Rhyacian-Orosirian orogenic system
Hbl	Hornblende
Hf	Hafnium
IGC	Instituto de Geociências
ISCB	Itabuna-Salvador-Curaçá belt
JF	Juiz de Fora
JF-Po	Juiz de Fora-Pocrane
JU-ROOS	Juvenile Rhyacian-Orosirian orogenic system
LA-ICP-MS	Laser Ablation Inductively Coupled Mass Spectrometry
LREE	Light Rare Earth Element
Lu	Lutetium
Ma	Million years
M	Mantiqueira arc/complex
MB	Mineiro belt
N	North
Opx	Orthopyroxene
Pb	Lead
Pl	Plagioclase
Po	Pocrane
Qtz	Quartz
ROOS	Rhyacian-Orosirian orogenic system
S	South

SHRIMP	Sensitive High Resolution Ion Micro Probe
U	Uranium
UERJ	Universidade do Estado do Rio de Janeiro
UFMG	Universidade Federal de Minas Gerais
UFOP	Universidade Federal de Ouro Preto
UTM	Universal Transverse Mercator
W	West
W- ROOS	West-Continental Rhyacian-Orosirian orogenic system

1. Introduction

The obvious linked geological history of the South American- and African continent before the Atlantic Ocean opening in the Mesozoic is still traceable today. The shared geotectonic evolution is reflected by stratiform correlative rocks units located to the east and the west of the Atlantic Ocean. Those units include among others, documented Palaeoproterozoic complexes as remnants of the Brazil Africa Rhyacian-Orosirian orogenic system (ROOS) and Neoproterozoic orogens of the Brasiliano-Pan-African orogeny (BPAO), Table 1A. The focused Araçuaí-Ribeira orogenic system (AROS) in southeast Brazil represents the climax of the BPOA orogeny among Western Gondwana. In western Africa, the Neoproterozoic geology of the West Congo belt (WCB; Alkmim et al., 2006; Tack et al., 2010; Affaton et al., 2016) forms the AROS geotectonical counterpart, Table 1A. After the opening of the Atlantic Ocean two third of this former connected landmass (West Congo and Araçuaí-Ribeira orogen) remained as the AROS in Brazil. Today the AROS is located in SE Brazil between the São Francisco craton and the Atlantic coast (E-W) and further between 15° and 23°S (N-S), (Fig. 1). It is a conjunction of the confined and well preserved Neoproterozoic Araçuaí orogen (Pedrosa-Soares and Noce, 1998; 2000; 2001) in the north and the Neoproterozoic Ribeira belt (Almeida et al., 1976; Trouw et al., 2000; Heilbron et al., 2008) in the south. The northern part of the AROS represents a derivate orogen, with evidence for an oceanic basin and subduction to the east. The northern part of the basin is considered to be back-arc (Pedrosa-Soares, 2001). The central part shows ophiolites from the Atlantic opening (c. 660-600 Ma; Queiroga et al., 2007; Queiroga, 2010; Pedrosa-Soares et al., 1998) and magmatic arc sequences, for example the Rio Doce magmatic arc (Gradim et al., 2014; Tedeschi et al., 2016), representing a former active continental margin environment. To the south the Ribeira belt as part of the Brazilian-Pan-African orogenic system can be subdivided from NW to SE in four tectonic domains: the Occidental Terrane, representing reworked margin of the São Francisco craton; the Paraíba do Sul-Embu Terrane, a docked terrane of granulite facies; the Oriental Terrane, composed of paragneisses and the Cabo Frio tectonic domain composed by a reworked Paleoproterozoic basement (Tupinambá et al., 2012; Heilbron et al., 2013); Fig. 2.

A consciously large-scale sampling of paragneisses (Figs. 1 and 2) was implemented to attempt correlations of these two orogenic belts. Since the beginning, this was an overarching focus and mainly objected by detailed analyses of metasedimentary rocks provenances and metamorphism in the first part of the study (Publication 2). Although at first sight, the two belts do not seem to have much in common an attempted correlation of the geotectonic domains from the Araçuaí and Ribeira belt are illustrated in Table 1B. It quickly became clear that further and older Pre-Gondwana

relations between geotectonic domains of the AROS and former marginal domains of the São Francisco-Congo palaeocontinent are very obvious. Accidently, by sampling the paragneiss interlaid Palaeoproterozoic basement the study focus changed to intense analyses on AROS units representing the Rhyacian-Orosirian basement, the Juiz de For a (JF), Pocrane (Po) and Quirino (Q) complexes (Fig. 1 and Publication 1). To relate the widespread geotectonism of the South American and African continents displayed in the AROS to geological settings along the São Francisco and Congo craton it was indispensable to focus documented geological rock units from Palaeoproterozoic to Neoproterozoic ages. The breakdown in rock analyses of different ages, composition and genesis in this study permits a comprehensive outline of the AROS rocks through time.
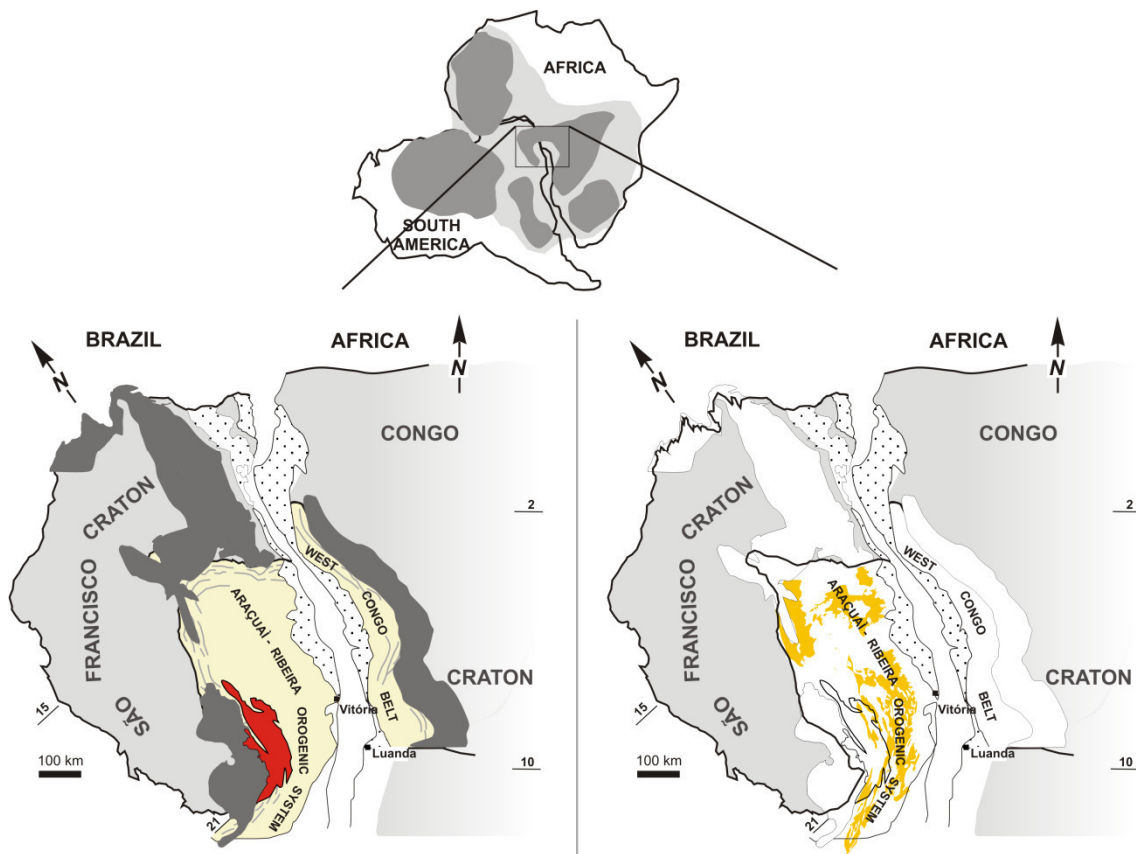
Fig. 1: Simplified geological maps showing the Araçuaí-Ribeira orogenic system(AROS) and its African counterpart the West Congo belt (WCB), as confined orogen between the Congo-and São Francisco cratons (modified from Pedrosa-Soares at al., 2008). Left, highlighted in grey and red remnants of the Brazil Africa Rhyacian-Orosirian orogenic system (ROOS), red: JF, Po and Q complexes, objected in Publication 1 and right, highlighted metasedimentary units (yellow) objected in Publication 2.

1.1 Characterisation of the problem and objectives

A big disadvantage of geological studies is the fact that they are regionally limited and mostly only focus small areas and spots. Contrasting, this focusing can be seen as an advantage, as at best it guarantees detailed high quality data. The geological discovery of the AROS is a combined product of these two study approaches. The sum of locally detailed data and correlations of their results over widespread areas display the today's picture of the regional geology in SE Brazil. Thereby, most geological studies in relation to the AROS are focused on the Neoproterozoic intrusion events (e.g. Pedrosa-Soares et al., 2011; Gradim et al., 2014; Richter et al., 2015; Gonçalves et al., 2016; Tedeschi et al., 2016). The expanding interlaid metasedimentary units have been always some kind of cut out, less studied, and consequently so far show a small amount of published data. Further, it seems that the metasedimentary rocks of the AROS were very generalised and served as "filling" to correlate and simplify geotectonic settings (e.g. mapping projects in scale 1: 100 000), Tables 1B and 3.

Table 1: A, Fig. 1: Relevant factors for the present geology of the Rhyacian-Orosirian orogenic system and the role as basement units. CSFP = Congo-São Francisco palaeocontinent. B, Attempt of a correlation between Ribeira belt and Araçuaí belt units forming the Araçuaí orogenic system (AROS). The term "Andrelândia" for metasedimentary units is used universal in the Araçuaí region. Circled are the possible eastern basement units for both orogens, which could probably summarised.
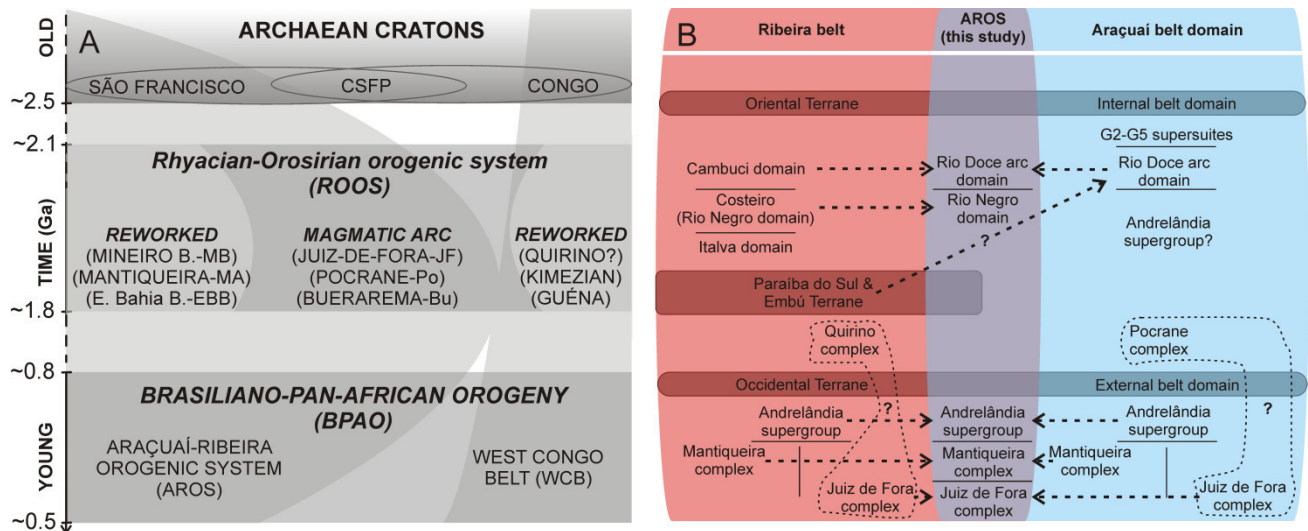
In big scales, sedimentary rocks (Fig. 1) are one of the best parameter to understand the geotectonic evolution of a large region as they contain important information about the composition, sediment transport and formation of continental crust. Their geochemical pattern is closely related to possible provenances and tectonic settings of their depositional basin. As the general regional geology in the

central part of the AROS can be described as a result of a change from passive- to active margin environment (basement, for-arc, arc, back-arc), different sources of material are assumed. The present Palaeoproterozoic basement rocks (Noce et al., 2007), ophiolite silvers (Queiroga, 2010) and Neoproterozoic intrusions (Gradim et al., 2014; Richter et al., 2015; Gonçalves et al., 2016; Tedeschi et al., 2016) in this part of the orogenic system could all be potential material sources for the sediments and leave speculations, whether there are more than only one depositional basin. Furthermore, the orogenesis is accompanied by different metamorphic events, which could be reflected and recorded in the today's metasediments.

In the course of the studies and analyses it became clear, that not all collected rock samples were really metasedimentary. It turned out that some para-derived considered rocks showed exact Concordia Ages, Palaeoproterozoic ages. Based on their appearance and geographical location this Rhyacian to Orosirian gneisses were allocated to the Juiz de Fora, Pocrance and Quirino complexes, being part of AROS basement (Figs. 1 and 2) in the earlier precursor basin stage. Macroscopically and hardly microscopically these ortho-derived Palaeoproterozoic rocks are very similar to the mostly younger para-derived rocks, only detailed age determination allowed their differentiation. In some AROS regions, the distinction between those completely different generated rocks seems not clear as both underwent the same metamorphic event in the Neoproterozoic (BPAO).

It is not unusual that objectives of scientific research studies change during their development and progress. This was also the case for the present study. New data along the path, field work observations, and findings concerning the interpretation of analytical data, but also opinions of colleagues have sustainable influence to the process of sciences.

The basic idea of this study was a differentiated consideration of the metasedimentary rocks in the AROS (Publication 2), further, caused by their similarity, Palaeoproterozoic basement rocks came to the fore. In the course of the study the basement rocks of the Juiz de Fora, Pocrane and Quirino complexes (JF, Po and Q; Publication 1) were considered independently and as possible source of the paragneissic cover units.

To identify these distinctive features the work focuses on detailed geochronological and isotopic data carried out by LA-ICP-MS in the main chronometers zircon and monazite. Analyses of U-Pb and Lu-Hf isotopes in detrital zircons and EMP-monazite dating, as well as geothermobarometry were performed to guaranty a profound understanding of the complex composition of para-derived and ortho-derived rocks of the AROS. A subordinated objective was the correlation of known collisional magmatic intrusions and Neoproterozoic collisional metamorphism imprinted in the metasedimentary rocks. It is attempted to interpret the data in context to evolutional stages of the Araçuaí-Ribeira-West Congo orogen and show possible correlations between the Araçuaí orogen

and the Ribeira belt (Fig. 2). On the basis of this new data a general evolutional model since the Precambrian for the AROS region is suggested.

1.2 Previous works and nomenclature

The independent consideration of the Araçuaí belt and the Ribeira orogen makes sense in large part. On one hand this is caused by obvious different geotectonic settings, but also has historical reasons in relation to studies of different scientists. However, the "geotectonic world" of these two orogens does not end at the 21°S meridian (in literature a geographical landmark for their limit) and there are surly correlative features like the investigated metasedimentary rocks and the Neoproterozoic arc domains (Table 1).

With a closer look to several published works (e.g. Costa et al., 1998; Noce et al., 2007; Tupinambá et al., 2013) objecting the Araçuaí and Ribeira belt it is out of question, that the basic idea of the geotectonic setting is almost the same. Generally, Palaeoproterozoic basement (Fig. 1), amalgamated to the Archaean São Francisco craton, Neoproterozoic magmatic arc intrusions and all this interlaid by metasedimentary units of distinct ages and provenances (Figs. 1 and 2). Further, the idea of geographical subdivision is quite equal, an external (western) and internal (eastern) part for the Araçuaí belt and an Occidental and Oriental terrene for the Ribeira belt (Table 1).

Table 2: Summarised selective historical achievements concerning the study of Palaeoproterozoic basement units in the AROS.

Pre-Neoproterozoic basement rocks in the Araçuaí-Ribeira orogenic system (chronological nomenclature chart)			
age	authors	nomen-clature	characterisation
1954	Barbosa	Mantiqueira complex	- defines the "Mantiqueira series"
1957	Ebert, Rosier	Juiz de Fora complex	- first field work on gneisses (today Juiz de Fora complex in Rio de Janeiro and Minas Gerais states
1968	Ebert	Mantiqueira complex	- in retrospect the Piedade gneiss complex is today considered as part of the Mantiqueira complex
1991	Brandalise	Mantiquueira complex	- first designation of the Mantiqueira complex as part of the São Francisco craton
1993-1995	Heilbron	Juiz de Fora complex	- detailed description of orthogneisses and their metamorphic conditions (granulite facies)
1996	Machado	Juiz de Fora complex	- first meaningful crystallisation age dating: 2134 Ma
1998	Fischel et al.	Juiz de Fora Mantiqueira complex	- detailed mineralogical and structural studies in the central AROS region
2002	Silva et al.	Mantiqueira complex	- extensive age determination (SHRIMP) in gneisses of the Mantiqueira complex, aging (2180 - 2041 Ma)
2003	Heilbron et al.	Mantiqueira Juiz de Fora complex	- correlative work based on mapping projects in SE Brazil, specific occurrences first isotopic analyses
2004	Duarte *et al.*	Mantiqueira complex	- consideration of the Mantiqueira complex as a continental magmatic arc setting
2007	Noce *et al.*	Mantiqueira Juiz de Fora complex	- age and geochemical determinations - differentiation of the complexes. correlations to West Africa units
2013	Novo	Juiz de Fora-Pocrane	- discovery of Juiz de Fora similar rocks to the east Pocrane complex - eastern basement
2015	Silva *et al.*	Porteirinhas domain	- correlation of various basement domains in the AROS and with units in MIB and ISCB

We have opted the use of the general generic term "metasedimentary rocks" (Andrelândia group) by the lack of definition regarding the stratigraphic nomenclature for metasedimentary rocks in the Araçuaí belt. Some authors choose the term Andrelândia group or megasequence, other opt Rio Doce group. The Andrelândia group (Ebert, 1956) occurs in distinct areas of the Ribeira and Araçuaí orogens, south and southeast of São Francisco craton and in the southern Brasilia belt

nappe system (Heilbron et al., 2004). In the studied area the term Andrelândia group was used by Romano and Noce, 2002; Tupinambá et al., 2003; Heilbron et al., 2003; Noce et al., 2003; 2006, 207; Horn et al., 2006; Novo et al., 2012;Gradim et al., 2012 and Queiroga et al., 2012. The Rio Doce group (Barbosa et al., 2004) occurs exclusively in the Araçuaí orogen, north of the presented area (Table 3).

Table 3: Overview of previous publication that refer to metasedimentary rocks in the Araçuaí orogen and the Ribeira belt.

	age	authors	nomen-clature	characterisation
Metasedimentary rocks in the Araçuaí-Ribeira orogenic system (chronological nomenclature chart)				
Ribeira belt	1956	Ebert	Andrelândia group	- by petrology, structural geology, stratigraphy based on quartzites
	1968	Ebert	Andrelândia group	- redefined as metasedimentary sequence including quartzites, garnet mica-schists, gneisses and marble
	1976	Almeida	Andrelândia group	- as part of the Uruaçu belt
	1984 and 1986	Ebert and Trouw	Andrelândia group	- correlation with the São João del Rei group, the Araxá group and the Canastra group
	1997	Paciullo *et al.*	Andrelândia group	- subdivision in the Carrancas sequence: (paragneisses interbeded by amphibolites) and the Serra dos Turvo sequence: (biotite schists) - sedimentation in passive margin basin
	2000	Paciullo *et al.*	Andrelândia group	- isotopic data of juvenile contribution from intrabasin igneous activity or magmatic arcs
	2000	Campos Neto	Andrelândia group	- relation between metasediments and magmatic arcs, as possible sources
	2000	Heilbron *et al.*	Andrelândia group	- metasediments as Neoproterozoic cover Paleoproterozoic basement units
	2003	Ribeiro *et al.*	Andrelândia group	- detrital zircons from the Carrancas sequence show mostly paleoproterozoic ages
	2004	Valeriano *et al.*	Andrelândia group	- detailed age determination of quartzites, as originated from Paleoproterozoic passive margin material
Araçuaí orogen	1998	Costa *et al.*	High Grade Mobile Belt	- detailed studies of the region around Manhuaçu/MG: describtion of metasedimentary and metavolcano-sedimentary sequences
	2004	Noce *et al.*	kinzigitic complex	- age determination of high-grade metasediments in the eastern Araçuaí orogen
	2007	Vieira	Rio Doce group	- description of paragneisses from the Nova Venecia complex in back-arc region
	2011	Belém *et al.*	Andrelândia group	- adaption of the terms 'upper' and 'lower' Andrelândia Group for the Araçuaí orogen
	2012	Novo, Gradim, Queiroga	Andrelândia group	- the term 'Andrelândia Group' is used for metasedimentary units in geological maps of Jequeiri, Manhuaçu, Manhumirim and Viçosa
	2014	Gradim *et al.*	Rio Doce group	- maximum depositional age of paragneisses 590 Ma

An overview on this unit can be found in Vieira (2007). In the focused region Féboli and Paes, 2000; Oliveira, 2000; Tuller, 2000; Vieira, 1993; Angeli et al., 2004; Carvalho and Pereira, 2000 and Pereira and Zucchetti, 2000 adopted Rio Doce group terminology. As the purpose of this study is independent of stratigraphic nomenclature, mostly the term "metasedimentary rocks" or "paragneisses" will be used for the Andrelândia or Rio Doce group, to represent para-derived rocks of the region.

The sampled rocks representing the AROS basement are summarised under the name of Brazil (Africa) Rhyacian-Orosirian orogenic system (ROOS); Table 2. The historical geological description of the AROS basement is illustrated in Table 2. In relation to the Ribeira belt distinct units of the Quirino complex (Valladares et al., 2002) make also part of the ROOS.

1.3 Location and field work

The study area extends over circa 20 000 km^2 between 19°30'S and 22°00'S (N-S) and 41°30'W to 43°00'W (E-W), 150 km WSW of Belo Horizonte, Minas Gerais (Figs. 2 and 3). Basically, it covers the geological maps in scale of 1:100 000 of Leopoldina (Heilbron et al., 2003); Pirapetinga (Tupinambá et al., 2003); Ubá (Noce et al., 2003); Muriaé (Romano and Noce, 2002; Noce et al.,2003), Viçosa (Gradim et al., 2012); Carangola (Noce et al.,2012); Espera Feliz (Horn et al., 2006); Jequeri (Queiroga et al., 2012); Manhuaçu (Noce et al., 2006); Manhumirim (Novo et al. 2012); Ipanema (Tuller et al., 2002) and Caratinga (Signorelli et al., 2003); Itanhomi (Féboli and Paes, 2000) in eastern Minas Gerais, southern Espirito Santo and northern Rio de Janeiro state (Figs. 2 and 3).

Two trips to the field over a period of together five weeks in 2014 and a third excursion of one week in 2016 are the basis of this study. Main objectives of the field work were a profound knowledge of the regional geology, outcrop detection and description, as well as collection of a representative quantity of samples. All this observations were primarily focused on metasedimentary rocks and their interaction with other outcropping lithologies. Further basement units, especially of the northern Pocrane complex were collected in the second part of the field work.

After an evaluation of large scale physical maps it was decided to sample along sections of west-east orientation to cut the predominant morphology (N-S) vertically. Also considered was the general geological interpretation of the study area, which proposed more geological variation in east-west extension. Along four sections with an average extent of 100 km 66 samples were taken

(Figs. 2 and 3a-3e). A fifths section of Palaeoproterozoic ROOS rocks was created in N-S direction. Out of almost 100 samples (i.a. represented in Figs. 3a-3e) from the five sections 16 were analysed in detail (Table 4).

Table 4: Compilation of analysed samples from the AROS region. Whites are ortho-derived basement samples of Publication 1, grey highlighted are para-derived samples of Publication 2. The 16 samples are highlighted in Figs. 3a-3e.

Sample	UTM coordinates	Mineralogy	LA-ICP-MS U-Pb zircon / SHRIMP U-Pb zircon	LA-ICP-MS U-Pb monazite	EMP Th-U-Pb monazite	LA-ICP-MS Lu-Hf zircon	Geothermobarometry
RC-02	755214/7747628	Qtz-Pl-Bt-Grt-Kfs	X	X	X	X	
RC-03	755935/7734053	Qtz-Pl-Kfs-Bt-Grt	X	X	X	X	X
RC-15	233235/7770064	Qtz-Bt-Pl-Kfs-Grt	X			X	
RC-17	211141/7699888	Qtz-Bt-Pl-Grt-Kfs	X			X	
RC-30	777133/7714568	Qtz-Pl-Bt-Grt-Sil	X				
RC-34	753654/7710340	Qtz-Pl-Bt-Grt	X		X	X	X
RC-38	742122/7636281	Qtz-Bt-Pl-Grt-Sil	X			X	X
RC-43	789405/7621752	Qtz-Bt-Pl-Amp-Grt	X			X	
RC-46	719626/7605780	Qtz-Bt-Grt-Kfs	X			X	X
RC-90	220250/7846557	Qtz-Pl-Amp-Px-Hbl-Bt	X				
RC-93	218323/7843555	Qtz-Pl-Hbl-Bt	X			X	
RC-94	221385/7840162	Qtz-Bt-Amp-Kfs	X			X	
RC-95	262843/7863012	Qtz-Pl-Hbl-Bt-Kfs	X				
RC-99	220250/7846557	Qtz-Pl-Hbl-Bt-Kfs	X				
RC-101	204009/7740522	Qtz-Pl-Kfs-Px-Hbl	X			X	
RC-103	202107/7739164	Qtz-Pl-Kfs-Px-Hbl	X				

The further Figures (2 to 3e) should give an idea of the study area expansion and the created sections. The listed samples in Table 4 are the result of detailed outcrop description and microscopical analyses.
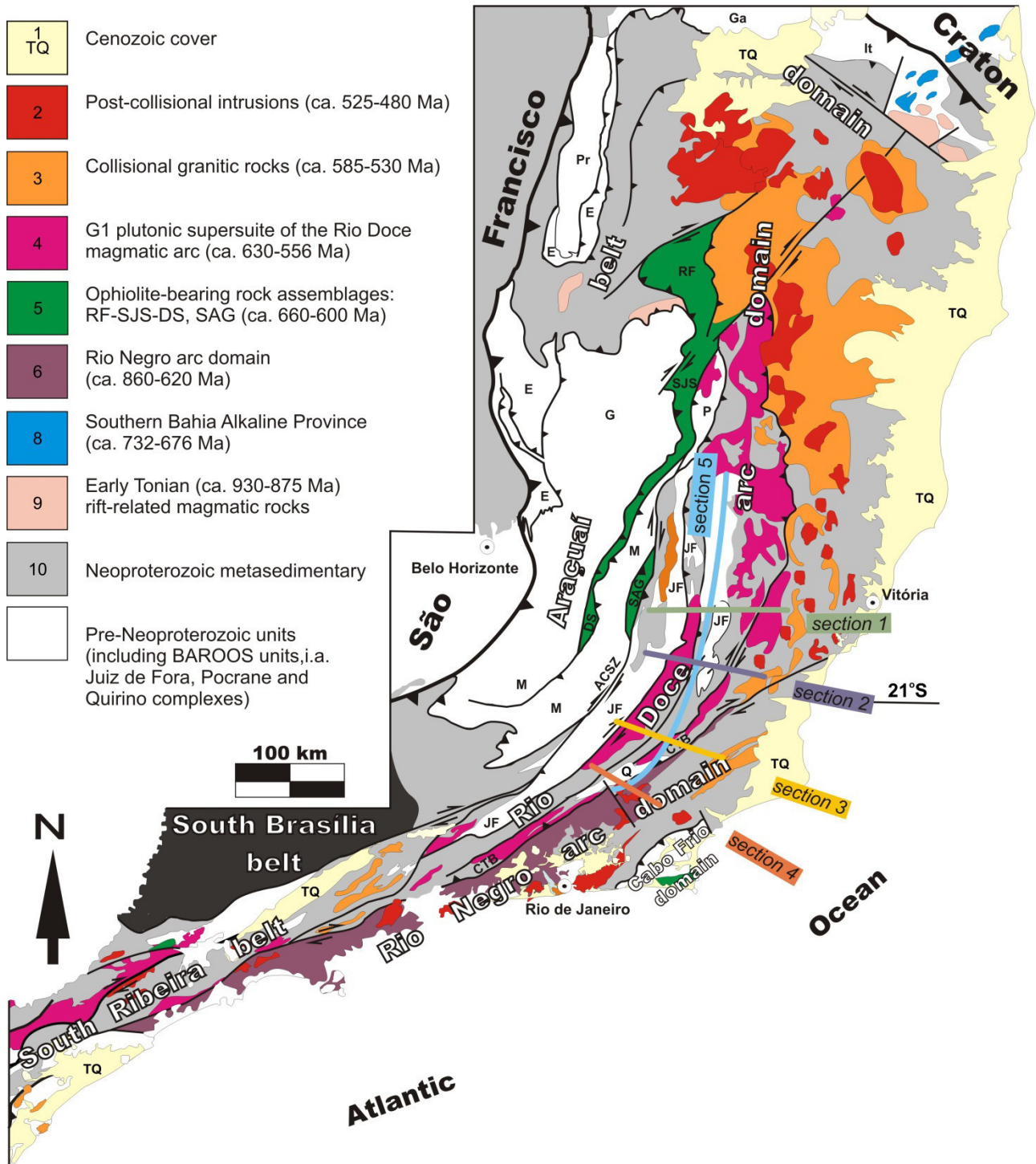
Fig.2: The Araçuaí-Ribeira orogenic system (AROS) in SE Brazil and the five sample sections. Section 1-4 in direction W-E for paragneisses (Publication 2) and section 5 in N-S direction for the JF, Po and Q complexes samples (Publication 1). B, AROS simplified geological map (modified from Silva et al., 2005, and Tedeschi et al., 2016): 1, Cenozoic cover (TQ - Tertiary, Quaternary); 2, Post-collisional intrusions (c. 525-480 Ma); 3, Collisional granitic rocks (ca. 585-530 Ma); 4, G1 plutonic supersuite of the Rio Doce magmatic arc (ca. 630-556 Ma) and probable correlatives; 5, Ophiolite-bearing rock assemblages: RF-SJS-DS, Ribeirão da Folha-São José da Safira-Dom Silvério schist belt (ca. 660-630 Ma); SAG, Santo Antônio do Grama metamafic-ultramafic suite (ca. 600 Ma); 6, Rio Negro arc domain (Rio Negro and Serra da Prata magmatic arcs, and related units; ca. 860-620 Ma); 7, Southern Bahia Alkaline Province (ca. 732-676 Ma); 8, Early Tonian (ca. 930-875 Ma) rift-related magmatic rocks; 9, Neoproterozoic metasedimentary and metavolcanic successions; 10, Pre-Neoproterozoic units: E, Espinhaço Supergroup; and Archaean-

10

Palaeoproterozoic blocks and complexes (including ROOS): G, Guanhães; Ga, Gavião; It, Itapetinga; JF, Juiz de Fora; M, Mantiqueira; Po, Pocrane; Pr, Porteirinha; Q, Quirino. ACsz, Abre Campo shear zone. CTB, central tectonic boundary.

The created geological sample sections were the basis of the entire study (Publication 1 and 2). Under mineral aspects, the paragneiss samples are almost similar but show variations in grain size and grade of mylonitisation. The modal mineral content is illustrated by balk diagrams in percent of hundred. Dip and strike measurement always represent the regional main foliation (most probably S_2). The problem of paleosome and melanosome can be clearly identified in the paragneiss samples (Figs. 3a-3d). This was regarded while sample preparation.

Illustrated sampled rocks of the JF-, Po- and Quirino complex (Fig. 3e) partially show the chaotic banding and the typical greenish colour (if not surface weathered). Further petrographical descriptions can be found in Publication 1 and 2.
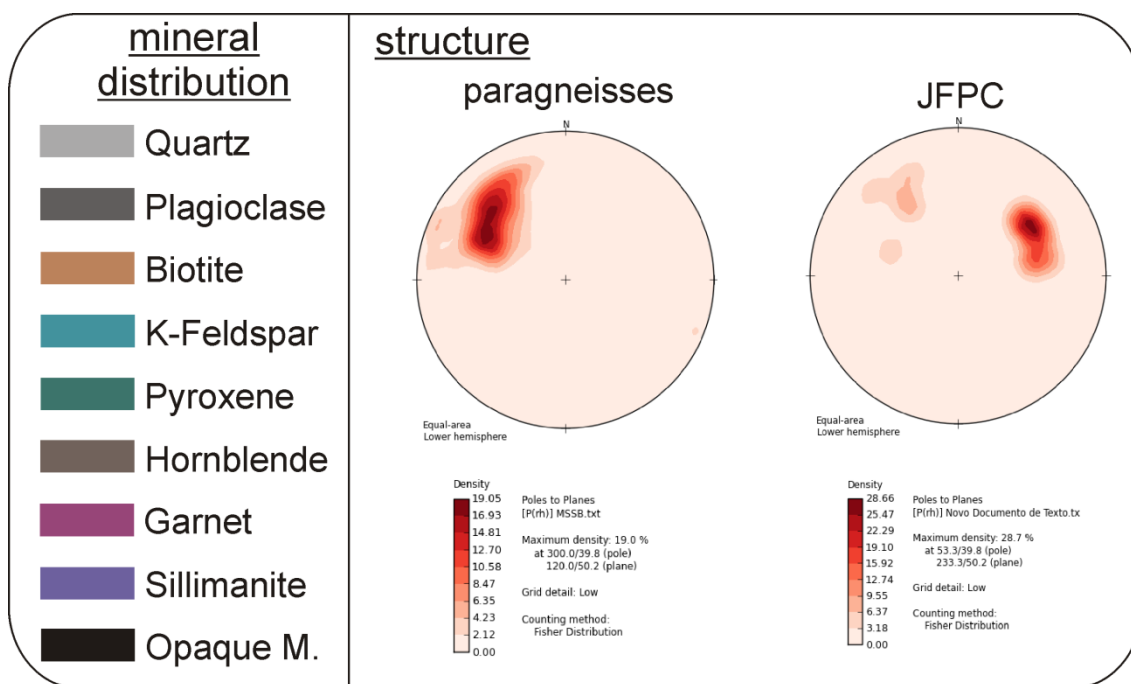

Fig. 3: Legend for mineral distribution observed in thin sections of the 5 samples sections (Fig. 3a-3e).The recorded regional main foliation for the paragneisses has maximum of 120°/50° (n = 38 measurements). For ROOS orthogneisses the maximum plots at 233°/50° (n = 16). Analysed samples listed in Table 4 are marked in blue.

section 1

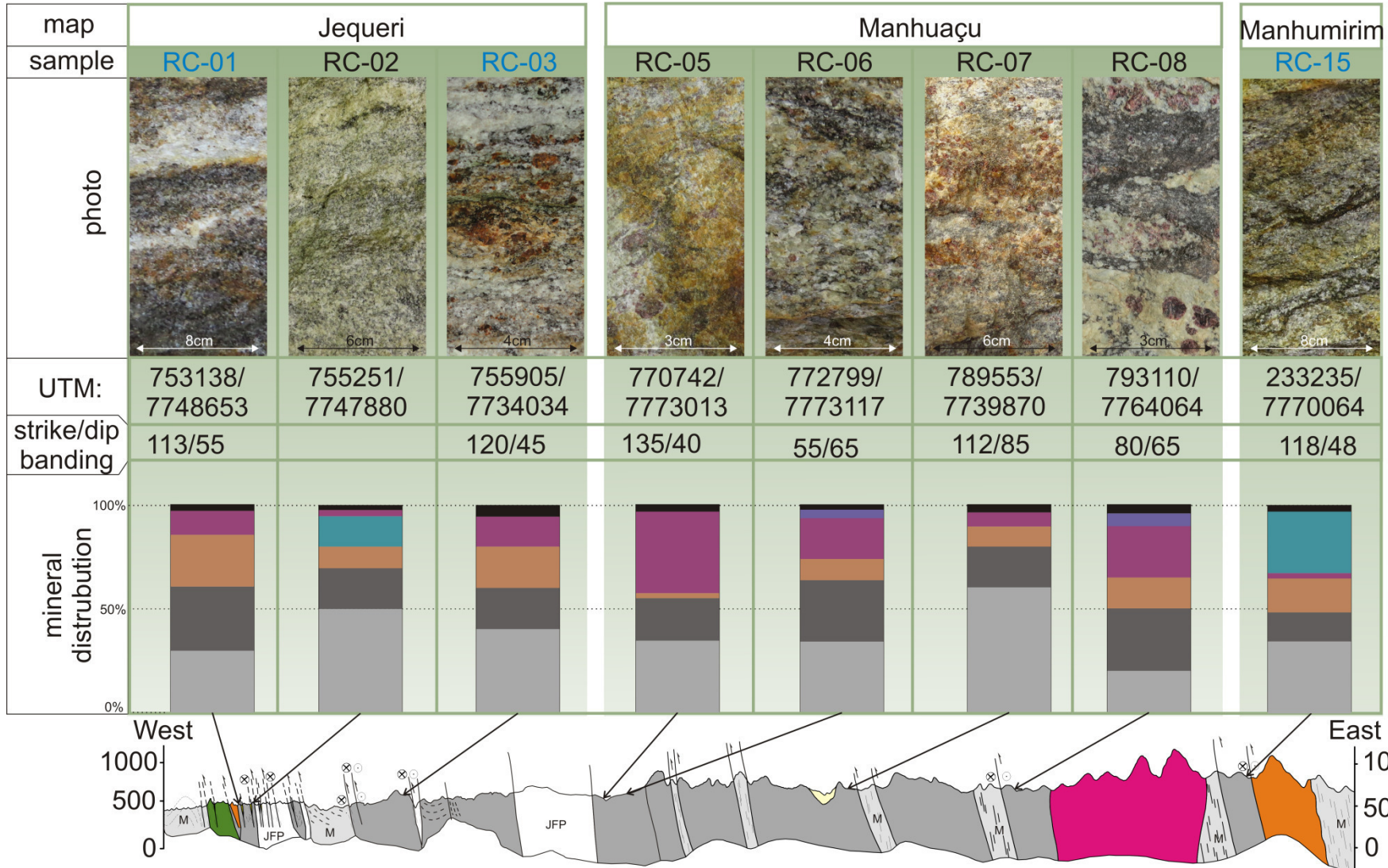| map	Jequeri			Manhuaçu				Manhumirim
sample	RC-01	RC-02	RC-03	RC-05	RC-06	RC-07	RC-08	RC-15
photo	8cm	6cm	4cm	3cm	4cm	6cm	3cm	8cm
UTM:	753138/ 7748653	755251/ 7747880	755905/ 7734034	770742/ 7773013	772799/ 7773117	789553/ 7739870	793110/ 7764064	233235/ 7770064
strike/dip banding	113/55		120/45	135/40	55/65	112/85	80/65	118/48

Fig. 3a: Field work and microscopical information of cross section 1 consisting of 8 representative samples. Lithotype-colours refer to Fig. 2.
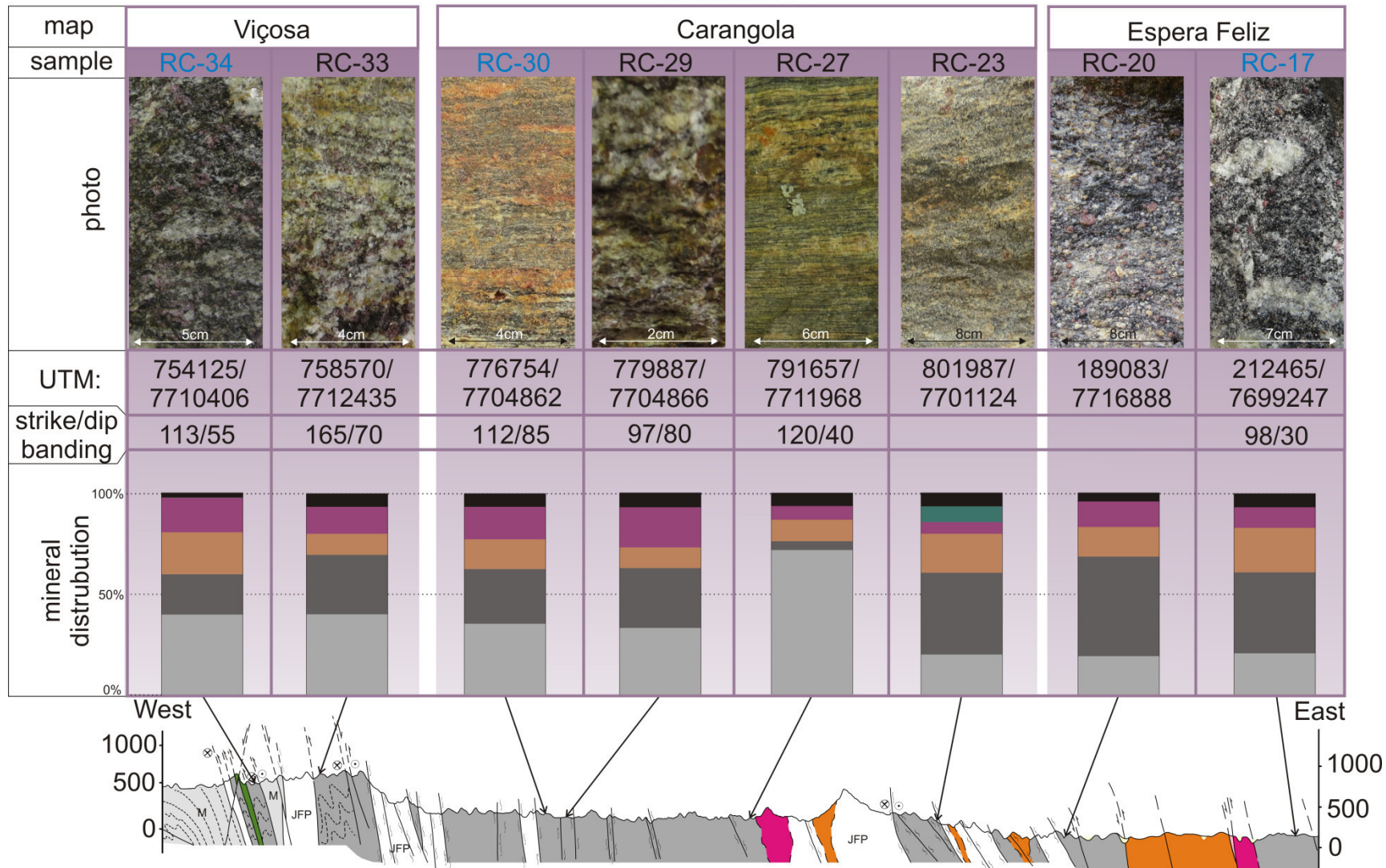
12

Fig. 3b: Field work and microscopical information of cross section 2 consisting of 8 representative samples. Lithotype-colours refer to Fig. 2.
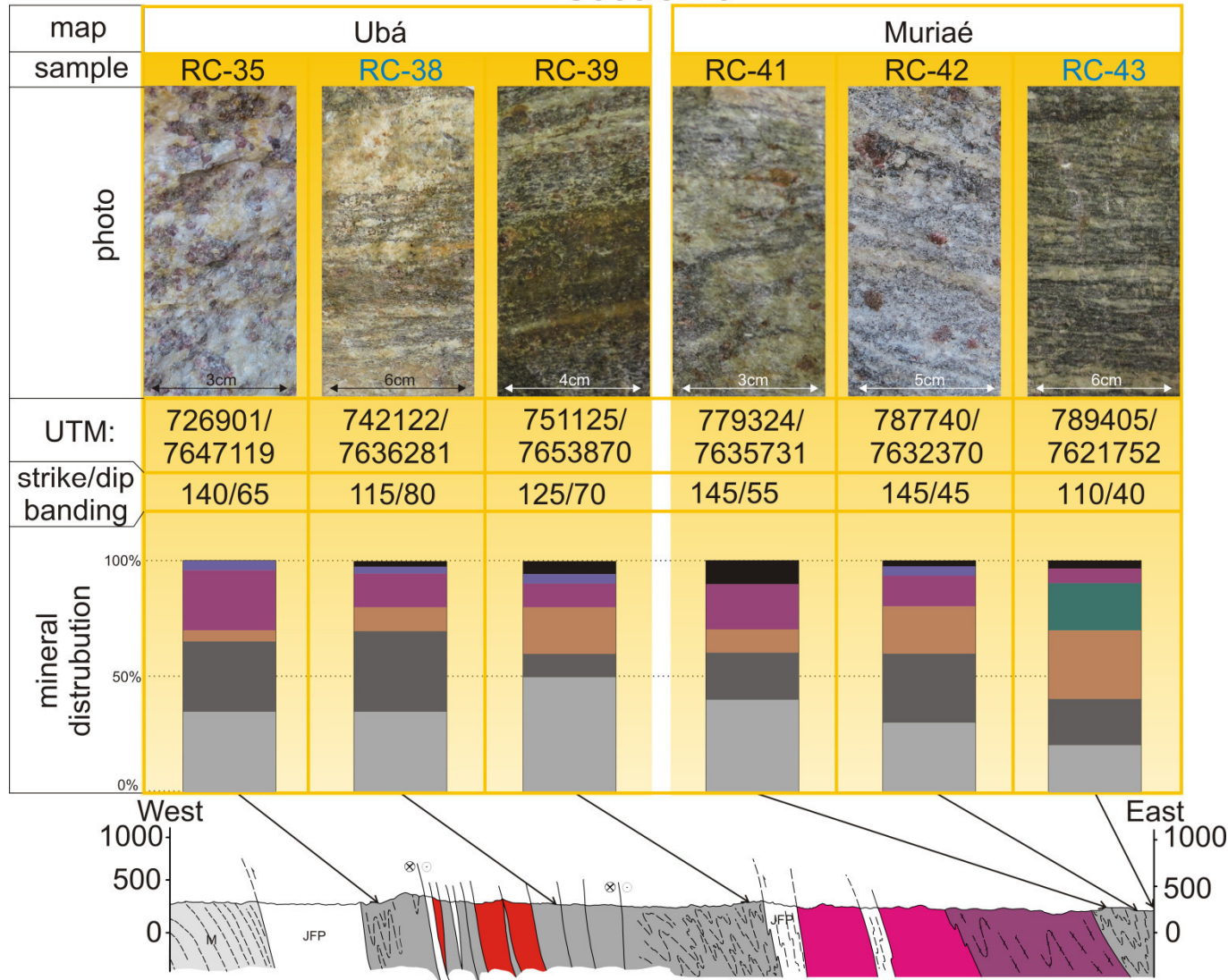
13

section 3

map	Ubá			Muriaé		
sample	RC-35	RC-38	RC-39	RC-41	RC-42	RC-43
photo	3cm	6om	4cm	3cm	5cm	6cm
UTM:	726901/ 7647119	742122/ 7636281	751125/ 7653870	779324/ 7635731	787740/ 7632370	789405/ 7621752
strike/dip banding	140/65	115/80	125/70	145/55	145/45	110/40
mineral distrubution						

Fig. 3c: Field work and microscopical information of cross section 3 consisting of 6 representative samples. Lithotype-colours refer to Fig. 2.
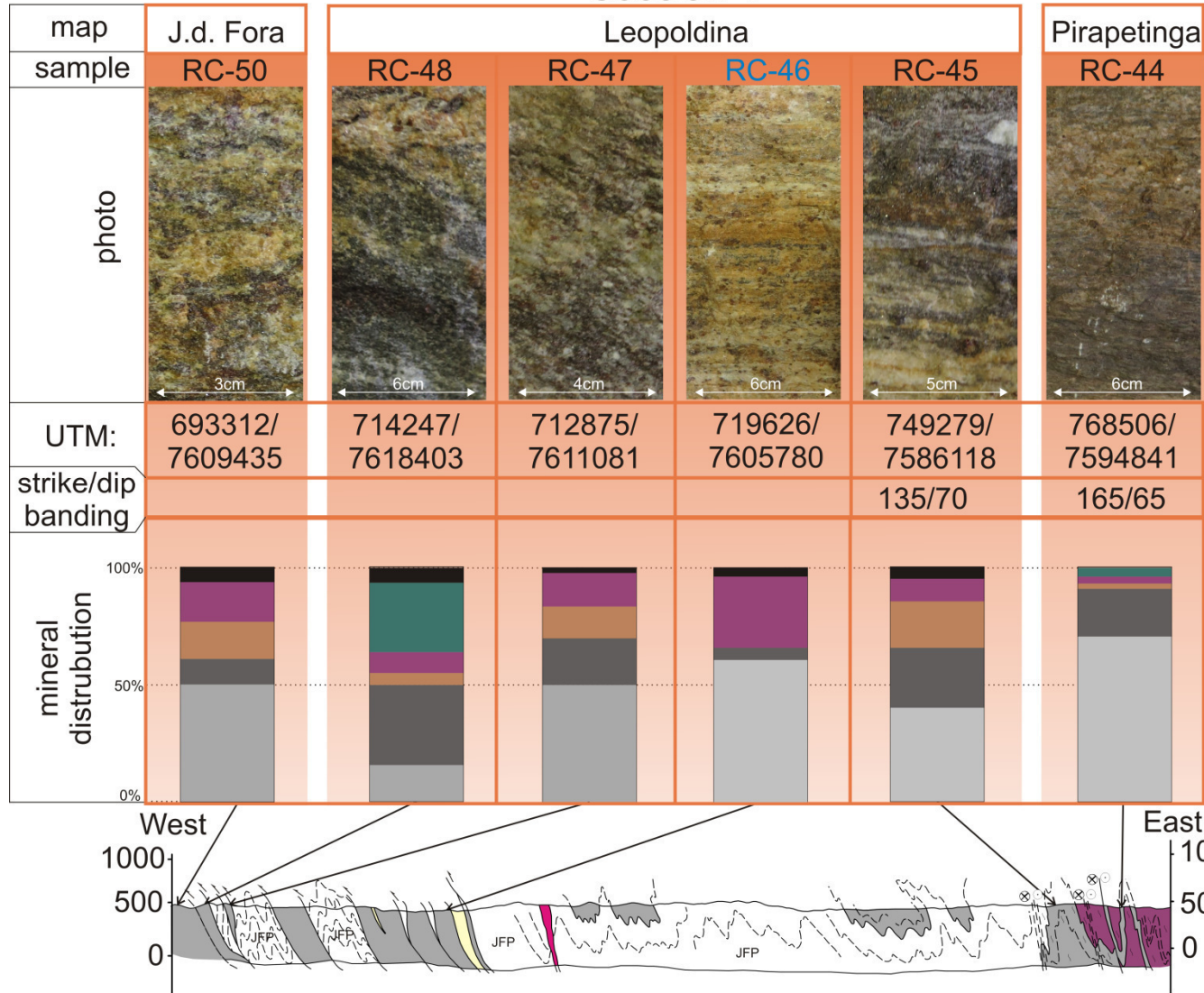
14

Fig. 3d: Field work and microscopical information of cross section 4 consisting of 6 representative samples. Lithotype-colours refer to Fig. 2.
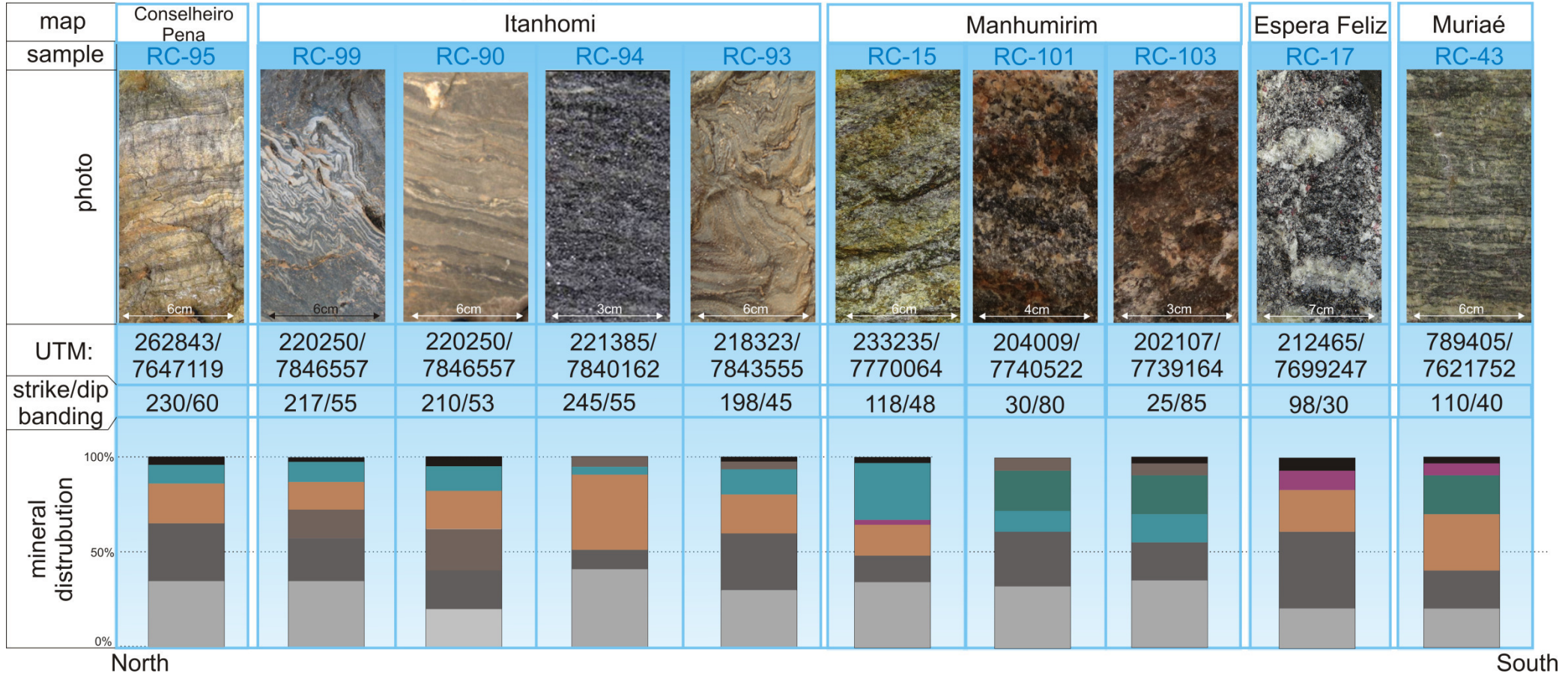
15

Fig. 3e: Field work and microscopical information of cross section 4 consisting of 6 representative samples.

16

2. Publication 1

Rhyacian–Orosirian links in the Congo-São Francisco palaeocontinent: Isotopic records from the basement of the Araçuaí–Ribeira orogenic system, Brazil

(published in Precambrian Research 317, 179-195)

(https://doi.org/10.1016/j.precamres.2018.08.018)

Rhyacian-Orosirian isotopic records from the basement of the Araçuaí-Ribeira orogenic system (SE Brazil): Links in the Congo-São Francisco palaeocontinent

Reik Degler[a],[*], Antonio Pedrosa-Soares[a], Tiago Novo[a], Mahyra Tedeschi[a],[b], Luiz Carlos Silva[b], Ivo Dussin[c], Cristiano Lana[d]

[a] Universidade Federal de Minas Gerais, Programa de Pós-Graduação em Geologia, CPMTC-IGC-UFMG, Campus Pampulha, 31270-901 Belo Horizonte, MG, Brazil
[b] Serviço Geológico do Brasil, CPRM, Avenida Brasil 1731, 30140-003 Belo Horizonte, MG, Brazil
[c] Universidade do Estado do Rio de Janeiro, Faculdade de Geologia, MULTILAB, Rua Francisco Xavier 524, Maracanã, 20550-900 Rio de Janeiro, RJ, Brazil
[d] Universidade Federal de Ouro Preto, DEGEO, Laboratório de Geoquímica Isotópica, Campus do Cruzeiro, 35400-000 Ouro Preto, MG, Brazil

ARTICLE INFO

ABSTRACT

Assembled during the Rhyacian-Orosirian boundary, the Congo-São Francisco palaeocontinent remained linked by a continental bridge from ca. 2 Ga to the Atlantic Ocean opening in the Cretaceous. To the south of that bridge, precursor basins and orogenic outcomes encompassed by the Neoproterozoic-Cambrian Araçuaí-Ribeira orogenic system (AROS) and its African counterparts, developed. The AROS discloses reworked basement units, like the Juiz de Fora, Pocrane and Quirino complexes, which are key units to retrieve the Palaeoproterozoic history of the Congo-São Francisco palaeocontinent. This paper presents new U-Pb ages, and the first Lu-Hf in zircon signatures from those complexes. All magmatic zircon grains show Rhyacian and Orosirian ages, ranging from c. 2250 Ma to c. 1850 Ma. The best Concordia ages range from 2184 ± 9 Ma to 2080 ± 19 Ma. Hf in zircon and whole-rock Sm-Nd data disclose mantle-related signatures for both, the Pocrane and Juiz de Fora complexes, suggesting igneous protoliths with no or very few involvement of continental crust, similarly to juvenile magmatic arcs. Conversely, Hf in zircon data for the Quirino complex show an evolved signature compatible with a magmatic arc developed on a continental older crust with Archaean components. Together with a thorough compilation on Rhyacian-Orosirian orogenic systems (ROOS), our data allow us to envisage links within the Congo-São Francisco palaeocontinent, comprising orogens characterised by mostly evolved isotopic signatures and zircon inheritance. They are grouped into the: (i) W-ROOS, including the Mantiqueira complex, the west segment of the Eastern Bahia belt, intrusions in the south Gavião and Porteirinha blocks, and parts of the Mineiro belt; and (ii) E-ROOS, comprising the Quirino complex, basement rocks of the Cabo Frio tectonic domain, the coastal Eastern Bahia belt, and, in Africa, Eburnean and Kimezian complexes, as well as the western Angola shield. Assembled between the W-ROOS and E-ROOS, an orogenic system with prominent juvenile to moderately juvenile isotopic signature (JU-ROOS) includes the Juiz de Fora and Pocrane complexes, and the Buerarema complex at the central segment of the Eastern Bahia belt.

1. Introduction

Rhyacian-Orosirian orogenic systems (also called Transamazonian-Eburnean belts) are recognised on nearly all continents, including an important framework of Palaeoproterozoic belts nowadays located in South America and Africa (Zhao et al., 2002). Segments of those orogenic systems and Archaean blocks were stitched together around 2 Ga (Fig. 1), forming the Congo-São Francisco palaeocontinent (Ledru et al., 1994; Trompette, 1994; Noce et al., 2007; Heilbron et al., 2010, 2017;

De Waele et al., 2008). This palaeocontinental landmass has been related to the Columbia supercontinent assembly (Rogers and Santosh, 2002; Zhao et al., 2002; Evans, 2009; Meert and Santosh, 2017; Teixeira et al., 2017a), but updated palaeomagnetic studies suggest it was not part of Columbia neither of Rodinia (D'Agrella-Filho and Cordani, 2017).

Once amalgamated in Early Orosirian time, the Congo-São Francisco palaeocontinent experienced a series of taphrogenic events from the Statherian to Ediacaran (Pedrosa-Soares and Alkmim, 2011),

acting as basement for precursor basins involved in the Araçuaí-Ribeira orogenic system and its African counterparts (Fig. 1). This Neoproterozoic-Cambrian orogenic system formed during the West Gondwana assembly, establishing well-known links between the proto-continents of South America and Africa (Pedrosa-Soares et al., 2001, 2008; Cordani et al., 2003; Alkmim et al., 2006; Heilbron et al., 2008; Schmitt et al., 2004, 2016; Degler et al., 2017).

A unique link formed long before the assembly of West Gondwana

was the Bahia-Gabon cratonic bridge (Fig. 1; Porada, 1989; Pedrosa-Soares et al., 2008). This long-lasting continental landmass once connected the São Francisco and Congo counterparts between c. 2 Ga and c. 140 Ma (Ledru et al., 1994; Trompette, 1994; D'Agrella-Filho and Cordani, 2017; Heilbron et al., 2017). Indeed, the Bahia-Gabon cratonic bridge shows no evidence of continental breakup and orogeny from the Rhyacian-Orosirian boundary until the Atlantic Ocean opening in the Cretaceous (Feybesse and Milési, 1998; Feybesse et al., 1998; Barbosa
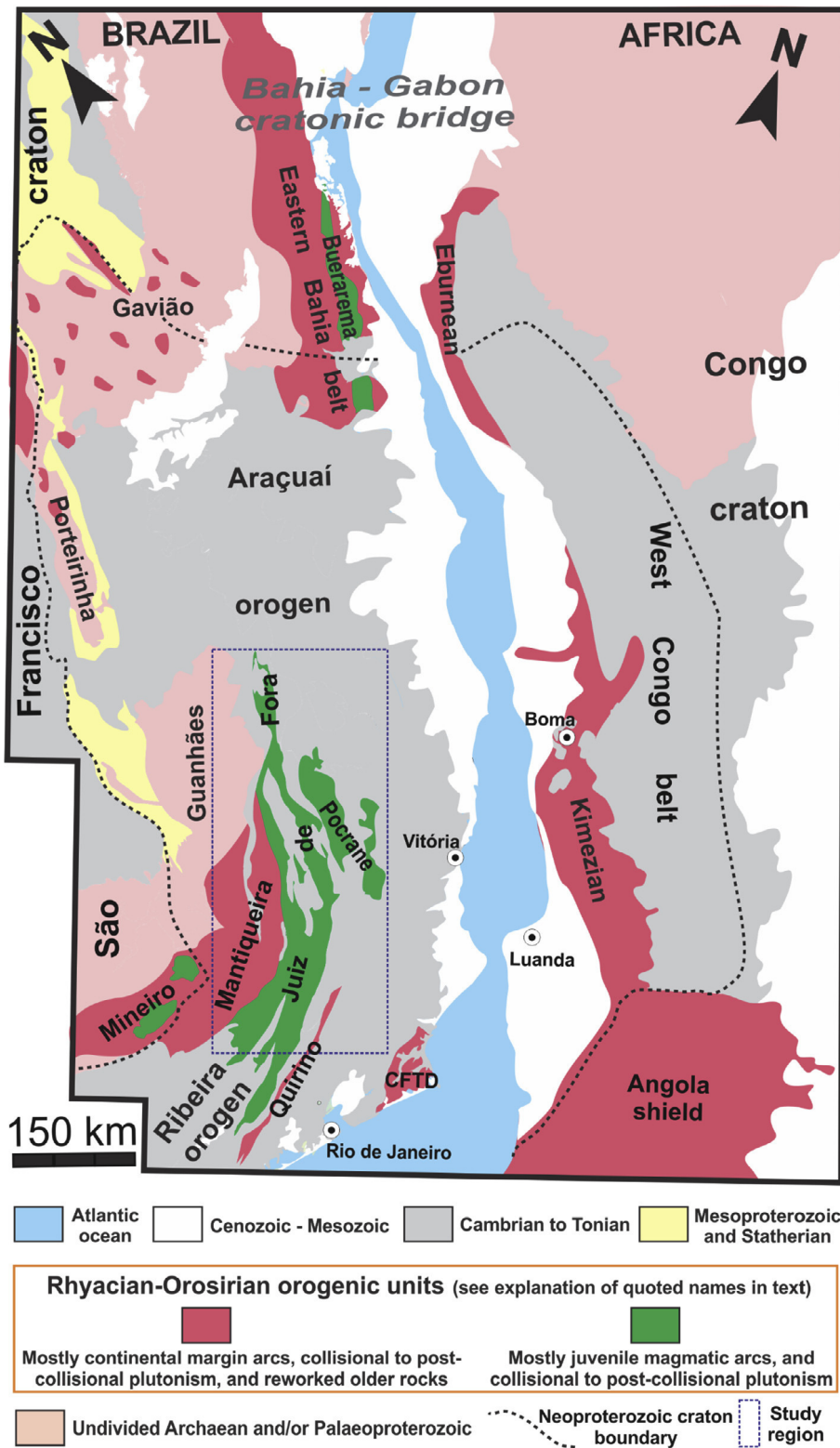

Fig. 1. Sketch maps on the focused region of the Congo-São Francisco palaeocontinent and its location in Western Gondwana. A, the Brasiliano-Pan-African orogenic system and related cratons (PC-LA-RPC, Paranapanema, Luiz Alves and Rio de la Plata cratons), highlighting the Congo and São Francisco (SFC) cratons linked by the Bahia-Gabon cratonic bridge (BGB). B, Brasiliano-Pan-African orogenic belts related to the Bahia-Gabon cratonic bridge and adjacent cratonic region (MFZ, Malange fault zone); C, the Rhyacian-Orosirian orogenic system in the focused region of the Congo-São Francisco palaeocontinent (modified from Brito-Neves et al., 1999; Silva et al., 2011; Barbosa and Barbosa, 2017).
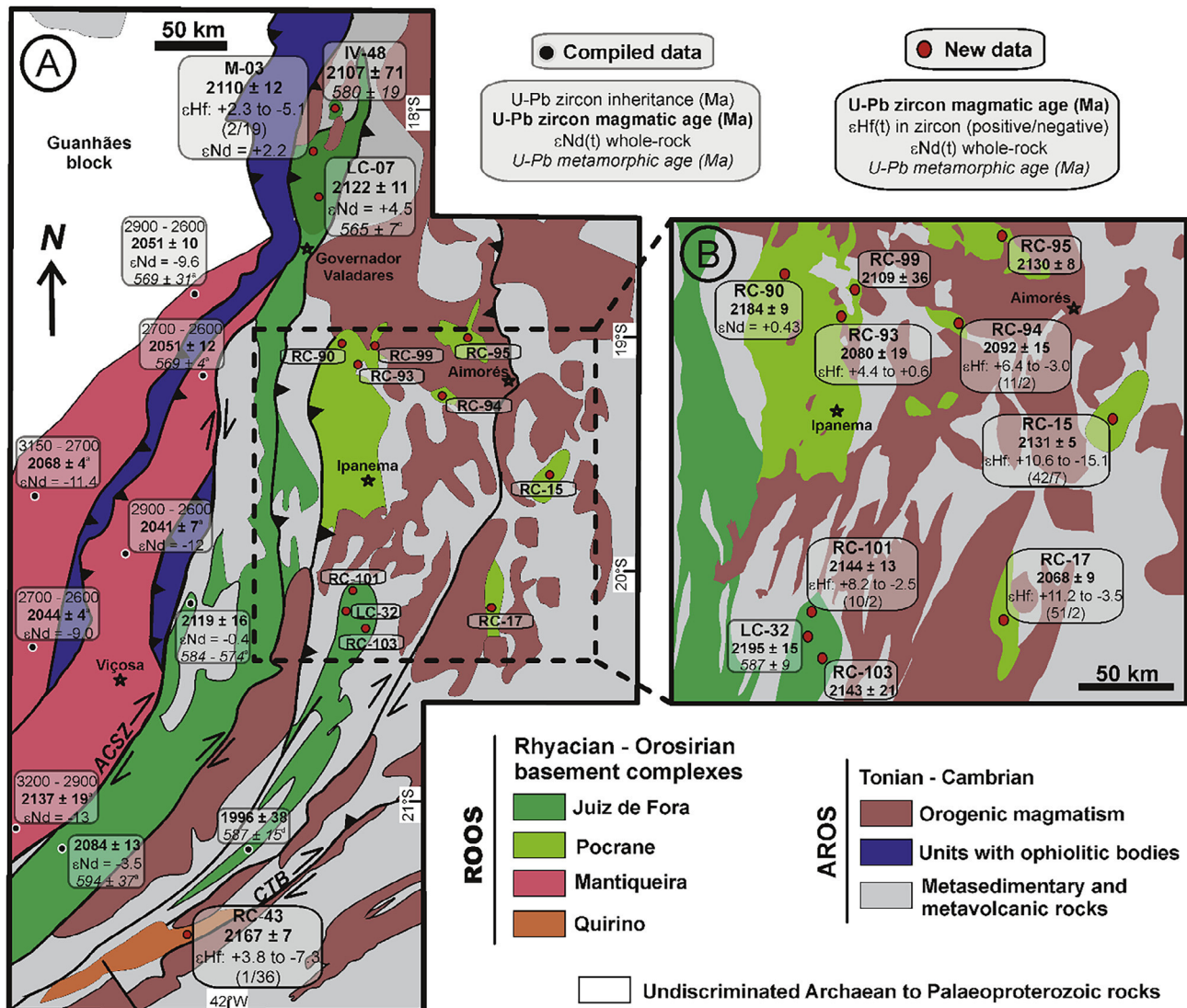
Fig. 2. The Rhyacian-Orosirian orogenic system (ROOS) from the northern to central Araçuaí-Ribeira orogenic system, highlighting: A, the new U-Pb and Lu-Hf in zircon, and Sm-Nd whole-rock data for the samples of the Quirino (RC-43) and Juiz de Fora (IV-48, M-03, LC-07, LC-32) complexes, as well as the compiled U-Pb data for the Mantiqueira and Juiz de Fora complexes ([a]Noce et al., 2007; [b]Silva et al., 2002b, [c]Silva et al., 2011); B, sample distribution with new U-Pb (SHRIMP and LA-ICP-MS) and Lu-Hf in zircon, and isotopic Sm-Nd whole-rock data for the Juiz de Fora and Pocrane complexes. ACsz, Abre Campo shear zone; CTB, central tectonic boundary (modified from Tuller, 2001).

and Sabaté, 2004; Lerouge et al., 2006; Thiéblemond et al., 2009; Barbosa and Barbosa, 2017). Therefore, the Bahia-Gabon cratonic bridge keeps the best evidence of the prior existence of the Congo-São Francisco palaeocontinent (Fig. 1). Farther south, within the Araçuaí-Ribeira orogenic system, remarkable outcomes of Rhyacian-Orosirian orogenies are the Juiz de Fora, Mantiqueira, Pocrane and Quirino complexes, representing Palaeoproterozoic magmatic arcs (Silva et al., 2002a; Valladares et al., 2002; Noce et al., 2007; Heilbron et al., 2010; Novo 2013). On the African side (Fig. 1), the Eburnean and Kimezian belts and parts of the Angola shield are also relics of Rhyacian-Orosirian orogens (Carvalho et al., 2000; Vicat and Pouclet, 2000; De Waele et al., 2008; Pedrosa-Soares et al., 2008, 2016; Thiéblemond et al., 2009; McCourt et al., 2013).

We present a detailed U-Pb and Lu-Hf in zircon isotopic study on selected orthogneiss samples from the Juiz de Fora, Pocrane and Quirino complexes (Figs. 2, 3 and 4; Table 1). Our data reveal the following important outcomes: (i) the first Lu-Hf data for those complexes, distinguishing between crustal and juvenile protoliths; (ii) the Rhyacian magmatic age and juvenile nature of the Pocrane orthogneiss protoliths, formerly considered to be Archaean in age; (iii) the

significant extension of the Juiz de Fora complex to the north of its prior known area; (iv) a solid correlation between the Juiz de Fora and Pocrane complex, both including juvenile crust; and, (v) the magmatic age and crustal nature of a part of the Quirino complex not described in the literature. Our data (Table 1; Figs. 2, 6, 7) and a full compiled dataset (Table 2, Fig. 8) disclose a reliable correlation scenario, comprising Rhyacian-Orosirian juvenile and continental orogenic systems involved in the Congo-São Francisco palaeocontinent assembly.

In this paper, geographical coordinates and orientations refer to the present-day position of continents, even in palaeotectonic interpretations. The geological time subdivisions here cited (e.g., Rhyacian, 2.30–2.05 Ga; Orosirian, 2.05–1.80 Ga) are those from the International Chronostratigraphic Chart (Cohen et al., 2013, updated in 2017).

2. Geological setting

In eastern Brazil and southwestern Africa, the basement of the Congo-São Francisco palaeocontinent mostly comprises Archaean blocks and Rhyacian-Orosirian orogenic systems (Fig. 1). Some Archaean blocks, e.g., Gavião, Guanhães and Porteirinha (Fig. 1) record

orogenic reworking in the Palaeoproterozoic and/or Neoproterozoic (Cruz et al., 2016; Silva et al., 2016; Aguillar et al., 2017; Alkmim and Teixeira, 2017; Teixeira et al., 2017b).

As part of the Bahia-Gabon cratonic bridge (Fig. 1), the Eastern Bahia belt mostly includes Archaean infracrustal rocks reworked by a Rhyacian-Orosirian orogeny (Silva et al., 1997, 2002b; Barbosa and Sabaté, 2004; Souza et al., 2014; Barbosa and Barbosa, 2017). Flanked to the east and west by the reworked Archaean crust of the Eastern Bahia belt (Fig. 1), the Buerarema complex consists of low-K calc-alkaline tonalite and trondjhemite, metamorphosed from the amphibolite to granulite facies (Silva et al., 2002; Pinho, 2005; Pinho et al., 2011). This complex shows U-Pb magmatic (2191–2096 Ma) and metamorphic ages (2109–2069 Ma) relatively close to each other, and $^{\varepsilon}Nd_{(2.1\ Ga)}$ values (+3.1 to −1.7) suggesting a moderately juvenile magmatic arc (Silva et al., 2002b; Peucat et al., 2011; Silva, 2006), the Buerarema arc (Silva et al., 2016).

Even farther south, the Mineiro belt involved accretions of igneous bodies with both, juvenile and continental signatures, from the Siderian to Late Rhyacian (Teixeira et al., 2000, 2015, 2017b; Avila et al., 2010; Seixas et al., 2013; Ávila et al., 2014; Barbosa et al., 2015, 2018; Aguillar et al., 2017; Alkmim and Teixeira, 2017; Moreira et al., 2018). To the east of the Mineiro belt (Figs. 1 and 2A), the Mantiqueira complex represents a magmatic arc built on a Late Rhyacian continental margin with remarkable inheritance of Archaean continental crust (Silva et al., 2002a; Noce et al., 2007; Heilbron et al., 2010; Aguillar et al., 2017; Alkmim and Teixeira, 2017). Farther east, segments of Palaeoproterozoic magmatic arcs are the Juiz de Fora, Pocrane and Quirino complexes, which are the focus of the present paper (Figs. 1, 2A and 2B).

The Juiz de Fora complex extends to the east of the Abre Campo shear zone (ACSZ in Fig. 2). This remarkable NE-SW-trending shear zone sutured the Mantiqueira and Juiz de Fora magmatic arcs in the Early Orosirian (Alkmim et al., 2006; Noce et al., 2007; Heilbron et al., 2017). The Juiz de Fora complex mostly includes tholeiitic mafic granulites and calc-alkaline enderbites with mafic enclaves, and granitic leucosomes. To the south of Governador Valadares city, the Juiz de Fora complex is rich in greenish orthopyroxene-bearing rocks (Fig. 2A, 3A, 3B, 4A, 4Ax). Taking into account our new results, the greenish to greyish, banded orthogneisses enriched in hornblende and biotite, found from Governador Valadares towards north, are also included in the Juiz de Fora complex (Fig. 2A). These orthogneisses are granodioritic to tonalitic rocks with metamafic enclaves and granitic leucosomes (Tedeschi, 2013). The greyish orthogneisses are richer in biotite and frequently show mylonitic features (Fig. 3C, 3D, 4C, 4Cx). The Juiz de Fora enderbites and mafic granulites have yielded zircon U-Pb magmatic ages from c. 2.2 to 2.08 Ga, relatively close to their Nd T_{DM} model ages (2.4–2.2 Ga) with $^{\varepsilon}Nd(t)$ from +7.7 to −3.5, suggesting a juvenile magmatic arc (Fischel et al.,1998; Heilbron et al., 1998, 2010; Noce et al., 2007; André et al., 2009). Leucosomes composed of garnet-bearing charnockite represent, in general, an Ediacaran anatectic event related to the Brasiliano orogeny (Duarte et al., 2000; Silva et al., 2002b; Heilbron et al., 2010).

The Pocrane complex consists of banded to laminated orthogneisses, with intercalations of ortho-amphibolites and metasedimentary rocks (Novo, 2013). The orthogneisses show alternating bands and laminae variably rich in biotite and hornblende, tending to dark grey tints (Fig. 3E, 4B, 4Bx). The lighter bands and laminae are rich in quartz and feldspars (generally plagioclase > K-feldspar), and poor in mafic minerals. The fine-grained bands may show features resembling volcanic rocks, like corroded quartz and plagioclase phenocrysts. Although most orthogneisses show relatively low partial melting rates, migmatisation is a common feature in the Pocrane complex, forming granitic

Table 1

Summary of the main data for the studied samples. U-Pb (SHRIMP and LA-ICP-MS) ages and Lu-Hf (LA-ICP-MS) isotopic data obtained from spot analysis on zircon grains. Sm-Nd (TIMS) isotopic data obtained from analysis on pulps from whole-rock samples.

Sample (C.S.U.)[*]	Studied rock	Location (UTM)	A.I.M.[**]	U-Pb age (Ma) magmatic *metamorphic*	$\varepsilon Hf_{(t)}$ (N+/N−)[***]	Hf T_{DM} age (Ga)[****]	$\varepsilon Nd_{(t)}$	Nd T_{DM} age (Ga)
IV-48 (JF)	granodioritic orthogneiss	E190863 N7970418	1	2107 ± 71 *580 ± 19*				
M-03 (JF)	tonalitic orthogneiss	E188779 N7963791	1,2,3	2110 ± 12	+2.3 to −5.1 (2/19)	2.69–2.30	+2.2	2.18
LC-07 (JF)	tonalitic orthogneiss	E205219 N7960172	2,3	2122 ± 11 *565 ± 7*			+4.5	2.03
RC-101 (JF)	enderbiticorthogneiss	E204009 N7740522	1	2144 ± 13	+8.2 to −2.5 (10/2)	2.59–2.11		
RC-103 (JF)	enderbiticorthogneiss	E202107 N7739164	1	2143 ± 21				
LC-32 (JF)	charnockiticorthogneiss	E199781 N7742627	2	2195 ± 15 *587 ± 9*				
RC-90 (P)	dioritic orthogneiss	E220250 N7846557	2	2184 ± 9			+0.43	2.34
RC-93 (P)	tonalitic orthogneiss	E218323 N7843555	1,2	2080 ± 19	+4.4 to +0.6 (8/0)	2.33–2.12		
RC-94 (P)	tonalitic orthogneiss	E221385 N7840162	1,2	2092 ± 15	+6.4 to −3.0 (11/2)	2.53–2.09		
RC-95 (P)	granodioritic orthogneiss	E262843 N7863012	2	2130 ± 8				
RC-99 (P)	tonalitic orthogneiss	E220250 N7846557	2	2109 ± 36				
RC-15 (P)	tonalitic orthogneiss	E233235 N7770064	1	2131 ± 5	+10.6 to −15.1 (42/7)	2.79–2.05		
RC-17 (P)	tonalitic orthogneiss	E211141 N7699888	1	2068 ± 9 *609 ± 3*	+11.2 to −3.5 (51/2)	2.39–2.02		
RC-43 (Q)	tonalitic orthogneiss	E789405 N7621752	1	2167 ± 7 *613 ± 5*	+3.8 to −7.3 (1/36)	2.81–2.25		

* C.S.U. (corresponding stratigraphic unit): Juiz de Fora (JF), Pocrane (P) or Quirino (Q) complex.
** A.I.M. (applied isotopic method): 1, U-Pb and/or Lu-Hf LA-ICP-MS; 2, U-Pb SHRIMP; 3, Sm-Nd TIMS.
*** N+/N− ratio: number of positive $\varepsilon Hf_{(t)}$ values/number of negative $\varepsilon Hf_{(t)}$ values.
**** Hf T_{DM} age range corresponding to the most positive $\varepsilon Hf_{(t)}$ value and the most negative $\varepsilon Hf_{(t)}$ value.
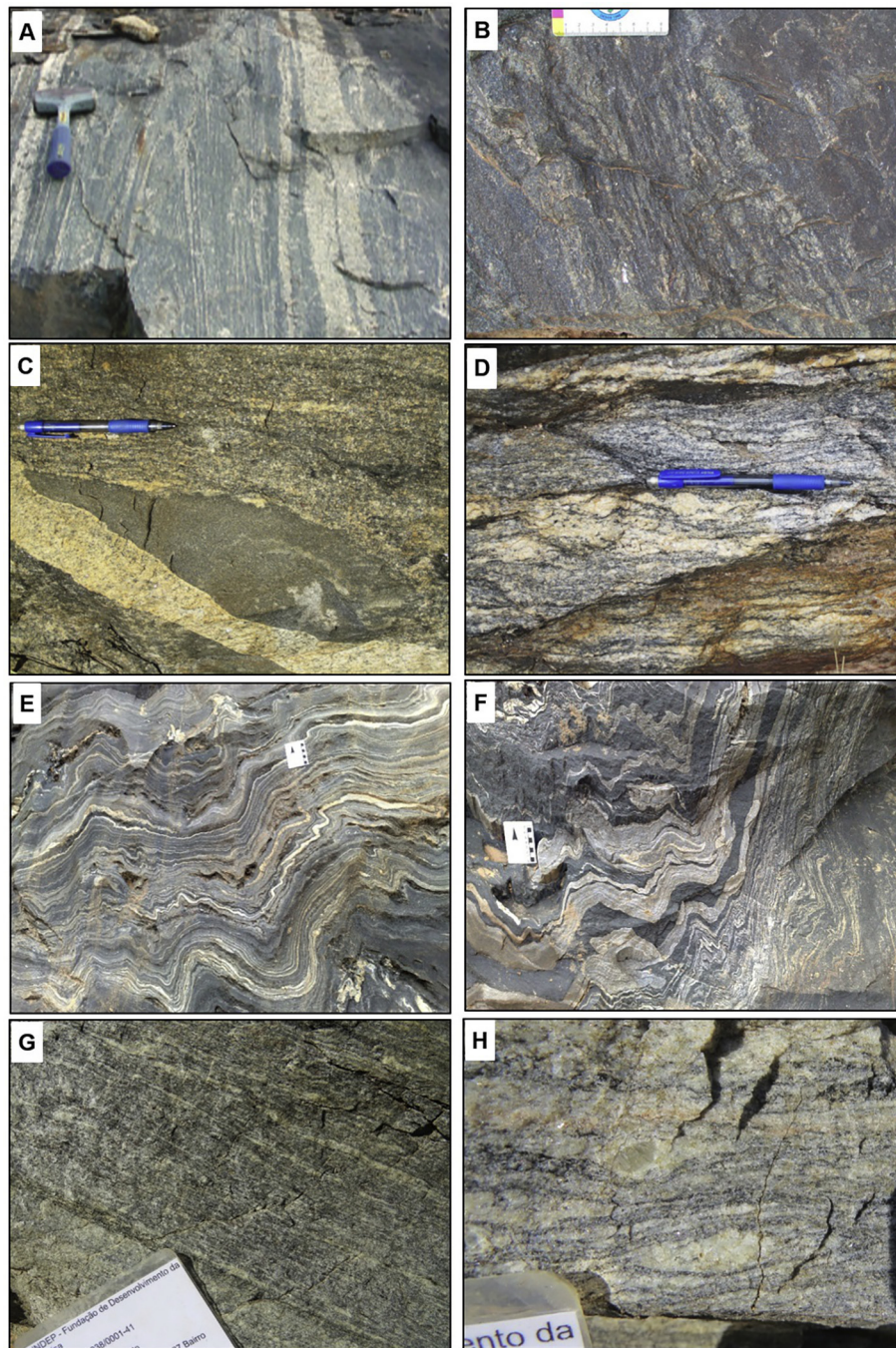
Fig. 3. Typical features of the studied Rhyacian orthogneisses: A, banded enderbitic granulite with charnockitic leucosomes, southern Juiz de Fora complex; B, banded mafic granulite, southern Juiz de Fora complex; C, tonalitic orthogneiss with metamafic enclave, cut by leucogranite vein, northern Juiz de Fora complex; D, mylonitic features in a granodioritic orthogneiss, northern Juiz de Fora complex; E, banded biotite-hornblende orthogneiss, Pocrane complex; F, Mesoproterozoic ortho-amphibolite intercalations (black) in the Pocrane orthogneiss; G, laminated Quirino orthogneiss; H, banded Quirino orthogneiss rich in leucosomes.

leucosomes parallel to the banding. Progressive mylonitic features can be observed from macroscopic to microscopic scales. That process results in series of increasingly deformed and leached rocks that, locally, disclose the transformation of an orthogneiss in rocks very rich in quartz and/or biotite (Novo, 2013). Formerly interpreted as Archaean in age (Tuller, 2001), the Pocrane orthogneisses represent Rhyacian magmatic protoliths roughly coeval to those of the Juiz de Fora and Quirino complexes (see new data and discussions in next sections).

The Quirino complex includes greyish to greenish, tonalitic to granitic orthogneisses with intercalations of meta-mafic and meta-

ultramafic rocks, metamorphosed in the high amphibolite facies (Fig. 2A, 3G, 3H). The Quirino orthogneisses show a medium-K to high-K calc-alkaline signature (Valladares et al., 2002; Viana, 2008). Most magmatic ages from the Quirino orthogneisses and their enclaves are in the range of c. 2.14–2.31 Ga, with εNd(t) from +1.6 to −9.5 and Nd T_{DM} model ages from c. 3.9 Ga to c. 2.2 Ga (Valladares et al., 2002; Viana, 2008; Machado et al., 2010). According to these authors, the Quirino complex represents a Rhyacian magmatic arc built on a continental margin, with significant Archaean inheritance.
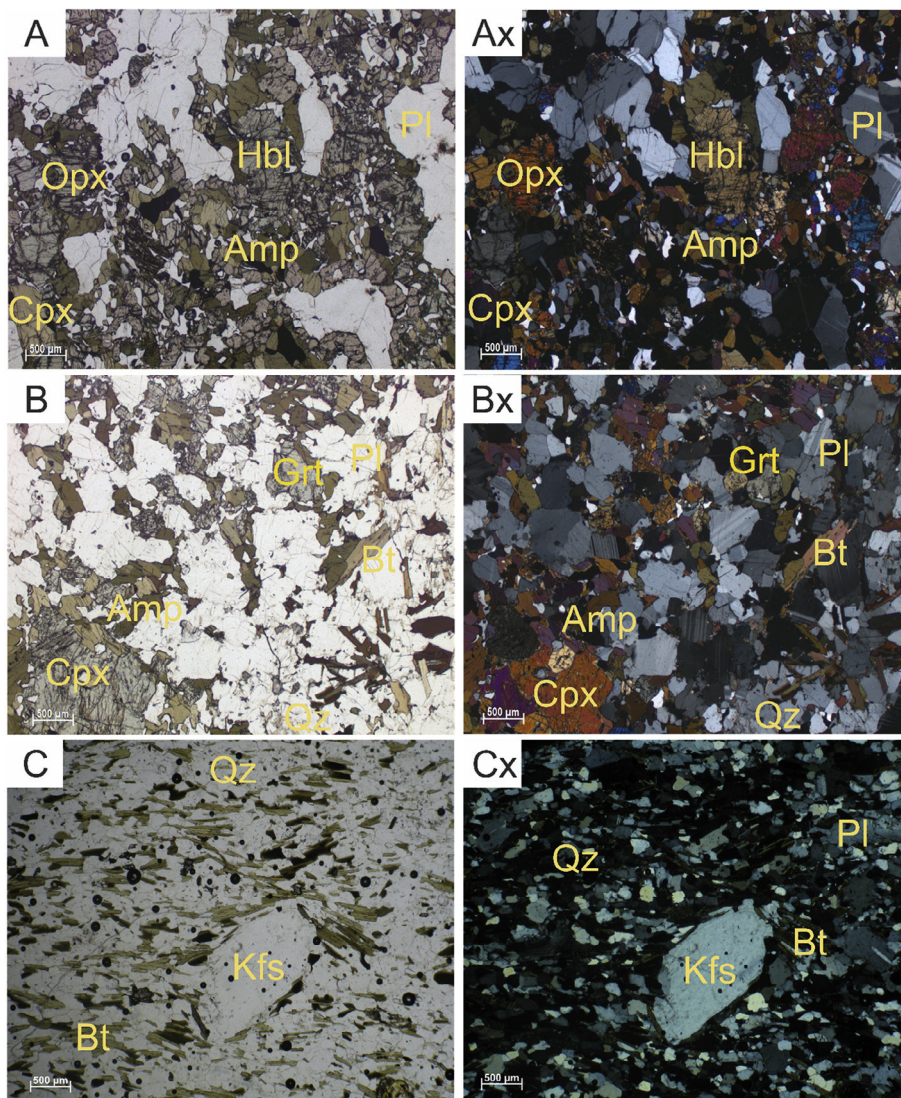
Fig. 4. Photomicrographs from thin sections of the Juiz de Fora orthogneisses in the granulite and amphibolite facies (x indicates polarized light). A and Ax, enderbitic to noritic granulite of the southern Juiz de Fora complex (e.g., samples RC-101 and RC-103), showing retrograde (uralitisation) process of a probable Brasiliano orogeny age; B and Bx, tonalitic amphibole-biotite orthogneiss of the Pocrane complex (e.g., RC-90); C and Cx, granodioritic biotite orthogneiss of the northern Juiz de Fora complex (e.g., sample RC-104), showing the regional foliation associated with important retrograde (Bt-rich) metamorphism related to the Brasiliano orogeny.

3. Sample selection and analytical methods

This article presents new isotopic (U-Pb and Lu-Hf in zircon; and whole-rock Sm-Nd) data for 14 orthogneiss samples collected from the Juiz de Fora (six samples: RC-101, RC-103, LC-07, LC-32, M-03, IV-48), Pocrane (seven samples: RC-15, RC-17, RC-90, RC-93, RC-94, RC-95, RC-99) and Quirino (one sample: RC-43) complexes (Supplementary Data File 1). Before starting the preparation processes, the samples were inspected for mineral concentrates and whole-rock pulps. Afterwards, all samples were broken in fragments of ~ 5 cm in size, and carefully cleaned to remove weathered materials, alteration coats, mineral veins and leucosomes. The cleaned rock samples were processed by conventional methods, like crushing, milling, sieving and fractionation. Pulps of the fractionated material were obtained for isotopic Sm-Nd analyses. From each sample concentrate, around 100 zircon grains were picked and mounted on standard sections for the cathodoluminescence (CL) imaging, and isotopic U-Pb and Lu-Hf analysis on LA-ICP-MS or SHRIMP equipment.

Supplementary data associated with this article can be found, in the online version, at https://doi.org/10.1016/j.precamres.2018.08.018.

3.1. LA-ICP-MS U-Pb in zircon

All separated zircons were mounted and photographed for cathodoluminescence (CL) imaging using the electron microscope (SEM) Quanta-250-FEI. The zircon grains were spotted by microprobe Laser (Excimer Laser 193 μm by Photon-Machines Inc. Model ATLEX SI), pulsed with ArF, attached to a MC-ICP-MS (Neptune-Plus), in the MULTILAB-UERJ (State University of Rio de Janeiro). Isotopic data were acquired by static mode with a laser beam spot of 25 μm under operating conditions presented in Supplementary Data File 1. Element fractionation by induction of the Laser and essential mass discrimination were monitored by analyses of external zircon standard (GJ-1 of 609 ± 0.6 Ma, Jackson et al., 2004). External inaccuracies were compensated by quadratic addition of individual measures of the external standard GJ-1 and individual measurement of every sampled zircon (or spot). For detailed method conditions see (Chemale et al., 2012). The quality data control of the sample sets and the GJ-1 standard was controlled by complement analyses of 91,500 standard grains with an age of 1065 ± 0.3 Ma (Wiedenbeck et al., 1995).

3.2. SHRIMP U-Pb in zircon

U-Pb analyses were performed with Sensitive High Resolution Ion Microprobe (SHRIMP) equipment at the SHRIMP laboratory of the Australian National University (Canberra) and at the SHRIMP Laboratory of CPGEO-USP, São Paulo University. Backscattered (BSE) and CL images were taken using SEM JEOL 6200. Before starting the

SHRIMP analyses, the mounts were re-polished and gold coated. The isotopic U-Pb investigations were performed with the SHRIMP II equipment following the methodology by Compston et al. (1984, 1992) and the operating routine described by Smith (1998). Measured uranium, lead and thorium concentrations were referenced to the TE-MORA zircon standard (417 ± 0.2 Ma, Black et al., 2003). The determination of the standard was done after every third measurement. Every single analytical spot has a 15–25 μm diameter, depending on the laboratory routine.

3.3. LA-ICP-MS Lu-Hf in zircon

The Lu-Hf analyses in zircons were performed at the Isotope Geochemistry Laboratory of the Federal University of Ouro Preto, Brazil. Out of six samples 170 Lu-Hf isotopic analyses were obtained via Laser Ablation Multicollector Inductively Coupled Plasma Mass Spectrometry (LA-MC-ICP-MS, Photonmachines 193/Neptune Thermo Scientific) on the same zircon grain domains already spotted for U-Pb dating. Zircons of Temora (416 Ma, $^{176}Hf/^{177}Hf = 0.282680$); 91,500 (1065 Ma $^{176}Hf/^{177}Hf = 0.282307$); Mudtank (732 Ma $^{176}Hf/^{177}Hf = 0.282504$) and Plešovice (337 Ma $^{176}Hf/^{177}Hf = 0.282482$) served as standards during the measurement process. The laser was operated with a spot of 40 μm in diameter (65% power) and fluence of $3 J/cm^2$ 36 s, and a pulse rate of 5 Hz. Helium was used as carrier gas to minimize oxide formation and increase Hf sensitivity (Bahlburg et al., 2011). For calculation of $\varepsilon_{Hf(t)}$ values, we adopted a decay constant for ^{176}Lu of 1.867×10^{-11} (Söderlund et al., 2004) and present-day chondritic ratios of $^{176}Hf/^{177}Hf = 0.282785$ plus $^{176}Lu/^{177}Hf = 0.0336$ (Bouvier et al., 2008). The depleted mantle Hf evolution curve was determined from present-day depleted mantle values of $^{176}Hf/^{177}Hf$ ratio of 0.28325 and $^{176}Lu/^{177}Hf$ ratio of 0.0388 (Griffin et al., 2000; updated by Andersen et al., 2009). Following (Pietranik et al., 2008) the continental model of felsic crust was calculated using the initial $^{176}Hf/^{177}Hf$ of zircon and the $^{176}Lu/^{177}Hf = 0.022$ ratio.

3.4. Whole-rock Sm-Nd isotopic analysis

Sm-Nd isotopic determination was conducted in the Laboratory of Geochronology at the University of Brasília (UnB). Sm and Nd followed the method as described by Gioia and Pimentel (2000). Whole-rock powders (~ 50 mg) were mixed with a ^{149}Sm-^{150}Nd spike solution and dissolved in Savillex capsules. The lanthanides were extracted under use of ionic exchange conventional techniques in quartz columns of added BIO-RAD-AG-50W-X8 resin. Sm and Nd extraction of whole-rock samples followed conventional cation exchange techniques, using Teflon columns containing LN-Spec resin di-(2-ethylhexyl) phosphoric acid (HDEHP) supported on PTFE powder. The fractions of Sr, Sm and Nd samples were loaded on re-evaporation filaments of double filament assemblies. The isotopic measurements were carried out on a multi-collector Finnigan MAT 262 mass spectrometer in static mode. Uncertainties for $^{87}Sr/^{86}Sr$ are smaller than 0.01% (2σ), and for Sm/Nd and $^{143}Nd/^{144}Nd$ ratios are better than ± 0.1% (2σ) and ± 0.005% (1σ), respectively, based on repeated analyses of international rock standards BHVO-1 ($^{87}Sr/^{86}Sr = 0.7034$, $^{143}Nd/^{144}Nd = 0.5129$ and BCR-1 ($^{87}Sr/^{86}Sr = 0.7049$, $^{143}Nd/^{144}Nd = 0.5126$). $^{143}Nd/^{144}Nd$ ratios were normalised to $^{146}Nd/^{144}Nd = 0.7219$ and the decay constant (λ) used was $6.54 \times 10^{-12} y^{-1}$. T_{DM} ages were calculated according to DePaolo (1981).

4. Results

In this section we describe the results obtained from the isotopic analyses (Figs. 2, 6 and 7). Detailed data, sample references and location coordinates are given in Table 1 and Supplementary Data File 1. To guaranty best precision and accuracy for calculated Concordia ages, it was attempted to keep the probability and MSWD values as low as possible. Exclusion criteria for data were imprecise ratios values (± 0.15) and calculated errors (Disc. % ± 0). Used data for accurate Concordia age determination of each sample (Fig. 6) are highlighted in Supplementary Data File 1. Acceptable data besides Concordia ages were not included in Isoplot calculation but considered to discuss age ranges in the following sections.

4.1. Juiz de Fora complex

Sample IV-48: This sample, collected from the granodioritic palaeosome of a migmatitic orthogneiss, yielded zircon grains with magmatic domains of oscillatory zoning, and metamorphic overgrowths at the rims (Fig. 5A). Although the grains are mostly fragments, it is possible to identify their prismatic shapes and magmatic features. The calculated ages for the upper and lower intercepts are 2107 ± 17 Ma (MSWD = 0.36), representing the magmatic crystallisation of the granodioritic protolith, and 580 ± 19 Ma, indicating metamorphism and migmatisation in the Brasiliano orogeny (Fig. 6A). This outcrop is a new finding of an exposure of the Juiz de Fora complex in an area previously ascribed to the Mantiqueira complex.

M-03: Collected from a greyish band of tonalitic composition in a migmatitic and mylonitic orthogneiss (Fig. 3D), this sample only shows elongated and prismatic zircons grains (Fig. 5A). The zircon grains have a homogenous inner texture with weak oscillatory zoning being interpreted as magmatic crystals. The best calculated Concordia age for the magmatic crystallisation is 2110 ± 12 Ma (MSWD = 0.091; Fig. 6A). The M-03 outcrop is also a further discovery for an extension of the Juiz de Fora complex to the north of its formerly known area of occurrence.

LC-07: This sample represents the greenish tonalitic bands of a biotite-hornblende orthogneiss with mafic enclaves, cut by leucogranite veins (Fig. 3C). It shows prismatic zircon crystals with magmatic domains of oscillatory zones, surrounded by metamorphic overgrowths towards the grain rims. The fourteen spotted zircon grains provide a Discordia line with a calculated upper intercept age of 2122 ± 11 Ma (MSWD = 0.91). This age represents the magmatic age of the zoned igneous grain cores that crystallised in the tonalitic protolith (Fig. 6A). The calculated lower intercept age of 561 ± 9 Ma represents the metamorphic rim overgrowths related to the collisional stage of the Brasiliano orogeny. Although in the same deviation range, a more precise age for the Brasiliano metamorphism (565 ± 7 Ma; MSWD = 0.62; probability = 95%) was calculated using only data from four spots on rim overgrowths (Silva et al., 2011).

RC-101 and RC-103: These samples represent the typical greenish enderbitic (Opx-bearing) orthogneiss of the Juiz de Fora complex (also known as Caparaó suite in the sampling area). They show typical magmatic zircon grains of prismatic habitus and oscillatory zonation (Fig. 5A). Owing to intense Pb loss, it was only possible to calculate upper intercept ages, representing the magmatic crystallisation at 2144 ± 13 Ma (RC-101) and 2143 ± 21 Ma (RC-103; Supplementary Data File 1). The ages are in good agreement with the other samples of the same unit and, therefore, considered for the present paper (Fig. 2B).

LC-32: This sample, also collected from the Caparaó suite of the Juiz de Fora complex, is composed of a greenish Opx-bearing charnockitic orthogneiss with elongated K-feldspar porphyroclasts. The zircons are characterised by a magmatic grain core with oscillatory zoning, as well as zircon grains typical for recrystallisation under high-T conditions in the granulite facies (e.g., grains with soccer ball morphology and fir tree texture, and pseudo-rounded grains with thick metamorphic rims; Silva et al., 2011). Nine spots furnished a Discordia line with an upper intercept at 2195 ± 15 Ma (MSWD = 0.62), representing the magmatic crystallisation. The lower intercept at 599 ± 79 Ma reflects the metamorphic overprint by the Brasiliano orogeny (Fig. 6A). A more precise calculation with nine spots on metamorphic domains yielded an age of 587 ± 9 Ma (MSWD = 0.89; probability = 0.54; Silva et al., 2011). Data from a few metamorphic grains with soccer ball morphology and fir tree texture suggest a Rhyacian high-grade
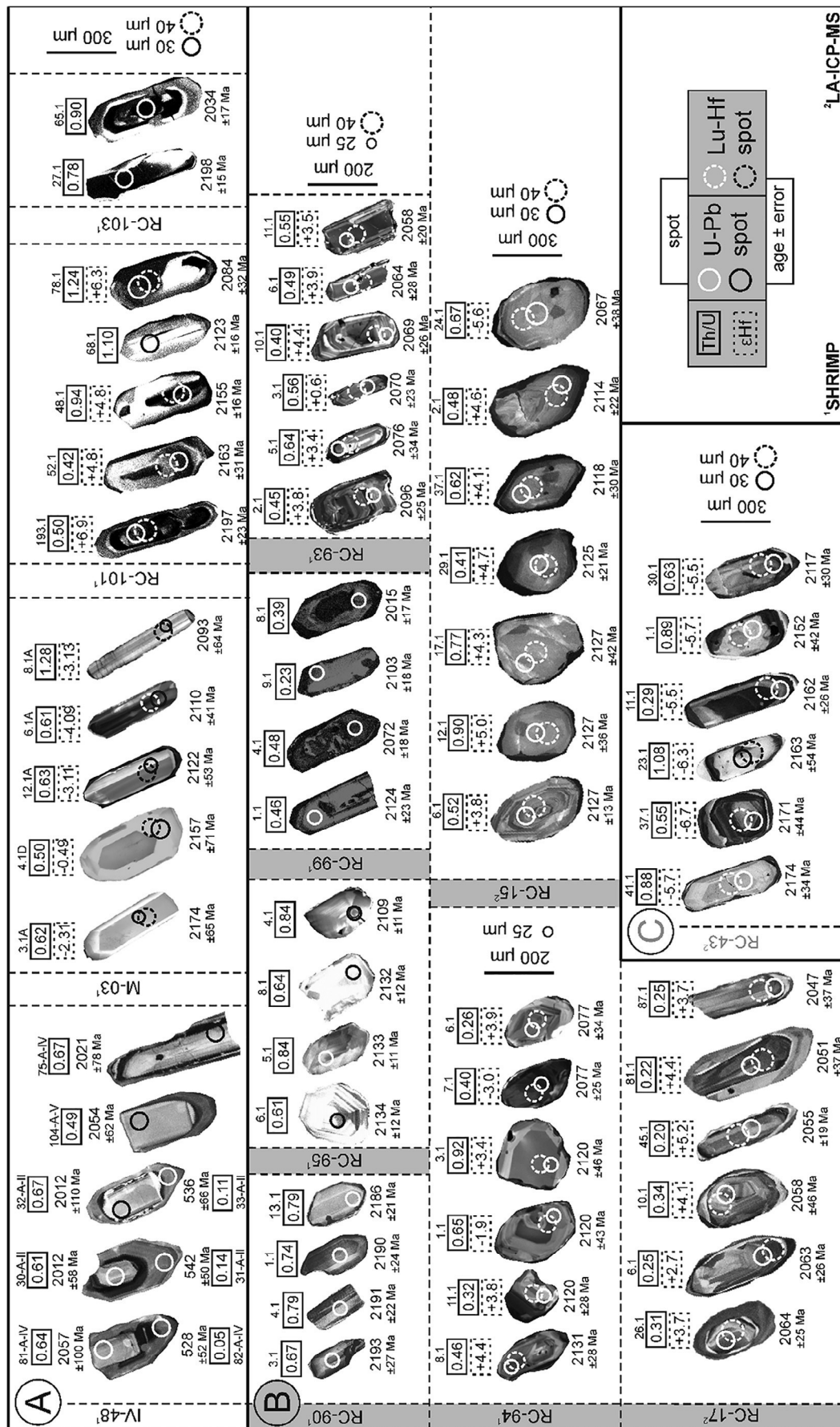
Fig. 5. Cathodoluminescence (CL) images of analysed zircons from orthogneiss samples of the Juiz de Fora, Pocrane and Quirino complexes.

metamorphism at 2095 ± 9 Ma (Silva et al., 2011).

4.2 Pocrane complex

RC-90: This sample was collected from an outcrop of the laminated to banded hornblende-biotite orthogneiss (Fig. 3E) and represents one of the most typical rocks of the Pocrane complex. The sampled rock shows bands with corroded quartz and plagioclase crystals within a fine-grained matrix, suggesting an origin related to volcanic processes. Zircon crystals were extracted from dioritic/andesitic bands of the orthogneiss. The CL images show a homogenous group of short and prismatic zircons (Fig. 5B). Most of the grains display a thin overgrowth at the rims (not wide enough for spot analyses), which could indicate metamorphic recrystallisation. Fifteen zircon grains were analysed using the U-Pb SHRIMP method. Data from eight spots yielded a Concordia age at 2184 ± 9 Ma (MSWD = 0.011; probability = 0.92), representing the magmatic crystallisation age of the igneous protolith (Fig. 6B). Only one grain with Archaean age (c. 2710 Ma) suggests a scanty contamination by continental material, which is a common process in volcanic rocks, even in juvenile magmas of Andean-type arcs. However, as this is the only case among more than one hundred analysed grains from the Pocrane samples, we cannot definitely rule out an unlikely but possible contamination during sample preparation.

RC-95: This sample represents an ultramylonite formed from the intense shear deformation of an orthogneiss of the Pocrane complex. The sampled outcrop consists of a banded rock with feldspar-bearing bands enriched in quartz and alternating bands of thin phyllonitic biotite bands, with pods preserving the typical Pocrane orthogneiss. The CL images show predominant igneous prismatic zircons with oscillatory zoning. Some small pseudo-rounded zircons with soccer ball morphology indicate high-T metamorphism. Both zircon groups have thin rims of metamorphic overgrowth, not wide enough to spot analysis. From SHRIMP analysis, eight spots yielded the best fitting Concordia age of 2130 ± 8 Ma (Fig. 6B), representing the crystallisation of the igneous protolith.

RC-99: The sampled rock is a laminated hornblende-biotite orthogneiss of tonalitic composition (Fig. 3F). The CL images show zircon grains of the same size and with evidence of magmatic features (Fig. 5B). Another evidence for an igneous origin are the high Th/U ratios. From SHRIMP analysis on sixteen zircon grains, four spots yielded a Concordia age of 2109 ± 36 Ma (MSWD = 0.034; probability = 0.85), interpreted as the crystallisation age of the magmatic protolith (Fig. 6B).

RC-93: The analysed zircon crystals were extracted from the tonalitic palaeosome of a migmatitic hornblende-biotite orthogneiss. Twelve elongated prismatic zircon grains of magmatic origin were selected for SHRIMP analysis (Fig. 5B). A Concordia age yielded by five spots indicate the crystallisation age (2080 ± 13 Ma; MSWD = 0.80; probability = 0.37) of the magmatic protolith (Fig. 6B).

RC-94: This sample represents a mylonitic orthogneiss of the Pocrane complex, relatively poor in feldspars, and rich in biotite and quartz. As in outcrop RC-95, pods wrapped by the mylonitic foliation preserve small relicts of the typical Pocrane orthogneiss. The analysed zircon grains are similar in size, habitus and texture in relation to most zircons from the typical Pocrane orthogneisses (Fig. 5B). The oscillatory zoning of the grains suggests that they are of magmatic origin. Small rims of metamorphic overgrowth are not wide enough for spot analysis in the SHRIMP. Five among 24 analysed grains show a Concordia age of 2092 ± 15 Ma (MSWD = 1.4), related to the crystallisation of the magmatic protolith (Fig. 6B). The spot spreading along the Concordia, from the Rhyacian to Cambrian, can be explained by Pb loss caused by high-grade metamorphism followed by low temperature processes of mylonitisation and mineral leaching.

RC-15: This sample is a migmatitic biotite-rich orthogneiss of tonalitic composition. The zircon grains look very similar and have a prismatic shape in proportion 2:1, with weak oscillatory zoning and

almost no evidence of metamorphic rims (Fig. 5B). U-Pb (LA-ICP-MS) analyses were performed on 32 grains, yielding a Concordia age of 2131 ± 5 Ma (MSWD = 0.20; Fig. 6B), interpreted as the crystallisation age of the igneous protolith.

RC-17: This sample is also a fine-grained tonalitic orthogneiss rich in plagioclase and biotite. The zircon features indicate igneous origin represented by striking oscillatory zoning (Fig. 5B). The zircons are elongated and show very thin rims of metamorphic overgrowth. Fourteen zircon grains were analysed by LA-ICP-MS. Data from ten spots resulted in a Concordia age of 2068 ± 9 Ma (MSWD = 0.23), representing the crystallisation age of the magmatic protolith (Fig. 6B).

4.3 Quirino complex

RC-43: This sample is a fine-grained orthogneiss of tonalitic composition with a weak greenish tint (Fig. 3G). The CL images show grains of prismatic habitus and oscillatory zoning (Fig. 5C). U-Pb (LA-ICP-MS) analyses were performed on 39 zircon grains. Data from 18 spots yielded a Concordia age of 2167 ± 7 Ma (MSWD = 0.042; probability = 0.84), being interpreted as the crystallisation age of the protolith (Fig. 6C). This sample, collected from an exposure that has been assigned to other units, represents a new finding of a rock that can be correlated with the Quirino complex (see forthcoming sections).

4.4 U-Pb ages from neoformed metamorphic zircons

Besides the described magmatic zircon grains, a small number of neoformed metamorphic zircons was detected throughout the studied samples. Only small amounts of neoformed metamorphic zircons were identified for samples IV-48, LC-07, RC-17 and RC-43. Low Th/U ratios (< 0.2) and typical grain appearance of small pseudo-rounded zircons with soccer ball morphology are the main characteristics to classify those few grains as neoformed metamorphic crystals. Their individual U-Pb ages range from c. 630 Ma to c. 565, covering a broad timing related to the Brasiliano orogeny (cf. Degler et al., 2017).

4.5 Lu-Hf in zircon and whole-rock Sm-Nd data

The Lu-Hf in zircon isotopic analysis was applied as a robust tool to characterise the origins of the studied rocks from the Juiz de Fora, Pocrane and Quirino complexes. Besides reinforcing some previous interpretations, the Lu-Hf in zircon data coupled with the U-Pb spot ages and whole-rock Sm-Nd data allow us to present a new approach for the basement of the Araçuaí-Ribeira orogenic system. The Lu-Hf (LA-ICP-MS) analyses were performed on 193 zircon domains of best concordance in U-Pb ages (Figs. 5, 7 and 8, Table 1 and Supplementary Data File 1). The analysed grains represent seven samples: two correlated to the Juiz de Fora complex (M-03 and RC-101), four from the Pocrane complex (RC-15, RC-17, RC-93 and RC-94), and one (RC-43) ascribed to the Quirino complex (Fig. 2, Table 1). Our detailed illustration of the Lu-Hf data shows the εHf values in relation to the corresponding U-Pb spot ages (Fig. 7A, enlarged in Fig. 7B). The distribution of the magmatic crystallisation age ranges of each sample can be associated with εHf clusters (Fig. 7C and 7D), and the spectra of Hf model ages (T_{DM}) (Fig. 7A and E). Altogether, the εHf$_{(t)}$ data (193 values) reveal a major juvenile to moderately juvenile signature for the studied basement complexes. 125 positive εHf$_{(t)}$ (65%) values face 68 negative (35%) values (Fig. 7A and B; Table 1). The Hf diagram points out the shared evolutionary trend of the Pocrane and Juiz de Fora complexes samples, as well as the distinct position of the data cluster from the Quirino sample (Fig. 7A and B). Overall, the studied samples record a wide range of U-Pb spot ages (c. 2.22 to c. 1.86 Ga; Fig. 7C and D) corresponding to an even wider interval of Hf model ages (c. 2.74 Ga to c. 1.93 Ga; Fig. 7E). Most of the Hf model ages also suggest a major juvenile to moderately juvenile nature for the main studied basement complexes, being concentrated in the range of c. 2.4–2.1 Ga (Fig. 7E).
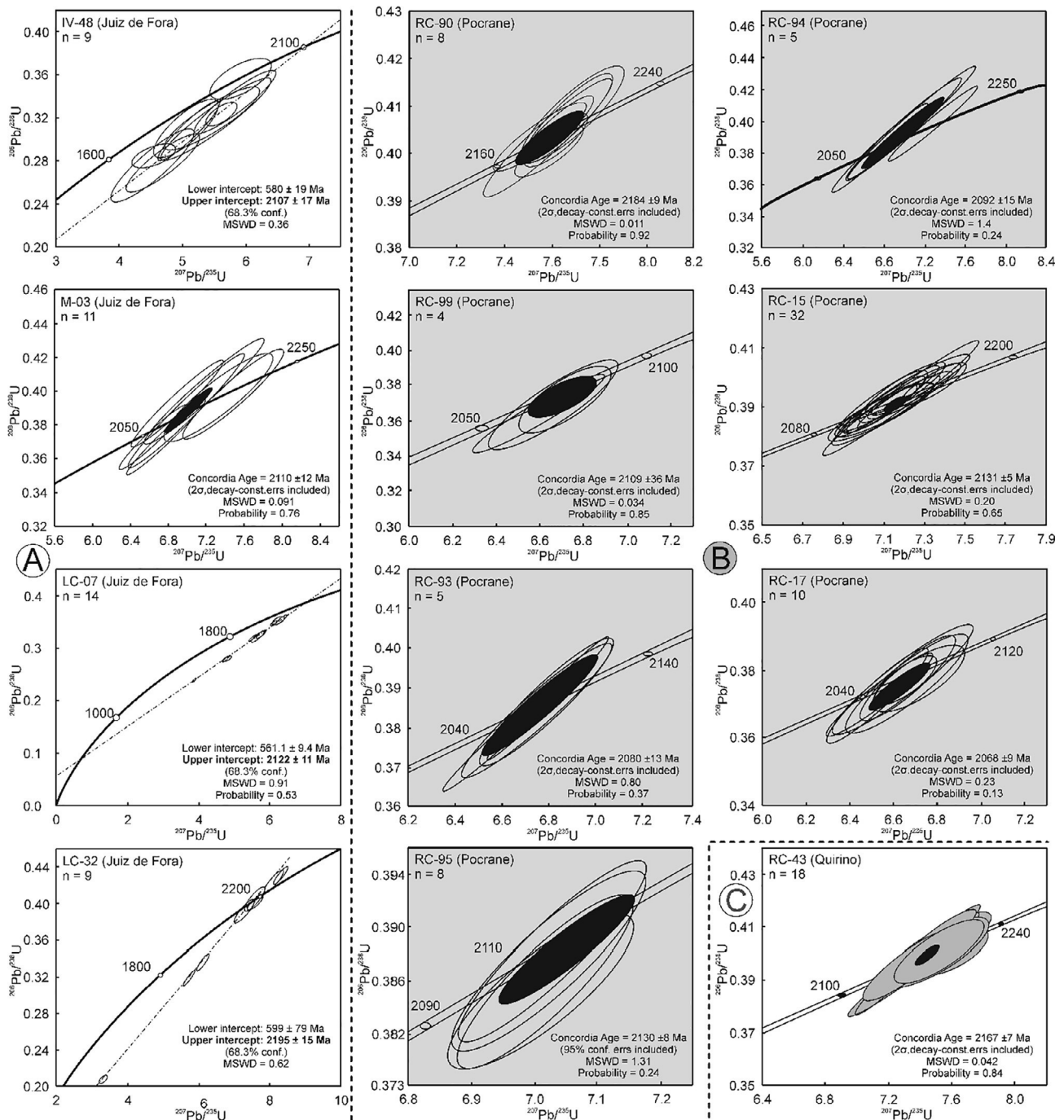
Fig. 6. Diagrams of calculated Concordia ages for the Juiz de Fora, Pocrane and Quirino complexes.

The determined $\varepsilon Hf_{(t)}$ values allow us to distinguish two clearly distinct sets of samples (Figs. 2 and 8, Table 1). The first group (I) is characterised by far mostly positive $\varepsilon Hf_{(t)}$, with 122 positive spots (> 90%) against only 13 negative values. It includes the samples RC-93 ($\varepsilon Hf_{(t)} = +4.4$ to $+0.6$), RC-94 ($\varepsilon Hf_{(t)} = +6.4$ to -3.0; with the ratio positive/negative values, p/n = 11/2), RC-17 ($\varepsilon Hf_{(t)} = +11.2$ to -3.5; p/n = 42/7), RC-15 ($\varepsilon Hf_{(t)} = +6.4$ to -3.0; p/n = 51/2), and RC-101 ($\varepsilon Hf_{(t)} = +8.2$ to -2.5; p/n = 10/2). Except the sample RC-101, which is a typical greenish enderbitic orthogneiss of the Juiz de Fora complex, all other samples of the group (I) (RC-15, RC-17, RC-93, RC-94) represent rocks assigned to the Pocrane complex. The group (I) shows a clear tendency from juvenile to moderately juvenile signatures with spot ages decreasing for each sample (Fig. 7B). The largely predominant positive $\varepsilon Hf_{(t)}$ values and Hf model ages relatively close to the

U-Pb magmatic crystallisation ages demonstrate the juvenile to moderately juvenile signatures for both, the Juiz de Fora and Pocrane complexes. This interpretation is in good agreement with our isotopic Sm-Nd data for the Juiz de Fora (LC-07, $\varepsilon Nd_{(t)} = +4.5$; M-03, $\varepsilon Nd_{(t)} = +2.2$) and Pocrane (RC-90, $\varepsilon Nd_{(t)} = +0.43$) samples, as well as with the data available in the literature for the Juiz de Fora complex ($\varepsilon Nd_{(t)}$: +7.7 to -3.5, Nd T_{DM} model ages: 2.4–2.2 Ga; Fischel et al.,1998; Heilbron et al., 1998, 2010; Noce et al., 2007; André et al., 2009). The very small number (< 10%) of negative $\varepsilon Hf_{(t)}$ values given by the group (I) samples can be related to metamorphic and partial melting processes.

The second group (II), characterised by far most negative (55 or 95%) $\varepsilon Hf_{(t)}$ values, includes only the samples RC-43 ($\varepsilon Hf_{(t)} = +3.8$ to -7.3; p/n = 1/36), assigned to the Quirino complex, and M-03
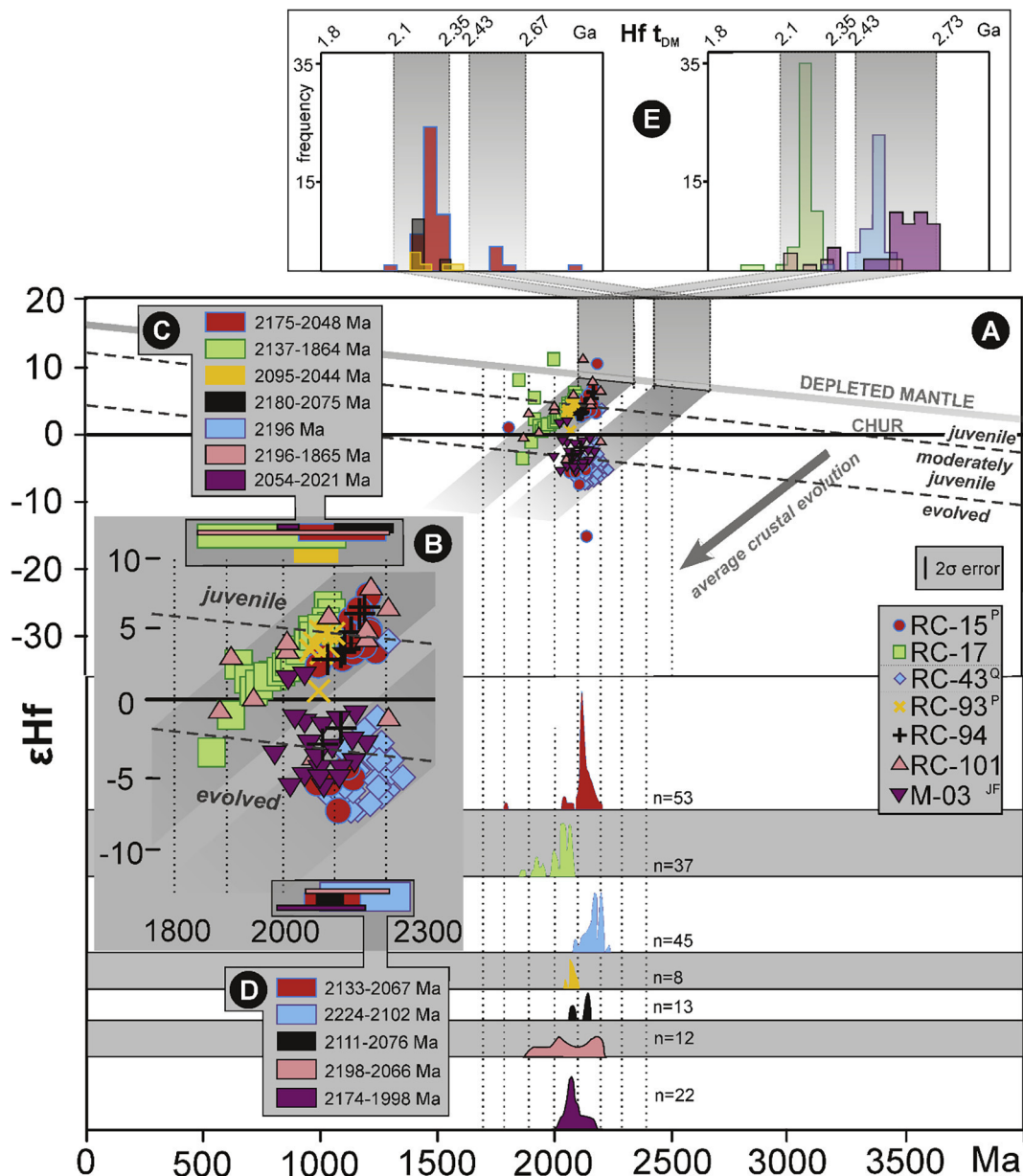
Fig. 7. Hf isotope data for magmatic zircons from samples of the Juiz de Fora (RC-101), Pocrane (RC-15, RC-17, RC-93 and RC-94) and Quirino (RC-43) complexes. A and B, distribution of εHf values in relation to the corresponding U-Pb spot ages. C and D, distribution of the magmatic crystallization age ranges with regard to each sample and εHf clusters. E, Hf model ages (T$_{DM}$) for the studied samples in relation to their εHf plots. Reference lines: CHUR (chondritic uniform reservoir; Bouvier et al., 2008); grey dashed lines classify fields of juvenile (0–5 ε-units below DM), moderately juvenile (5–12 ε-units below DM) and evolved (> 12 ε-units below DM), according to Bahlburg et al., 2011.

(εHf$_{(t)}$ = +2.3 to −5.1; p/n = 2/19), correlated with the Juiz de Fora complex (Fig. 2). However, these samples show quite distinct signatures, with small overlaps between the clusters of their εHf$_{(t)}$ values (Fig. 7). The sample RC-43 displays a clear crustal origin, with 33 (89%) εHf$_{(t)}$ negative values supporting an evolved signature against only four εHf$_{(t)}$ values plotting in the moderately juvenile field. Tending to a Hf evolved signature with εHf$_{(t)}$ values from +2.3 to −5.1, the sample M-03 shows Nd parameters (εNd$_{(2.1Ga)}$ = +2.2; Nd T$_{DM}$ model age = 2.18) and no inherited zircon grain. Indeed, the Mantiqueira complex, another candidate to include outcrop M-03, always show inherited zircon grains. Moreover, sample M-03 comes from an outcrop of the basement that hosts the Rio Doce magmatic arc (Tedeschi et al., 2016), therefore located in the upper plate of the Araçuaí orogen. All these data allows us to correlate sample M-03 with the Juiz de Fora complex (Fig. 2).

5. Discussion

Based on the new dataset and a thorough compilation of data from the literature, we addressed the following discussions: (i) the nature (juvenile versus crustal) of the studied rocks and their correlations in the focused region (Fig. 2); (ii) correlation attempts involving basement units in the focused region of the Araçuaí-Ribeira orogenic system and São Francisco craton, and their counterparts in the West Congo belt and Congo craton (Fig. 8).

5.1. The studied complexes

Traced back in the literature, the Juiz de Fora complex is the classical Rhyacian granulitic (Opx-bearing) unit from the basement of the Araçuaí-Ribeira orogenic system basement (Heilbron et al., 1998, 2010;

Duarte et al., 2000; Noce et al., 2007). With no isotopic study of its typical rocks until now, the Pocrane complex was formerly considered Archaean in age (Tuller, 2001; Pinto et al. 2001). In fact, the main difference between the Juiz de Fora and Pocrane complexes is the metamorphic grade. The Pocrane rocks were metamorphosed in the high amphibolite facies but did not reach the Opx-bearing granulite facies. However, both complexes mostly include tonalitic to granodioritic orthogneisses, with dioritic to gabbroic enclaves and, as we demonstrate here, their magmatic protoliths cover similar age ranges (Figs. 6 and 7; Table 1). The U-Pb ages for the magmatic protoliths of the Juiz de Fora complex range from 2195 ± 15 Ma to 2107 ± 17 Ma, and for the Pocrane complex between 2184 ± 9 Ma and 2069 ± 9 Ma (Fig. 6; Table 1). A comparative study on lithochemical data showed striking conformities between the Juiz de Fora and Pocrane complexes, both of them representing segments of a magmatic arc (synthesis and new data in Novo, 2013). Furthermore, a comparative distribution of lithogeochemical data shows striking conformities in relation to several Pocrane, Juiz de Fora and Quirino samples (Supplementary Data File 1). Although all of them represent rocks from Rhyacian-Orosirian magmatic arcs, the Lu-Hf in zircon and whole-rock Sm-Nd data support a solid correlation between thePocrane and Juiz de For a complexes, representing only one juvenile to moderately juvenile magmatic arc, the Juiz de Fora-Pocrane arc (Figs. 2 and 8). This is in good agreement with prior models portraying the Juiz de Fora complex as an intra-oceanic island arc (Noce et al., 2007; Heilbron et al., 2010), but now with the complement of the Pocrane complex in the same arc system. In the field, the Juiz de Fora and Pocrane complexes seem to represent distinct crustal levels of the same geologic unit. Thereby, the Pocrane migmatitic orthogneisses are the shallower equivalents of the Juiz de Fora granulitic orthogneisses. This can be explained by the general tendency of the crustal levels get shallower from south to north in the Araçuaí orogen (Pedrosa-Soares et al., 2001, 2008).

Lacking clear field relations and despite its greenish colour (generally related to the Juiz de Fora complex rocks), the orthogneiss sample (RC-43, Fig. 3G) is here correlated to the Quirino complex. This is due to the Concordia U-Pb age of its magmatic protolith (2167 ± 9 Ma) and the prominent evolved Hf signature (Fig. 7). Our data arein good agreement with published U-Pb and Sm-Nd data for the Quirino complex, as a continental magmatic arc (Valladares et al., 2002).

5.2. Correlations across the Araçuaí-Ribeira orogenic system and the São Francisco craton, and their African counterparts

All reliable U-Pb ages, and Nd and Hf isotopic data available for units of the Rhyacian-Orosirian orogenic systems (ROOS) represented in Fig. 8 are quoted in Table 2. This compilation comprises the Araçuaí-Ribeira orogenic system (AROS), the eastern São Francisco craton, the West Congo belt, and the western Congo craton including the Angola shield (Fig. 8). For the correlation of the ROOS segments it is important to bear in mind that: (i) The remarkable tectonic influence of the Late Ediacaran-Cambrian Brasiliano-Pan-African collisional event imprinted the main structural trends on ROOS segments located within the AROS and the West Congo belt. (ii) Because of the lack of data, all correlations also involved collisional and post-collisional units, not only pre-collisional magmatic arcs.

The outstanding Hf and Nd primitive signatures (Figs. 2 and 7), and lack of inherited zircons, are the most striking features of the Juiz de Fora and Pocrane complexes, which represent segments of the same juvenile to moderately juvenile orogenic system, the JU-ROOS, located in the central zone of the focused region (Fig. 8). A probable correlative of the JU-ROOS is the Buerarema complex, linking the Juiz de Fora-Pocrane arc and the central segment of the Eastern Bahia belt (Fig. 8). Although it lacks isotopic Hf in zircon data, the Buerarema complex is a candidate to be a slight evolved to moderately juvenile arc segment, as it shows no zircon inheritance, slightly negative $\varepsilon Nd_{(2Ga)}$ values (−1.7

to −3.1), and magmatic and metamorphic ages within a relative narrow range (2191–2069 Ma) with maximum Nd T_{DM} ages around 2.5 Ga (Silva et al., 2002a, Silva, 2006; Peucat et al., 2011). Additionally, it follows the structural N-S trend of the JU-ROOS, although Neoproterozoic rocks overlap the northern continuation of the Juiz de Fora-Pocrane arc (Fig. 8). The Mineiro belt also includes some juvenile Rhyacian plutons, but it occurs far to the west of JU-ROOS, adjacent to the western border of the Mantiqueira complex, and is not in the same structural trend of the Juiz de Fora-Pocrane arc (Fig. 8).

The JU-ROOS, including the mostly juvenile Juiz de Fora-Pocrane arc and, probably, the Buerarema arc, fundamentally differs from virtually all other ROOS units. These include the Mantiqueira complex, the western and coastal segments of the Eastern Bahia belt, and from plutons of the Mineiro belt, Gavião and Porteirinha blocks, and the basement of the Cabo Frio tectonic domain (Figs. 2 and 8; references in Table 2). All these units were formed on older continental crust, similarly to modern arcs developed on active continental margins, because they show striking Archaean and Siderian inheritances attested by inherited zircon grains, and isotopic Nd and Hf parameters (Figs. 2, 7 and 8; Table 2). To the west of JU-ROOS, Rhyacian-Orosirian segments of continental margin orogens, comprising evolved magmatic arcs, collisional and post-collisional plutons, are grouped into the W-ROOS (Fig. 8; references in Table 2). It includes the Mantiqueira complex, parts of the Mineiro belt, plutons found in the Porteirinha and southern Gavião blocks, and the western segment of the Eastern Bahia belt. Evolved igneous rocks with significant crustal inheritance, including segments of continental margin magmatic arcs, collisional belts and associated plutons, and post-collisional intrusions characterise the W-ROOS (ages, isotopic data and references in Table 2).

Along its southeastern margin, the JU-ROOS is flanked by the Quirino complex, another relic of a Rhyacian magmatic arc with striking crustal inheritance (Valladares et al., 2002; Viana, 2008; Machado et al., 2010). Farther southeast (Fig. 8), the Região dos Lagos complex makes up the Early Orosirian basement of the Cabo Frio tectonic domain, composed of evolved orthogneisses and granitoids with early Archaean to Siderian Nd fingerprints (Schmitt et al., 2004, 2016). From this southernmost region northwards, bordering the JU-ROOS eastern flank, no basement rocks occur up to the coastal segment of the Eastern Bahia belt, represented by Archaean rocks reworked by a Late Rhyacian orogeny (Silva et al., 1997, 2002b; Peucat et al., 2011; Barbosa and Barbosa, 2017). The Quirino and Região dos Lagos complexes and the coastal Eastern Bahia belt are grouped within the E-ROOS (Fig. 8; Table 1 and 2).

Defined the major ROOS sectors in the Brazilian counterpart, it is now important to appraise correlations with their equivalents located at SW Africa. A promising option is, indeed, through the E-ROOS segment in the Bahia-Gabon cratonic bridge. Actually, this long-lived continental bridge has provided reliable correlations between the São Francisco and Congo palaeocontinental regions (Fig. 1), since the pioneer studies of the 1960's (Hurley et al., 1967; Porada 1989; Ledru et al., 1994; Trompette, 1994; Pedrosa-Soares et al., 2008; D'Agrella-Filho and Cordani, 2017). Accordingly, the coastal Eastern Bahia belt has been correlated with the Eburnean belt of the Congo craton at western Gabon (Caen-Vachette et al., 1988; Ledru et al., 1994, Feybesse and Milési, 1998; Feybesse et al., 1998; Barbosa and Sabaté, 2004; Lerouge et al., 2006; Thiéblemond et al., 2009; Barbosa and Barbosa, 2017). The Eburnean belt extends southwards to the Kimezian gneissic complexes and granitic to syenitic intrusions of the northern (Maurin et al., 1990, 1991; Djama et al., 1992) and southern (Delhal and Ledent, 1978) West Congo belt (Fig. 1). Zircon ages obtained from the Kimezian tonalitic-granodioritic orthogneisses and felsic intrusions range between c. 2140 Ma-1900 Ma, with εNd(t) of −4.8 to −6.2, and Nd T_{DM} ages of 3.0–2.6 Ga (Fig. 8, Table 2), recording evolved magmatic arc processes on a continental margin (Cahen et al., 1979; Maurin et al., 1990, 1991; Djama et al., 1992). For the Boma region (Lower Congo River), the U-Pb (SHRIMP) and Lu-Hf (LA-ICP-MS) in zircon data for a
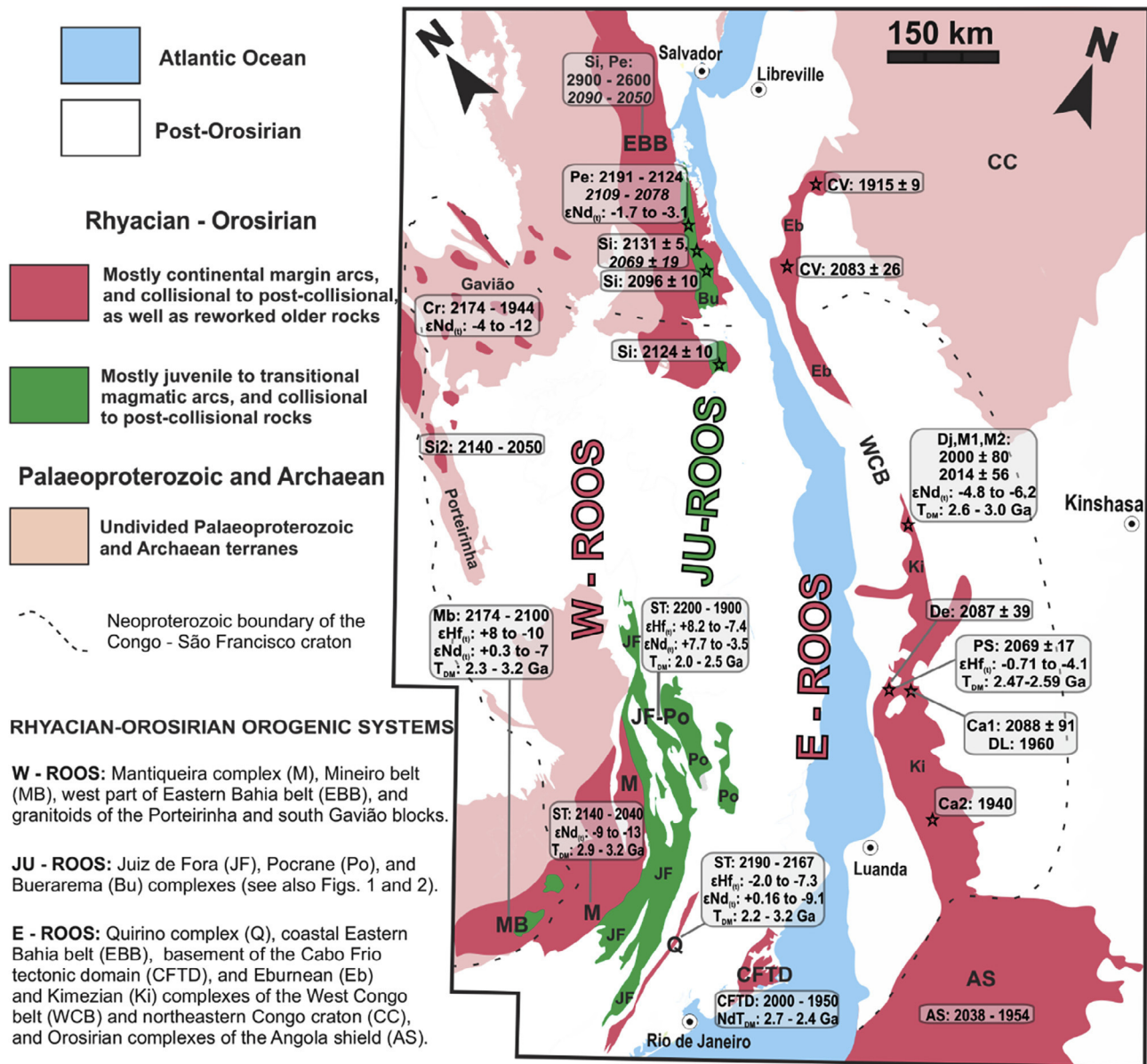
Fig. 8. Rhyacian-Orosirian orogenic systems (ROOS: W – western, JU – mostly juvenile, and E – eastern), including basement units located in Brazil and Africa (geology compiled and modified from BRGM, 2016, and CPRM, 2004). Geochronological and isotopic data, and references summarised in Tables 1 and 2.

granodioritic orthogneiss of the Kimezian basement indicate a less evolved signature ($\varepsilon Hf_{(t)}$: -0.71 to -4.1; Hf T_{DM}: 2.59–2.47 Ga) for an igneous protolith crystallised at 2069 $\pm$ 17 Ma (Pedrosa-Soares et al., 2016). Farther south, the basement of the western Angola shield records Early Orosirian igneous episodes (c. 2038 Ma – 1954 Ma; Table 2, Fig. 8), suggesting the evolution of a magmatic arc built on an active continental margin (Delor et al., 2006; Jelsma et al., 2011; McCourt et al., 2013). Accordingly, from the Bahia-Gabon cratonic bridge to the Angola shield there are a series of Rhyacian-Orosirian orogenic units that can be correlated to the E-ROOS (Figs. 1 and 8). Therefore, the E-ROOS includes both the coastal Eastern Bahia belt and its counterpart now located at Gabon, the Eburnean belt of the western Congo craton, extending southwards, along the West Congo belt, to the Kimezian and western Angola magmatic arcs. In turn, the western Angola basement correlates with the Região dos Lagos complex (Cabo Frio tectonic domain; Fig. 8), a palaeotectonic connection already established in the literature (Schmitt et al., 2004, 2016). Lastly, the Quirino complex

seems to fit well with the Kimezian complexes found in the West Congo belt (Figs. 1 and 8; data and references in Tables 1 and 2).

6. Conclusion

Besides the first Lu-Hf in zircon analysis from basement complexes of the Araçuaí-Ribeira orogenic system, we also present numerous spot U-Pb zircon ages, and some isotopic Sm-Nd data for the Juiz de Fora, Pocrane and Quirino complexes. Regarding the established field geology of the focused Brazilian region and the robust analytical dataset gained, linked to literature, we suggest new correlations within the Rhyacian-Orosirian orogenic systems found in the AROS basement and adjacent São Francisco craton. Furthermore, an attempt is made to correlate counterparts located in Eastern Brazil and SW Africa (Figs. 1 and 8).

The first conclusion is the solid demonstration of the remarkable juvenile nature of the Pocrane complex. It represents a correlative to

Table 2
Data compilation from Rhyacian-Orosirian basement belts, complexes and intrusions, located in the Araçuaí-Ribeira orogenic system, the West Congo belt, the São Francisco and Congo cratons, and the Angola shield (see data summaries and locations in Fig. 8). U-Pb ages in Ma, Nd and Hf t_{DM} model ages in Ga.

Unit name and reference abbreviation	Main lithotypes	Isotopic data and age (Ma), and data sources
W-ROOS (Fig. 8)		
Mineiro belt		$\varepsilon_{Nd(t)}$ +0.3 to −7 $\varepsilon_{Hf(t)}$ +8 to −10 T_{DM} 3.2–2.3 Ga
MB	diorite, granodiorite	2180–2100 Ma Teixeira et al., 2000, 2015, 2017a,b; Ávila et al., 2010, 2014; Barbosa et al., 2015, 2018; Aguillar et al., 2017; Alkmim and Teixeira, 2017; Moreira et al., 2018.
Mantiqueira complex		$\varepsilon_{Nd(t)}$ −9 to −13.0 Nd T_{DM} 3.2–2.9 Ga
ST	granodioritic orthogneiss	2068–2041 Ma Noce et al., 2007
ST	tonalitic orthogneiss	2102–2050 Ma Silva et al., 2002a
ST	granodioritic orthogneiss	2040 ± 8 Ma Heilbron et al. 2010
Porteirinha complex		
Si	granitoids	2050 ± 10 Ma, 2140 ± 14 Ma Silva et al., 2016
Gaviao complex		$\varepsilon_{Nd(t)}$ −4 to −12
Cr	granitoids	2140–2038 Ma Cruz et al., 2016
West and Coastal Eastern Bahia belt		$\varepsilon_{Nd(2.1\ Ga)}$ = −8 to −11 T_{DM} 3.3–2.7 Ga
Pe, Si	orthogranulite	2090–2050 Ma Silva et al., 2002a; Silva, 2006; Peucat et al., 2011
JU-ROOS (Fig. 8)		
Juiz de Foracomplex		$\varepsilon_{Nd(t)}$ +7.7 to −3.5 $\varepsilon_{Hf(t)}$ +8.2 to −5.1 (80% positive ε_{Hf} values) T_{DM} 3.2–2.1 Ga
ST	tonaliticgneiss	2195–2107 Ma **This study**
ST	enderbitic gneiss	2084 ± 13 Ma, 2119 ± 10 Ma Noce et al., 2007
ST	tonalitic gneiss	2116–2099 Ma Gonçalves et al., 2014
ST	charnockitic gneiss	2195 ± 15 Ma Silva et al., 2002a
ST	enderbitic gneiss	2127 ± 33 Ma; 2154 ± 11 Ma Heilbron et al., 2010
ST	charnockitic gneiss	2134 ± 5 Ma Machado et al., 1996
Pocrane complex		$\varepsilon_{Hf(t)}$ +6.9 to −7.4 (91% positive ε_{Hf} values) T_{DM} 2.8–2.0 Ga
ST	tonalitic gneiss	2184–2068 Ma **This study**
Buerarema complex Central Eastern Bahia belt		$\varepsilon_{Nd(t)}$ −1.7 to −3.1 Nd T_{DM} c. 2.5 Ga
Pe	meta-tonalite, enderbite	2191–2124 Ma Peucat et al., 2011
Si	meta-tonalite and enderbite	2131–2096 Ma Silva et al., 2002a; Silva, 2006
E-ROOS (Fig. 8)		
Quirino complex		$\varepsilon_{Nd(t)}$ +0.16 to −9.1 $\varepsilon_{Hf(t)}$ +3.8 to −7.3 (87% negative ε_{Hf} values) Nd T_{DM} 3.2–2.2 Ga
ST	tonalitic gneiss	2167 ± 7 Ma **This study**

Table 2 (*continued*)

Unit name and reference abbreviation	Main lithotypes	Isotopic data and age (Ma), and data sources
ST	tonalitic gneiss and mafic enclaves	2169 ± 3 Ma, 2185 ± 8 Ma Valladares et al., 2002;Machado et al., 2010
Região dos Lagos complex Cabo Frio Tectonicdomain		Nd T_{DM} 2.7–2.4 Ga
CFTD	orthogneiss	2000–1940 Ma Schmitt et al., 2004, 2016
E-ROOS in SW Africa (Fig. 8)		
Eburnean and Kimezian		$\varepsilon_{Hf(t)}$ −0.71 to −4.1 Hf T_{DM} 2.59–2.47 Ga $\varepsilon_{Nd(t)}$ −4.8 to −6.2 Nd T_{DM} 3.0–2.6 Ga
PS (Boma, D.R. Congo)	granodioritic orthogneiss	2069 ± 17 Ma $\varepsilon_{Hf(t)}$ −0.71 to −4.1 Hf T_{DM} 2.59–2.47 Ga Pedrosa-Soares et al., 2016
Ca1 (Mpozo, D.R. Congo)	gneiss	2088 ± 91 Ma Cahen et al., 1984
De (Boma, D.R. Congo)	migmatite	2087 ± 39 Ma Delhal, 1976
Dj (Guéna, Congo)	tonalitic orthogneiss	2014 ± 56 Ma $\varepsilon_{Nd(t)}$ −4.8 to −6.2 Nd T_{DM}: 3.0–2.6 Ga Djama et al., 1992
M1 (Les Saras, Congo)	granodiorite	2000 ± 80 Ma Maurin et al., 1990
M2 (Guéna, Congo)	tonalitic orthogneiss	2014 ± 56 Ma Maurin et al., 1991
CV (Fougamou, Gabon)	porphyritic diorite	1915 ± 9 Ma Caen-Vachette et al., 1988
CV (Gomboumassif, Gabon)	granodioritic orthogneiss	2083 ± 26 Ma Caen-Vachette et al., 1988
Ca2 (Vista Alegre, Angola)	granodiorite	c. 1940 Ma Cahen et al., 1979
DL (Mpozo, D.R. Congo)	syenite	c. 1960 Ma Delhal and Ledent, 1978
Angola shield		
AS (Chela group, Angola)	granitoids	2038 ± 28 Ma 1954 ± 6 Ma McCourt et al., 2013
AS (Huambo, Angola)	granitoids	1980 ± 9 Ma 1987 ± 16 Ma Delor et al., 2008
AS (Andulo, Angola)	granodiorite	1967 ± 5 Ma 1966 ± 3 Ma Jelsma et al., 2011

the Juiz de Fora complex, whose primitive signature has been a long time quoted in the literature and is now confirmed with the first Lu-Hf in zircon data given by Juiz de Fora granulites. We suggest that both complexes form only one magmatic arc system exposed in distinct crustal levels: the Juiz de Fora complex exposing arc roots, and the Pocrane complex representing medium to uppermost (volcanic) arc sections. We also found the northernmost segment of the Juiz de Fora-Pocrane magmatic arc in a region formerly assigned to other stratigraphic units (Figs. 2 and 8).

A second contribution is the first characterisation by Lu-Hf in zircon data of an orthogneiss correlated to the Quirino complex. The data corroborate its already known evolved signature of a magmatic arc developed on a continental margin (Figs. 2 and 8).

The geotectonic evolution of the entire focused region is characterised by at least three main Rhyacian-Orosirian orogenic systems (ROOS), separated in space, but widely overlapping in time: the W-ROOS, JU-ROOS, and E-ROOS (Fig. 8). One of them, probably the first in scene, formed a juvenile to moderately juvenile magmatic arc system, represented by the Juiz de Fora, Pocrane and Buerarema complexes: the JU-ROOS (Fig. 8). Its palaeotectonic scenario would be

similar to modern intra-oceanic island arc systems, like those envisaged by Noce et al. (2007), Heilbron et al. (2010), and Aguillar et al. (2017). To the west and the east, the JU-ROOS is flanked on both sides by systems of orogens with striking crustal signatures, the W-ROOS and the E-ROOS. Both of these orogenic systems comprise magmatic arcs developed on segments of older continental crust and show striking Archaean inheritances. Applying the modern Plate Tectonics concepts, the W-ROOS assembled a major part of the São Francisco block, whereas the E-ROOS developed in the eastern margin of the Congo block. In contrast, the JU-ROOS evolved as an intra-oceanic arc system within a large ocean separating the W-ROOS and E-ROOS continental blocks (Fig. 8). Therefore, those orogenic systems were separated in space, but not necessarily in time, as the available data suggest they evolved diachronically within a wide time range from the Rhyacian to the Orosirian. Indeed, our data describe a long-lasting period (c. 2.20 Ga to c. 1.86 Ga, Fig. 7C and 7D) for the whole evolution of the Rhyacian-Orosirian orogenic systems that amalgamated the Congo and São Francisco palaeocontinental blocks. Thereby, the oldest U-Pb ages of magmatic zircons record the earliest magmatic activities. The youngest ages (< 1.86 Ma), interpreted as post-collisional manifestations, represent magmatic zircons of late intrusions, zircon metamorphic domains and partially re-setting grains. It seems that the climax of magmatic development took place in between c. 2150 Ma and c. 2050 Ma (Fig. 7C, 7D and 8; Tables 1 and 2).

Finally, we suggest possible correlations between major segments of the Rhyacian-Orosirian orogenic systems, providing further links between Brazil and Africa in Palaeoproterozoic time (Figs. 1 and 8).

Acknowledgements

References

Aguillar, C., Alkmim, F.F., Lana, C., Farina, F., 2017. Palaeoproterozoic assembly of the São Francisco craton, SE Brazil: new insights from U-Pb titanite and monazite dating. Precambr. Res. 289, 95–115.

Alkmim, F.F., Teixeira, W., 2017. The Paleoproterozoic Mineiro Belt and the Quadrilátero Ferrífero. In: Heilbron, M., Cordani, U., Alkmim, F. (Eds.), São Francisco Craton, Eastern Brazil. Regional Geology Reviews. Springer, Cham.

Alkmim, F.F., Marshak, S., Pedrosa-Soares, A.C., Peres, G.G., Cruz, S.C.P., Whittington, A., 2006. Kinematic evolution of the Araçuaí-West Congo orogen in Brazil and Africa: Nutcracker tectonics during the Neoproterozoic assembly of Gondwana. Precambr. Res. 149, 43–63.

Andersen, T., Andersson, U.B., Graham, S., Åberg, G., Simonsen, S.L., 2009. Granitic magmatism by melting of juvenile continental crust: new constraints on the source of Palaeoproterozoic granitoids in Fennoscandia from Hf isotopes in zircon. J. Geol. Soc. 166, 233–247.

André, J.L.F., Valladares, C.S., Duarte, B.P., 2009. O Complexo Juiz de Fora na região de Três Rios (RJ): litogeoquímica, geocronologia U-Pb (LA-ICPMS) e geoquímica isotópica de Nd e Sr. Revista Brasileira de Geociências 39, 773–793.

Avila, C.A., Teixeira, W., Cordani, U.G., Moura, C.A.V., Pereira, R.M., 2010. Rhyacian (2.23–2.20 Ga) juvenile accretion in the southern São Francisco craton, Brazil: Geochemical and isotopic evidence from the Serrinha magmatic suite, Mineiro belt. J. S. Am. Earth Sci. 29, 464–482.

Ávila, C.A., Teixeira, W., Bongiolo, E.M., Dussin, I.A., 2014. The Tiradentes suite andits role in the Rhyacian evolution of the Mineiro belt, São Francisco Craton: geo-chemical and U-Pb geochronological evidences. Precambr. Res. 243, 221–251.

Bahlburg, H., Vervoort, J.D., DuFrane, S.A., Carlotto, V., Reimann, C., Cárdenas, J., 2011. The U-Pb and Hf isotope evidence of detrital zircons of the Ordovician Ollantaytambo Formation, southern Peru, and the Ordovician provenance and paleogeography of

southern Peru and northern Bolivia. J. S. Am. Earth Sci. 32, 196–209.

Barbosa, J.S.F., Sabaté, P., 2004. Archean and Paleoproterozoic crust of the São Francisco Craton, Bahia, Brazil: geodynamic features. Precambr. Res. 133, 1–27.

Barbosa, J.S.F., Barbosa, R.G., 2017. The Paleoproterozoic Eastern Bahia Orogenic Domain. In: Heilbron, M., Cordani, U., Alkmim, F. (Eds.), São Francisco Craton, Eastern Brazil. Regional Geology Reviews. Springer, Cham.

Barbosa, N.S., Teixeira, W., Ávila, C.A., Montecinos, P.M., Bongiolo, E.M., 2015. 2.17–2.10 Ga plutonic episodes in the Mineiro belt, São Francisco Craton, Brazil: U-Pb ages, geochemical constraints and tectonics. Precambr. Res. 270, 204–225.

Barbosa, N.S., Teixeira, W., Ávila, C.A., Montecinos, P.M., Bongiolo, E.M., Vasconcellos, F.F., 2018. U-Pb geochronology and coupled Hf-Nd-Sr isotopic-chemical constraints of the Cassiterita Orthogneiss (2.47–2.41 Ga) in the Mineiro belt, São Francisco craton: Geodynamic fingerprints beyond the Archaean-Paleoproterozoic Transition. Precambr. Res.

Black, L.P., Kamo, S.L., Allen, C.M., Aleinikoff, J.N., Davis, D.W., Korsch, R.J., Foudoulis, C., 2003. TEMORA 1: a new zircon standard for phanerozoic U-Pb geochronology. Chem. Geol. 200, 155–170.

Bouvier, A., Vervoort, J.D., Patchett, P.J., 2008. The Lu-Hf and Sm-Nd isotopic compo-sition of CHUR: Constraints from unequilibrated chondrites and implications for the bulk composition of terrestrial planets. Earth Planet. Sci. Lett. 273, 48–57.

Brito-Neves, B.B., Campos-Neto, M.C., Fuck, R.A., 1999. From Rodinia to Western Gondwana: An approach to the Brasiliano-Pan African cycle and orogenic collage. Episodes 22, 155–199.

BRGM, 2016. Geological Map of Africa, scale 1:10 million scale (http://www.brgm.fr).

Caen-Vachette, M., Vialette, Y., Bassot, J.P., Vidal, P., 1988. Apport de la geochronologie isotopique a la connaissance de la geologic gabonaise. Chronique Recherche Miniere 491, 35–54.

Cahen, L., Kriiner, A., Ledent, D., 1979. The age of the Vista Alegre pluton and its bearing on the reinterpretation of the Precambrian geology of Northern Angola. Annales Societé Geologique Belgique 102, 265–275.

de Carvalho, H., Tassinari, C., Alves, P.H., Guimarães, F., Simões, M.C., 2000. Geochronological review of the Precambrian in West Angola: links with Brazil. J. Afr. Earth Sc. 31, 383–402.

Cohen, K.M., Finney, S.C., Gibbard, P.L., Fan, J.-X., 2013. The ICS international chron-ostratigraphic chart. Episodes 36, 199–204 (updated 2017: http://www.strati-graphy.org/ICSchart).

Cordani, U.G., D'Agrella-Filho, M.S., Brito-Neves, B.B., Trindade, R.I.F., 2003. Tearing up Rodinia: the Neoproterozoic paleogeography of South American cratonic fragments. Terra Nova 15, 350–359.

Chemale Jr., F., Dussin, I.A., Alkmim, F.F., Martins, M.S., Queiroga, G., Armstrong, R., Santos, M.N., 2012. Unravelling a Proterozoic basin history through detrital zircon geochronology: the case of the Espinhaco Supergroup, Minas Gerais, Brazil. Gondwana Res. 22, 200–206.

Compston, W., Williams, I.S., Meyer, C., 1984. U-Pb geochronology of zircons from lunar breccia 73217 using a sensitive high-resolution ion-microprobe. J. Geophys. Res. 98, 525–534.

Compston, W., Williams, I.S., 1992. Ion probe ages for the British Ordovician and Silurianstrato types. In: Webby, B.D., Laurie, J.R. (Eds.), Global Perspectives on Ordovician Geology. Proceedings of the 6th International Symposium on the Ordovician System, Sydney, pp. 59–67.

CPRM, 2004. Geological Map of Brazil, 1:1.000.000 scale. CPRM-Geological Survey of Brazil, Brasília.

Cruz, S., Barbosa, J., Pinto, M., Peucat, J., Paquette, J., Souza, J., Martins, V., Chemale, F., Carneiro, M., 2016. The Siderian-Orosirian magmatism in the Gavião paleoplate, Brazil: U-Pb geochronology, geochemistry and tectonic implications. J. S. Am. Earth Sci. 69, 43–79.

D'Agrella-Filho, M.S., Cordani, U.G., 2017. The Paleomagnetic Record of the São Francisco-Congo Craton. In: Heilbron, M., Cordani, U.G., Alkmim, F.F. (Eds.), São Francisco Craton, Eastern Brazil. Regional Geology Reviews. Springer, Cham.

Degler, R., Pedrosa-Soares, A., Dussin, I., Queiroga, G., Schulz, B., 2017. Contrasting provenance and timing of metamorphism from paragneisses of the Araçuaí-Ribeira orogenic system, Brazil: hints for Western Gondwana assembly. Gondwana Res. 51, 30–50.

Delhal, J., Ledent, D., 1978. Donees geochronologiques dans la region de Matadi (Zaire) relatives a lasyenite de laMpozo et auxmetarhyolites. Departement Geologic et Mineralogie, Musee Royal Afrique Centrale, Rapport annuel 1977, Tervuren, Belgique, 99–110.

Delor, C., Lafon, J.M., Rossi, P., Cage, M., Pato, D., Chevrel, S., LêMetour, J., Matukov, D., Sergeev, S., 2006. Unravelling Precambrian crustal growth of Central West Angola: Neoarchean to Siderian inheritance main Orosirian accretion and discovery of the "Angolan" Panafrican Belt. In: 21st Colloquium of African Geology. Geological Mining Association of Mozambique, Abstract Book, pp. 40–41.

DePaolo, D.J., 1981. Neodymium isotopes in the Colorado front range and crust-mantle evolution in the Proterozoic. Nature 291, 193–196.

De Waele, B., Johnson, S.P., Pisarevsky, S.A., 2008. Palaeoproterozoic to Neoproterozoic growth and evolution of the eastern Congo Craton: its role in the Rodinia puzzle. Precambr. Res. 160, 127–141.

Djama, L.M., Leterrier, J., Michard, A., 1992. Pb, Sr and Nd isotope study of the basement of the Mayumbian Belt (Guéna gneisses and Mfoubu granite, Congo): implications for crustal evolution in Central Africa. J. Afr. Earth Sc. 14, 227–237.

Duarte, B.P., Heilbron, M., Campos-Neto, M.C., 2000. RBG. Granulite/charnockite from the Juiz de Fora domain, central segment of the Brasiliano Ribeira Belt. Revista Brasileira de Geociências 30, 358–362.

Evans, D.A., 2009. The palaeomagnetically viable, long-lived and all-inclusive Rodinia supercontinent reconstruction. Geol. Soc., London, Spec. Pub. 327, 371–404.

Feybesse, J.L., Milési, J.P., 1998. The Archean/Proterozoic contact zone in West Africa: a

mountain belt of decollement, thrusting and folding on a continental margin related to the 2.1 Ga convergence of Archean cratons. Precambr. Res. 69, 199–227.

Feybesse, J.L., Johan, V., Triboulet, C., Guerrot, C., Mayaga-Mikolo, F., Bouchot, V., EkoN'dong, J., 1998. The West Central African belt: a model of 2.5–2.0 Ga accretion and two-phase orogenic evolution. Precambr. Res. 87, 161–216.

Fischel, D.P., Pimentel, M.M., Fuck, R.A., Costa, A.G., Rosiere, C.A., 1998. Geology and Sm-Nd Isotopic Data for the Mantiqueira and Juiz de I Complexes (Ribeira Belt) in the Abre campo-Manhuaçú Region, Minas Gerais, Brazil. In: International Conference of Basement Tectonics, 14. Ouro Preto, Brazil, Abstracts, pp. 21–23.

Gioia, S.M.C.L., Pimentel, M.M., 2000. The Sm-Nd isotopic method in the geochronology laboratory of the University of Brasília. Anais da Academia Brasileira de Ciências 72, 219–245.

Gonçalves, L., Farina, F., Lana, C., Pedrosa-Soares, A.C., Alkmim, F., Nalini, H.A., 2014. New U-Pb ages and lithochemical attributes of the Ediacaran Rio Doce magmatic arc, Araçuaí confined orogen, Southeastern Brazil. J. South Am. Earth Sci. 52, 1–20.

Griffin, W.L., Pearson, N.J., Belousova, E., Jackson, S.E., van Achterbergh, E., O'Reilly, S.Y., Shee, S.R., 2000. The Hf isotope composition of cratonic mantle: LA-MC-ICPMS analysis of zircon megacrysts in kimberlites. Geochim. Cosmochim. Acta 64, 133–147.

Heilbron, M., Duarte, B.P., Nogueira, J.R., 1998. The Juiz de Fora complex of the Central Ribeira belt, SE Brazil: a segment of Palaeoproterozoic granulitic crust thrust during the Pan-African Orogen. Gondwana Res. 1, 373–382.

Heilbron, M., Valeriano, C.M., Tassinari, C.C.G., Almeida, J., Tupinambá, M., Siga, O., Trouw, R., 2008. Correlation of Neoproterozoic terranes between the Ribeira Belt, SE Brazil and its African counterpart: comparative tectonic evolution and open questions. Geol. Soc. Spec. Pub. 294, 211–237.

Heilbron, M., Duarte, B., Valeriano, C., Simonetti, A., Machado, N., Nogueira, J., 2010. Evolution of reworked Paleoproterozoic basement rocks within the Ribeira belt (Neoproterozoic), SE-Brazil, based on U Pb geochronology: Implications for palaeo-geographic reconstructions of the São Francisco-Congo paleocontinent. Precambr. Res. 178, 136–148.

Heilbron, H., Cordani, U., Alkmim, F., Reis, H., 2017. Tectonic Genealogy of a Miniature Continent. In: Heilbron, M., Cordani, U.G., Alkmim, F.F. (Eds.), São Francisco Craton, Eastern Brazil. Regional Geology Reviews. Springer, Cham.

Hurley, P.M., Almeida de, F.F.M., Melcher, G.C., Cordani, U.G., Rand, J.R., Kawashita, K., Vandoros, P., Pinson, W.H., Fairbairn Jr., H.W., 1967. Test of continental drift by comparison of radiometric ages. A pre-drift reconstruction shows matching geologic age provinces in West Africa and Northern Brazil. Science 157, 495–500.

Jackson, S.E., Pearson, N.J., Griffin, W.L., Belousova, E.A., 2004. The application of laser ablation-inductively coupled plasma-mass spectrometry to in situ U-Pb zircon geochronology. Chem. Geol. 211, 47–69.

Jelsma, H., Perritt, S.H., Armstrong, R.A., Ferreira, H.F., 2011. SHRIMP U–Pb zircon geochronology of basement rocks of the Angolan Shield, western Angola. In: Proceedings of the 23rd CAG. Johannesburg. Council for Geoscience, Pretoria, pp. 203.

Ledru, P., Johan, V., Milési, J.P., Tegyey, M., 1994. Makers of the last stage of the Paleoproterozoic collision: evidence for 2 Ga continent involving circum-South Atlantic provinces. Precambr. Res. 69, 169–191.

Lerouge, C.A., Cocherie, S.F., Toteu, J., PenayeMilési, J.-P., Tchameni, R., Nsifa, E.N.C., Fanning, M., Deloule, E., 2006. Shrimp U-Pb zircon age evidence for Paleoproterozoic sedimentation and 2.05 Ga syntectonic plutonism in the Nyong Group, South-Western Cameroon: consequences for the Eburnean-Transamazonian belt of NE Brazil and Central Africa. In: J. Afr. Earth Sci. 44. pp. 127–413.

Machado, N., Valladares, C., Heilbron, M., Valeriano, C., 1996. U-Pb geochronology of the central Ribeira Belt (Brazil) and implications for the evolution of the Brazilian Orogeny. Precambr. Res. 79, 347–361.

Machado, H.T., Valladares, C., Valeriano, C., Medeiros, S.R., Duarte, B.P., 2010. Orthogneisses of the Quirino Complex, Central Ribeira belt, Se Brazil: Sr and Nd isotopic data. In: VII SSAGI – South American Symposium on Isotope Geology. Brasília, Brazil, Short Papers, pp. 93–96.

Maurin, J.C., Mpemba-Bony, J., Pin, C., Vicat, J.P., 1990. La granodiorite Les Saras: untemoin de magmatisme Eburneen (2 Ga) au sein de la chaine panafricaine du Mayombe (Congo). Compte Rendu Academie Sciences Paris 310, 571–575.

Maurin, J.C., Boudzoumou, F., Djama, L.M., Gioan, P., Michard, A., Mpemba-Boni, J., Peucat, J.J., Pin, C., Vicat, J.P., 1991. La chaîne proterozoique oeust-congolienne et son avant-pays au Congo: Nouvelles donnes geochronologiques et structurales, implications en Afrique central. Compte Rendu Academie Sciences Paris 312, 1327–1334.

Meert, J.G., Santosh, M., 2017. The Columbia supercontinent revisited. Gondwana Res. 50, 67–83.

Moreira, H., Seixas, L., Storey, C., Fowler, M., Lasalle, S., Stevenson, R., Lana, C., 2018. Evolution of Siderian juvenile crust to Rhyacian high Ba-Sr magmatism in the Mineiro Belt, southern São Francisco Craton. Geosci. Front.

McCourt, S., Armstrong, R.A., Jelsma, H., Mapeo, R.B.M., 2013. New U-Pb SHRIMP ages from the Lubango region, SW Angola: insights into the Paleoproterozoic evolution of the Angolan Shield, southern Congo Craton, Africa. J. Geol. Soc. London 170, 353–363.

Noce, C.M., Pedrosa-Soares, A.C., Silva, L.C., Armstrong, R., Piuzana, D., 2007. Evolution of the polycyclic basement complexes in the Araçuaí orogen, based on U-Pb SHRIMP data: Implications for Brazil-Africa links in Paleoproterozoic time. Precambr. Res. 159, 60–78.

Novo, T.A., 2013. Caracterização do Complexo Pocrane, magmatismo básico mesoproterozóico e unidades neoproterozóicas do sistema Araçuaí-Ribeira, com ênfase em geocronologia U-Pb (SHRIMP e LA-ICP-MS). Universidade Federal de Minas Gerais, Belo Horizonte, pp. 193.

Pedrosa-Soares, A.C., Noce, C.M., Wiedemann, C.M., Pinto, C.P., 2001. The Araçuaí-West

Congo orogen in Brazil: an overview of a confined orogen formed during Gondwanland assembly. Precambr. Res. 110, 307–323.

Pedrosa-Soares, A.C., Alkmim, F.F., Tack, L., Noce, C.M., Babinski, M., Silva, L.C., Martins-Neto, M.A., 2008. Similarities and differences between the Brazilian and African counterparts of the Neoproterozoic Araçuaí-West-Congo orogen. Geol. Soc., London, Spec. Pub. 294, 153–172.

Pedrosa-Soares, A.C., Alkmim, F.F., 2011. How many rifting events preceded the development of the Araçuaí-West Congo orogen?.

Pedrosa-Soares, A.C., Dussin, I., Nseka, P., Baudet, D., Fernandez-Alonso, M., Tack, L., 2016. Tonian rifting events on the Congo-São Francisco palaeocontinent: New evidence from U-Pb and Lu-Hf data from the Shinkakasa plutonic complex (Boma region, West Congo Belt, Democratic Republic of Congo). In: 5th International Geologica Belgica Meeting. Mons, Belgium, Abstract Book, pp. 44.

Peucat, J.-J., Barbosa, J.S.F., de A. Pinho, I.C., Paquette, J.-L., Martin, H., Fanning, C.M., Menezes Leal, A.B., Cruz, S.C.P., 2011. Geochronology of granulites from the south Itabuna-Salvador-Curaçá Block, São Francisco Craton (Brazil): Nd isotopes and U-Pb zircon ages. J. S. Am. Earth Sci. 31, 397–413.

Pietranik, A.B., Hawkesworth, C.J., Storey, C.D., Kemp, A.I.S., Sircombe, K.N., Whitehouse, M.J., Bleeker, W., 2008. Episodic, mafic crust formation from 4.5 to 2.8 Ga: New evidence from detrital zircons. Slave craton, Canada Geology 36, 875–878.

Pinho, I.C.A., 2005. Geologia dos metatonalitos/metatrondhjemitos e granulitos básicos das regiões de Camamu-Ubaitaba-Itabuna, Bahia (Doctorate thesis). Instituto de Geociências, Universidade Federal da Bahia, Salvador, pp. 156.

Pinho, I.C.A., Barbosa, J.S.F., Leal, A.B.M., Martin, H., Peucat, J.J., 2011. Geochemical modelling of the tonalitic and trondhjemitic granulites from the Itabuna-Salvador-Curaçá Block, Bahia, Brazil. J. S. Am. Earth Sci. 31, 312–323.

Pinto, C.P., Drumond, J.B., Féboli, W.L., 2001. Projeto Leste, Etapas 1 e 2. CODEMIG, Belo Horizonte, pp. 192.

Porada, H., 1989. Pan-African rifting and orogenesis in southern to equatorial Africa and eastern Brazil. Precambr. Res. 44, 103–136.

Rogers, J.J., Santosh, M., 2002. Configuration of Columbia, a Mesoproterozoic super-continent. Gondwana Res. 5, 5–22.

Seixas, L.A.R., Bardintzeff, J.M., Stevenson, R., Bonin, B., 2013. Petrology of the high-Mg# tonalities and dioritic enclaves of the c. 2130 Ma Alto Maranhão suite: evidence for a major juvenile crustal addition event during the Rhyacian orogenesis, Mineiro Belt, southeast Brazil. Precambr. Res. 238, 18–41.

Schmitt, R.S., Trouw, R.A.J., Van Schmus, W.R., Pimentel, M.M., 2004. Late amalgamation in the central part of West Gondwana: new geochronological data and the characterization of a Cambrian collisional orogeny in the Ribeira Belt (SE Brazil). Precambr. Res. 133, 29–61.

Schmitt, R.S., Trouw, R.A.J., Van Schmus, W.R., Armstrong, R., Stanton, N.S.G., 2016. The tectonic significance of the Cabo Frio Tectonic Domain in the SE Brazilian margin: a Paleoproterozoic through Cretaceous saga of a reworked continental margin. Braz. J. Geol. 46, 37–66.

Silva, L.C., 2006. Geocronologia aplicada ao mapeamento regional, com ênfase na técnica U-Pb SHRIMP. Serviço Geológico do Brasil, Publicações Especiais 1, 132.

Silva, L.C., McNaughton, N.P., Melo, R.C., Fletcher, I.R., 1997. U-Pb SHRIMP ages in the Itabuna-Caraíba TTG high-grade complex: The first window beyond the Paleoproterozoic overprint of the eastern Jequié Craton, NE Brazil. In: International Symposium on Granites and Associated Mineralization (ISGAM). Salvador, Abstracts, pp. 282–283.

Silva, L.C., Armstrong, R., Noce, C.M., Carneiro, M., Pimentel, M., Pedrosa-Soares, A.C., Leite, C., Vieira, V.S., Silva, M., Paes, V., Cardoso-Filho, J., 2002a. Reavaliação da evolução geológica em terrenos pré-cambrianos brasileiros com base em novos dados U-Pb SHRIMP; parte II: Orógeno Araçuaí, Cinturão Móvel Mineiro e Cráton São Francisco Meridional. Revista Brasileira de Geociências 32, 513–528.

Silva, L.C., Armstrong, R., Delgado, I.M., Carneiro, M., Pimentel, M., Arcanjo, J.B., Melo, R.C., Teixeira, L.R., Jost, H., Cardoso-Filho, J., Pereira, L.H., 2002b. Reavaliação da evolução geológica em terrenos pré-cambrianos brasileiros com base em novos dados U-Pb SHRIMP; parte I: Limite centro-oriental do Cráton São Francisco na Bahia. Revista Brasileira de Geociências 32, 501–512.

Silva, L.C., Pedrosa-Soares, A.C., Armstrong, R., Noce, C.M., 2011. Determining the timing of the collisional period of the Araçuaí Orogen by using high-resolution U-Pb geochronology on zircon: a contribution to the history of Western Gondwana amalgamation. Geonomos 19, 180–197.

Silva, L.C., Pedrosa-Soares, A.C., Armstrong, R., Pinto, C.P., Magalhães, J.T.R., Pinheiro, M.A.P., Santos, G.G., 2016. Disclosing the Paleoarchean to Ediacaran history of the São Francisco craton basement: the Porteirinha domain (northern Araçuaí orogen. Braz. J. South Am. Earth Sci. 68, 50–67.

Smith, M.A., 1998. The Pattern of Continental Occupation: Late Pleistocene Colonization of Australia and New Guinea. In: Murray, T.A. (Ed.), Archaeology of Aboriginal Australia: a reader. Allen and Unwin, Sydney, pp. 41–49.

de Souza, J.S., Peucat, J.J., Barbosa, J.S.F., Correia-Gomes, L.C., Cruz, S.C.P., Leal, A.B.M., Paquette, J.L., 2014. Lithogeochemistry and geochronology of the subalkaline felsic plutonism that marks the end of the Paleoproterozoic orogeny in the Salvador-Esplanada belt, São Francisco craton (Salvador, state of Bahia, Brazil). Braz. J. Geol. 44, 221–234.

Söderlund, U., Patchett, J.P., Vervoort, J.D., Isachsen, C.E., 2004. The 176 Lu decay constant determined by Lu-Hf and U-Pb isotope systematics of Precambrian mafic intrusions. Earth Planet. Sci. Lett. 219, 311–324.

Tedeschi, M., 2013. Caracterização do arco magmático do Orógeno Araçuaí entre FreiInocêncio e Itambacuri, Minas Gerais (Master thesis). Universidade Federal deMinas Gerais, Belo Horizonte, Brazil, pp. 126.

Tedeschi, M., Novo, T., Pedrosa-Soares, A.C., Dussin, I., Tassinari, T., Silva, L.C., Gonçalves, L., Alkmim, F.F., Lana, C., Figueiredo, C., Dantas, E., Medeiros, S., De Campos, C., Corrales, F., Heilbron, M., 2016. The Ediacaran Rio Doce magmatic arc

revisited (Araçuaí-Ribeira orogenic system, SE Brazil). J. S. Am. Earth Sci. 68, 167–186.

Teixeira, W., Sabaté, P., Barbosa, J.S.F., Noce, C.M., Carneiro, M.A., 2000. Archean and Paleoproterozoic tectonic evolution of the São Francisco Craton. In: Cordani, U.G., Milani, E.J., Thomaz-Filho, A, Campos, D.A. (Eds.), Tectonic Evolution of South America. 31th International Geology Congress, pp. 101–138.

Teixeira, W., Ávila, C.A., Dussin, I.A., Corrêa Neto, A.V., Bongiolo, E.M., Santos, J.O.S., Barbosa, N.S., 2015. Zircon U-Pb-Hf, Nd-Sr constraints and geochemistry of the Resende Costa Orthogneiss and coeval rocks: new clues for a juvenile accretion episode (2.36–2.33 Ga) in the Mineiro belt and its role to the long-lived Minas accretionary orogeny. Precambr. Res. 256, 148–169.

Teixeira, W., Oliveira, E.P., Peng, P., Dantas, E.L., Hollanda, M.H., 2017a. U-Pb geochronology of the 2.0 Ga Itapecerica graphite-rich supracrustal succession in the São Francisco Craton: tectonic matches with the North China Craton and paleogeographic inferences. Precambr. Res. 293, 91–111.

Teixeira, W., Oliveira, E.P., Marques, L.S., 2017b. Nature and Evolution of the Archean Crust of the São Francisco Craton. In: Heilbron, M., Cordani, U.G., Alkmim, F.F. (Eds.), São Francisco Craton, Eastern Brazil. Regional Geology Reviews. Springer, Cham.

Thiéblemond, D., Castaing, C., Billa, M., Bouton, P., Préat, A., 2009. Notice explicative de la carte géologique et des ressources minerals de la Republique Gabonaise à 1/

1000000. Editions DGMG – Ministère des Mines, du Pétrole, des Hydrocarbures, Libreville, 348.

Trompette, R., 1994. Geology of Western Gondwana (2000–500 Ma). Pan-African-Brasiliano aggregation of South America and Africa. A.A. Balkema, pp. 350.

Tuller, M.P., 2001. Folha Ipanema 1:100.000. Projeto Leste. CODEMIG-CPRM, Belo Horizonte, Brazil.

Valladares, C., Souza, S., Ragatky, D., 2002. The Quirino Complex: a Transamazonian Magmatic Arc (?) of the Central Segment of the Brasiliano/Pan-African Ribeira Belt, SE Brazil. Revista Universidade Rural, Série Ciências Exatas e da Terra 21, 49–62.

Viana, S.M., 2008. Evolução geológica do Terreno Paraíba do Sul, Orógeno Ribeira, Sudeste do Brasil, com base em estudos litogeoquímicos e de geocronologia U-Pb (LA-ICPMS). Tese de Doutoramento, Programa de Pós-Graduação em Análise de Bacias e Faixas Móveis, Faculdade de Geologia, UERJ, 230.

Vicat, J., Pouclet, A., 2000. Palaeo- and Neoproterozoic granitoids and rhyolites from the West Congolian Belt (Gabon, Congo, Cabinda, north Angola): chemical composition and geotectonic implications. J. Afr. Earth Sci. 31, 597–617.

Wiedenbeck, M., Alle, P., Corfu, F., Griffin, W.L., Meier, M., Oberli, F., von Quadt, A., Roddick, J.C., Spiegel, W., 1995. 3 natural zircon standards for U-Th-Pb, Lu-Hf, trace-element and REE analyses. Geostandards Newsl. 19, 1–23.

Zhao, G., Cawood, C.A., Wilde, S.A., Sun, M., 2002. Review of global 2.1–1.8 Ga orogens: implications for a pre-Rodinia supercontinent. Earth Sci. Rev. 59, 125–162.

3. Publication 2

Contrasting provenance and timing of metamorphism from paragneisses of the Araçuaí-Ribeira

orogenic system, Brazil: Hints for Western Gondwana assembly

(published in Gondwana Research 51, 30-50)

Contrasting provenance and timing of metamorphism from paragneisses of the Araçuaí-Ribeira orogenic system, Brazil: Hints for Western Gondwana assembly

Reik Degler [a,*], Antônio Pedrosa-Soares [a], Ivo Dussin [b], Gláucia Queiroga [c], Bernhard Schulz [d]

[a] Universidade Federal de Minas Gerais, Programa de Pós-Graduação em Geologia, CPMTC-IGC-UFMG, Av. Antônio Carlos 6627, Pampulha, 31270-901 Belo Horizonte, MG, Brazil
[b] Universidade do Estado do Rio de Janeiro, Faculdade de Geologia, MULTILAB, Rua Francisco Xavier, 524, Maracanã, 20550-900 Rio de Janeiro, RJ, Brazil
[c] Departamento de Geologia, Escola de Minas, Universidade Federal de Ouro, Morro do Cruzeiro, 35400-000 Ouro Preto, MG, Brazil
[d] TU Bergakademie Freiberg, Institute of Mineralogy, 09596 Freiberg, Saxony, Germany

ARTICLE INFO

ABSTRACT

The Araçuaí orogen and the Ribeira belt make up a complex Neoproterozoic-Cambrian orogenic system, the Araçuaí-Ribeira orogenic system (AROS) located from the eastern to southeastern Brazil. Along the AROS, the Ediacaran Rio Doce magmatic arc represents a geotectonic connection between the Araçuaí and the Ribeira orogenic domains. Although the nature and evolution of the Rio Doce plutonic rocks is regionally well established, it lacks detailed studies on the paragneisses found along the western and central regions of this magmatic arc. Besides information on the nature and provenance of their sedimentary protoliths, the paragneisses provide data to unravel the palaeogeographic scenario from the precursor to arc-related basins. Six samples of Al-rich gneisses covering a large AROS region were selected for electron microprobe (EMP) mineral analyses in order to obtain geothermobarometric data and monazite ages, as well as for Laser Ablation-Inductively Coupled Plasma-Mass Spectrometry (LA-ICP-MS) isotopic analyses on zircon (U-Pb, Lu-Hf) and monazite (U-Pb). The different age spectra from detrital zircon grains and contrasting Hf isotopic signatures suggest a complex sedimentary history. Located in the western sector of the study region, the samples RC-02 and RC-34, with an 80% age peak of detrital zircon grains from 2158 Ma to 1830 Ma, $\varepsilon_{Hf(t)}$ from −2.2 to −22.7, and Hf T_{DM} model ages from 3530 Ma to 2440 Ma, suggest sediment sources located in the São Francisco craton basement. The samples RC-03, also from the western sector, and RC-46 from the southern sector, have a more complex assemblage of detrital zircon grains with an 87% age peak from 987 Ma to 592 Ma, $\varepsilon_{Hf(t)}$ from +14.9 to −2.9, and Hf T_{DM} model ages from 2220 Ma to 720 Ma, indicating provenance from mainly juvenile sources of distinct ages. Candidates to be juvenile sources for RC-03 and RC-46 sedimentary protoliths are the Rhyacian Juiz de Fora and Pocrane complexes in the basement of the Rio Doce arc, the Neoproterozoic Rio Negro arc system of the Ribeira belt, and AROS ophiolite complexes. Samples RC-30 and RC-38 from the eastern sector of the study region, with most detrital zircon ages between 650 Ma and 552 Ma and very negative $\varepsilon_{Hf(t)}$ (−25.3 to −16.5), suggest main sediment sources in the Rio Doce arc. By extending U-Pb analyses on metamorphic zircon and monazite, we have identified a complex timing of metamorphism, represented by metamorphic ages ranging from 621 Ma to 480 Ma, with the main collisional activity between 580 Ma and 540 Ma. Geothermobarometric studies on garnet porphyroblasts, syn-kinematic to the D_2 regional foliation, show a retrograde metamorphic path typical of continental collision belts, starting with P-T conditions of T_{max} = 733 °C and P_{max} = 6.43 kbar. Our data also suggest: i) the studied paragneisses represent distinct Neoproterozoic basin stages, shifting from passive to active margin settings; ii) if the Rio Negro arc system really provided sediments for the basin stage represented by the RC-03 and RC-46 paragneisses, it would have amalgamated with the AROS before 614 Ma; iii) the final amalgamation of Western Gondwana took place around 540 Ma in the focused region; iv) an important re-heating period (520–480 Ma) can be related to the AROS gravitational collapse, after Western Gondwana assembly.

1. Introduction

Extending for some 2000 km from eastern to southeastern Brazil, the Araçuaí-Ribeira orogenic system (AROS) includes the Araçuaí orogen (Pedrosa-Soares et al., 2008), to the north, and the Ribeira belt

* Corresponding author.
  E-mail address: reikdegler@gmail.com (R. Degler).

(Heilbron et al., 2008), to the south (Fig. 1). A rough boundary between the Araçuaí and Ribeira orogenic sectors is the 21°S meridian that assigns a major inflection of the AROS structural trend in relation to the southernmost tip of the São Francisco craton (Pedrosa-Soares et al., 2001). As segments of the complex orogenic system formed during the Western Gondwana assembly in Late Neoproterozoic time, those AROS sectors are very distinct in relation to their geotectonic setting, lithotectonic components and development timing (Heilbron et al., 2004). The Araçuaí orogen and its counterpart located in Africa, the West Congo belt, represent a confined orogen bounded by the São Francisco-Congo craton along their northern, western and eastern edges (Pedrosa-Soares et al., 2001, 2008; Alkmim et al., 2006). It includes ophiolite remnants and subduction-related accretionary wedges

(Pedrosa-Soares et al., 1998; Queiroga et al., 2007; Queiroga, 2010; Peixoto et al., 2015), only one continental magmatic arc, the Rio Doce arc (G.O. Gonçalves et al., 2016; L. Gonçalves et al., 2016, 2017; Tedeschi et al., 2016), and a huge amount of collisional and post-collisional granites (580–480 Ma) (Pedrosa-Soares et al., 2011a; Gradim et al., 2014; De Campos et al., 2016; Richter et al., 2016). On the other hand, the Ribeira belt represents a more complex orogenic system (Fig. 1), including the Rio Negro - Serra da Prata magmatic arc with juvenile signatures (Tupinambá et al., 2012; Heilbron, 2012), as well as at least one continental margin arc, the Rio Doce arc (Heilbron et al., 2013; Tedeschi et al., 2016). The northern Ribeira sector also includes the Cabo Frio domain, an Early Cambrian collisional zone (Schmitt et al., 2008; Fig. 1). Furthermore, the Ribeira belt shows rather complex
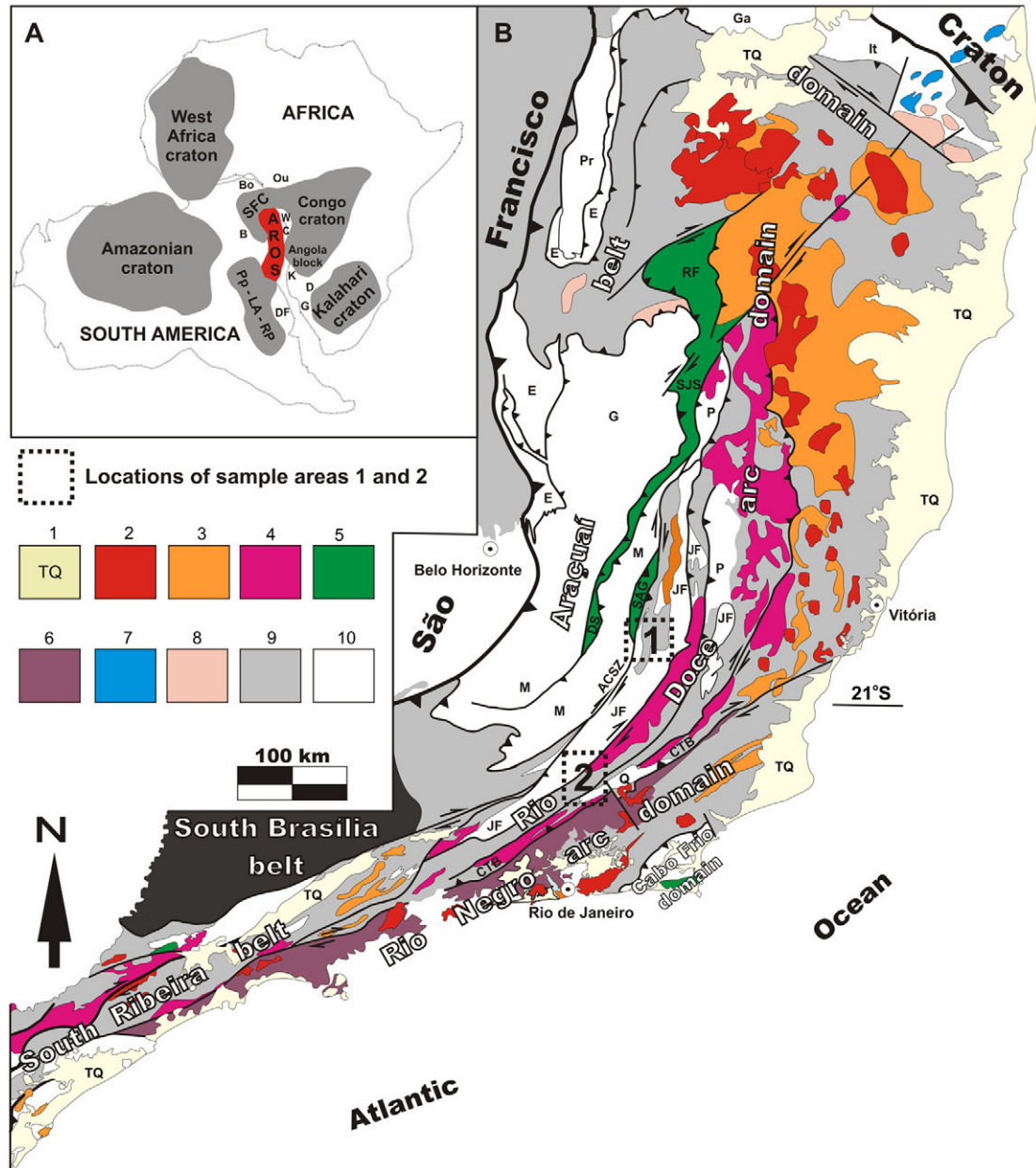
Fig. 1. A, Location of the Araçuaí-Ribeira orogenic system (AROS) in Western Gondwana (modified from Brito-Neves et al., 1999). Brasiliano - Pan-African orogenic belts: B, Brasília; Bo, Borborema; D, Damara; DF, Dom Feliciano; G, Gariep; K, Kaoko; WC, West Congo. Cratons: SFC, São Francisco; PP-LA-RP, Paranapanema-Luis Alves-Rio de La Plata. B, Simplified geological map of the AROS (modified from Silva et al., 2005, and Tedeschi et al., 2016): 1, Cenozoic cover (TQ - Tertiary, Quaternary); 2, post-collisional intrusions (c. 525–480 Ma); 3, collisional granitic rocks (c. 585–535 Ma); 4, G1 plutonic supersuite of the Rio Doce magmatic arc (c. 630–585 Ma) and probable correlatives; 5, ophiolite-bearing rock assemblages: RF-SJS-DS, Ribeirão da Folha-São José da Safira-Dom Silvério schist belt (c. 660–630 Ma); SAG, Santo Antônio do Grama metamafic-ultramafic suite (c. 600 Ma); 6, Rio Negro arc domain (Rio Negro - Serra da Prata magmatic arc, and related units; c. 860–605 Ma); 7, Southern Bahia Alkaline Province (c. 732–676 Ma); 8, Early Tonian (c. 930–875 Ma) rift-related magmatic rocks; 9, Neoproterozoic metasedimentary and metavolcanic successions; 10, pre-Neoproterozoic units: E, Espinhaço Supergroup; and Archaean-Palaeoproterozoic blocks and complexes: G, Guanhães; Ga, Gavião; It, Itapetinga; JF, Juiz de Fora; M, Mantiqueira; P, Pocrane; Pr, Porteirinha. ACsz, Abre Campo shear zone. CTB, central tectonic boundary.

palaeotectonic relations, being surrounded by the southern São Francisco craton, the southern Brasília belt, the Paranapanema, Luiz Alves and Angola cratonic blocks, the Kaoko and Damara belts and the northwestern border of the Kalahari craton (Trompette, 1994; Brito-Neves et al., 1999; Basei et al., 2008; Heilbron et al., 2008; Trouw, 2008).

Detrital zircon geochronology data for the AROS and its African counterparts have been published by several authors since the early 2000 (e.g., Pedrosa-Soares et al., 2000; Noce et al., 2004; Frimmel et al., 2006; Valladares et al., 2008; Basei et al., 2010; Belém et al., 2011; Gonçalves-Dias et al., 2011; Babinski et al., 2012). More recently, Affaton et al. (2015), Kuchenbecker et al. (2015) and Gonçalves-Dias et al. (2016) characterised material provenances related to passive margin sediments with sources of mostly Archaean to Early Tonian ages. In contrast, Novo (2013), Gradim et al. (2014), Peixoto et al. (2015) and Richter et al. (2016) presented detailed data supporting provenance from the Ediacaran Rio Doce magmatic arc. According to the sediment provenance studies by Fernandes et al. (2015) and Lobato et al. (2015), a broad spectrum of source material of Archaean to Ediacaran ages suggests a more complex scenario for the northern Ribeira belt. In view of the AROS, detailed studies based on U-Pb and Lu-Hf isotopic analyses in detrital zircon grains of metasedimentary rocks, together with geochronological studies on metamorphic zircon and monazite, can provide important data to unravel distinct sediment provenances and timing of metamorphism related to the palaeotectonic scenarios for the Western Gondwana assembly.

We present U-Pb geochronological and Lu-Hf isotopic (LA-ICP-MS) data from zircon and monazite grains, as well as EMP-monazite ages, together with quantitative geothermobarometric data that outline a reasonable understanding of the complex distribution of metasedimentary rocks and their distinct provenances in relation to a changing geological setting and metamorphic timing. In addition, we suggest new correlations and interactions of different sediment sources located in Brazil and Africa to better constrain the evolutionary context and timing of the Western Gondwana assembly. We also present a thorough compilation of zircon age data from primary and secondary sources in Supplementary File 1.

In this paper, if not otherwise specified, we use the name granite in a general sense. Geographical coordinates and orientations refer to the present-day position of continents, even in palaeotectonic interpretations.

2. Geotectonic setting

Our descriptions do not make use of the intricate terrane terminology presented in publications on the Ribeira belt, as it is not consensual and significantly differs from one region to another. Furthermore, it is not suitable for the Araçuaí orogen at all. Instead, we focus on the main AROS geotectonic components (e.g., magmatic arcs) and evolution stages, which are more appropriate for our research approach.

The AROS can be divided in five geotectonic domains (Fig. 1): i) the Araçuaí belt domain; ii) the Rio Doce arc domain; iii) the Rio Negro arc domain; iv) the Cabo Frio domain; v) the southern Ribeira belt.

The Araçuaí belt domain, corresponding to the marginal orogenic belt bordering the southeastern São Francisco craton, encompasses large portions of the Archaean-Palaeoproterozoic cratonic basement (the Guanhães, Gavião, Itapetinga and Porteirinha blocks; Fig. 1) reworked by the Brasiliano orogeny within the Araçuaí orogen (Cruz et al., 2016; Silva et al., 2015). To the south of the Guanhães block, the Mantiqueira complex represents a magmatic arc formed in the Late Rhyacian time (2.15–2.05 Ga) on the São Francisco continental margin (Noce et al., 2007). From the Statherian to Stenian, the Espinhaço Supergroup and related anorogenic magmatism (Fig. 1) represent three basin-forming events developed around 1.7 Ga, 1.5 Ga and 1.2 Ga (Pedrosa-Soares and Alkmim, 2011; Chemale et al., 2012; Guadagnin et al., 2015; Rolim et al., 2016). Two Neoproterozoic rifting events

formed the Early Tonian (c. 935–875 Ma) rift 1 and the Late Tonian-Early Cryogenian (c. 735–675 Ma) rift 2, both filled by sedimentary and volcanic successions of the Macaúbas Group and correlative units (Pedrosa-Soares and Alkmim, 2011; Pedrosa-Soares et al., 2011b; Babinski et al., 2012; Kuchenbecker et al., 2015; Gonçalves-Dias et al., 2011, 2016). The Macaúbas rift 2 evolved to an oceanic opening phase represented by the tectonic dismembered ophiolite complexes found in the Ribeirão da Folha - São José da Safira - Dom Silvério schist belt (RF-SJS-DS) and in the Santo Antônio do Grama suite (SAG; Fig. 1). They include tectonic slices of metamafic-ultramafic rocks and meta-plagiogranites with lithochemical and isotopic ($\varepsilon_{Nd(t)}$ from +7 to +1.1) oceanic signatures, forming an ophiolitic belt developed from c. 660 Ma to c. 600 Ma (Pedrosa-Soares et al., 1992, 1998, 2001; Suita et al., 2004; Queiroga et al., 2007; Queiroga, 2010; Peixoto et al., 2015). To the east, the Abre Campo shear zone (ACsz, Fig. 1), located between the Araçuaí belt and Rio Doce arc domains (Fig. 1), represents a segment of the suture zone of the Araçuaí orogen (Alkmim et al., 2006). The Araçuaí belt domain represents the lower plate in relation to the Rio Doce arc domain (Peixoto et al., 2015; Tedeschi et al., 2016).

Located in the upper plate margin, the Rio Doce arc domain encompasses the homonymous magmatic arc, as well as the related basins and basement (Fig. 1). The Rio Doce magmatic arc includes the plutonic rocks ascribed to the G1 supersuite, and the metavolcano-sedimentary succession of the Rio Doce Group (Tedeschi et al., 2016, and references therein). The G1 supersuite comprises magnesian, metaluminous, pre-collisional plutons of an expanded calc-alkaline series, ranging in composition from gabbro-norite to granite, with predominance of tonalites and granodiorites rich in dioritic to mafic enclaves. The large amounts of lithochemical and isotopic data clearly point to a magmatic arc formed on a continental margin setting, from c. 630 Ma to c. 580 Ma (G.O. Gonçalves et al., 2016; L. Gonçalves et al., 2016; Tedeschi et al., 2016; and references therein). The Rio Doce magmatic arc makes a clear geotectonic connection between the southern Araçuaí and northern Ribeira sectors of the AROS (Silva et al., 2005; Heilbron et al., 2013; Tedeschi et al., 2016), and can also be correlated to pre-collisional calc-alkaline plutonic suites found in the southern Ribeira belt domain (Campos-Neto, 2000; Basei et al., 2008). The basement of the Rio Doce arc domain comprises Rhyacian-Orosirian (c. 2.2–1.9 Ga) magmatic arcs with mainly juvenile signatures, represented by the Juiz de Fora, Pocrane and Quirino complexes (Noce et al., 2007; Heilbron et al., 2010; Novo, 2013). The basement complexes host minor Mesoproterozoic magmatic rocks dated at c. 1.7 Ga, 1.5 Ga and 1.1 Ga (Heilbron et al., 2008; Novo, 2013). The arc covers include the micaschists and paragneisses with intercalations of calc-alkaline metavolcanic rocks, as well as the meta-wackes and quartzites of the Rio Doce Group (Vieira, 2007; Novo, 2013; Tedeschi et al., 2016; Gonçalves et al., 2017). High-grade paragneisses and a huge amount of syn-collisional to late-collisional granites (G2 and G3 supersuites; c. 585–530 Ma), as well as a number of post-collisional intrusions (G5 supersuite, c. 530–480 Ma) characterise the back-arc region in the Rio Doce arc domain (Pedrosa-Soares et al., 2011a; Gradim et al., 2014; De Campos et al., 2016; Melo et al., 2016; Richter et al., 2016). The fore-arc region shows large areas of the Rhyacian basement (Juiz de Fora and Pocrane complexes), Neoproterozoic paragneisses, and collisional granites (Noce et al., 2007; Degler et al., 2016).

A central tectonic boundary (CTB, by Almeida et al., 1998), represented by thrust zones superimposed by late strike-slip shear zones, separates the Rio Doce and Rio Negro arc domains (Fig. 1). The Rio Negro domain includes the Rio Negro and Serra da Prata segments of a juvenile magmatic arc system, Neoproterozoic metasedimentary rocks metamorphosed under amphibolite to granulite facies, Ediacaran collisional granites, and Cambrian to Ordovician post-collisional intrusions (Heilbron et al., 2008; Valeriano et al., 2011, 2016; Tupinambá et al., 2012). Some important features, like the lack of a continental basement and the juvenile geochemical signatures found in the magmatic arc rocks, suggest that the Rio Negro domain represents an island arc

system that collided with the southern Rio Doce and Ribeira belt domains in the Late Neoproterozoic (Heilbron et al., 2008). The Rio Negro arc, with $\varepsilon_{Nd(t)}$ ranging from $+5$ to -3 (Tupinambá et al., 2012), is an important candidate to provide juvenile zircon grains to the adjacent basins.

The northern Ribeira belt also includes the Cabo Frio domain, a Cambrian collisional zone (530–501 Ma), involving a Rhyacian-Orosirian basement (the Região dos Lagos complex), Neoproterozoic metasedimentary rocks and the Palmital ophiolite complex (Schmitt et al., 2008).

The southern Ribeira belt encompasses terranes separated by strike-slip shear zones, including Palaeoproterozoic basement, Mesoproterozoic and Neoproterozoic metasedimentary and metavolcanic rocks, Ediacaran ophiolite complexes, pre-collisional calc-alkaline suites and collisional granites, as well as Cambro-Ordovician post-collisional intrusions (Campos-Neto, 2000; Juliani et al., 2000; Tassinari et al., 2001; Heilbron et al., 2004; Basei et al., 2008; Alves et al., 2013; Meira et al., 2015).

The Brasiliano orogenic evolution along the AROS shows differences in time and space. In the Araçuaí orogen, there are quite well-constrained time limits for the main orogenic stages related to the Rio Doce arc domain: the pre-collisional (630–585 Ma), collisional (585–535 Ma) and post-collisional (535–490 Ma) stages (Pedrosa-Soares et al., 2011a; Peixoto et al., 2015; De Campos et al., 2016; Melo et al., 2016; Richter et al., 2016; Tedeschi et al., 2016). However, the evolution timing for the Ribeira orogenic system is rather complex because it involves at least two distinct magmatic arc systems, the Rio Negro – Serra da Prata (c. 840–615 Ma) and the Early Ediacaran Rio Doce – Serra da Bolívia – Marceleza arcs (Heilbron et al., 2004, 2008, 2013; Tupinambá et al., 2012; Tedeschi et al., 2016). As the samples from areas 1 and 2 are located in the Araçuaí belt and Rio Doce arc domains,

we tried to correlate our data to the time limits for the orogenic stages related to the Araçuaí orogen.

3. Geological setting

The study areas cover parts of the eastern Araçuaí belt domain and the fore-arc to intra-arc regions of the Rio Doce arc domain, where the main metasedimentary successions, including the sampled paragneisses, have been ascribed to the Andrelândia Group (Figs. 1 and 2). The geological framework for both studied areas (1 and 2) resulted from systematic field mapping on the cartographic sheets named Jequeri (Queiroga et al., 2012a, 2012b), Viçosa (Gradim et al., 2012) and Manhuaçu (Noce et al., 2006), for area 1, and Ubá (Noce et al., 2003) and Leopoldina (Heilbron et al., 2003), for area 2 (Fig. 2).

Regarding the geotectonic scenario (Pedrosa-Soares et al., 2001, 2008; Alkmim et al., 2006), the sample area 1 covers parts of distinct plate margins, roughly limited by the Abre Campo shear zone (ABsz; Figs. 1 and 2A): the lower plate situated to the west and the upper plate to the east of the ACsz, respectively (Fig. 2). From west to east, the area 1 encompasses the Mantiqueira complex in the lower plate, a segment of the suture zone (the Abre Campo shear zone), and parts of the fore-arc and intra-arc regions of the southern Rio Doce magmatic arc, located on the upper plate margin (Figs. 1 and 2A). The Mantiqueira complex, representing a 2.15–2.05 Ga continental magmatic arc ($\varepsilon_{Nd(t)}$ = -9 to -13; Noce et al., 2007), makes up the basement to the west of the ACsz suture, where the Santo Antônio do Grama ophiolitic suite was thrust on top of that Rhyacian gneissic complex (Queiroga et al., 2012a, 2012b). The Santo Antônio do Grama ortho-amphibolites ($\varepsilon_{Nd(t)}$ = $+3.51$ to $+1.08$) yielded U-Pb zircon ages around 600 Ma for the magmatic crystallisation, and c. 570 Ma for the regional metamorphism (Queiroga, 2010). Further to the east, the Juiz de Fora
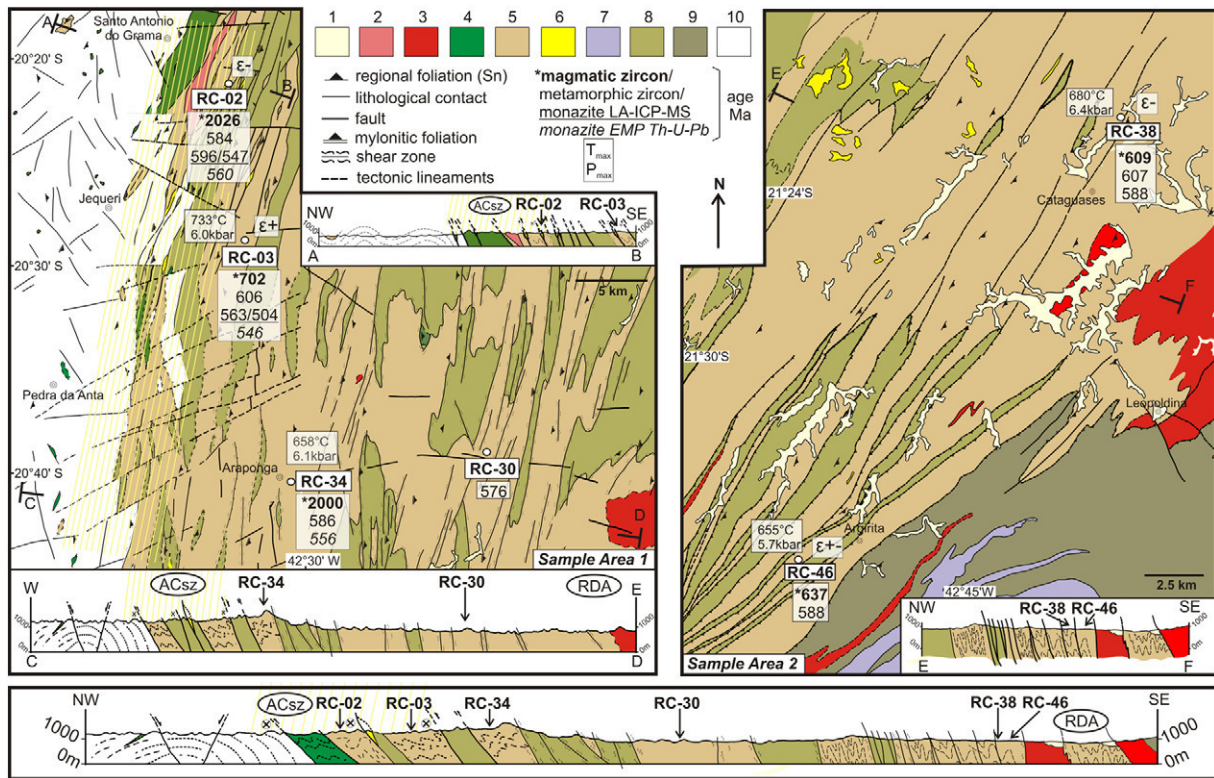
Fig. 2. Simplified geological maps and cross sections of the study areas 1 and 2. Labelled points show data from the paragneiss samples (see Table 1). In the lower part of the figure, a correlated cross section illustrates the position of the samples in relation to the Abre Campo shear zone (ABsz) and the Rio Doce magmatic arc (RDA). 1, Quaternary fluvial sediments. Neoproterozoic units: 2, Serra dos Vieiras collisional granite (G2, c. 570–540 Ma); 3, G1 plutons of the Rio Doce magmatic arc (c. 630–580 Ma); 4, Santo Antônio do Grama metamafic-ultramafic ophiolite suite (c. 600 Ma); Andrelândia Group: 5, mostly migmatitic Al-rich paragneisses; 6, mostly quartzites; 7, Paraiba do Sul metasedimentary rocks. Palaeoproterozoic basement complexes: 8, Juiz de Fora; 9, Quirino; 10, Mantiqueira. Labelled points show data from the selected paragneiss samples (see Table 1).

complex, representing an essentially juvenile magmatic arc formed around 2.2–2.08 Ga ($\varepsilon_{Nd(t)} = +7.7$ to -3.5; Fischel et al., 1998; Noce et al., 2007; André et al., 2009) is the basement of the Rio Doce arc domain in the fore-arc region (Fig. 2A). G1 plutons of the Rio Doce arc occur at the eastern border of the area. The Andrelândia Group represents the Neoproterozoic metasedimentary cover (Fig. 2). The typical rock of the Andrelândia Group is a migmatitic paragneiss variably rich in biotite, garnet and sillimanite. It was deformed together with ortho-granulites of the Juiz de Fora complex, forming complex tectonic structures (Fig. 2). Along the large Abre Campo shear zone, as well as in other shear zones of the region, pseudo-quartzites and iron formations represent distinct products of intense leaching and hydrothermal activity linked to the ductile deformation (Gradim et al., 2012; Queiroga et al., 2012a, 2012b). The Serra dos Vieiras pluton, a deformed granite rich in paragneiss xenoliths, is a typical representative of the collisional G2 supersuite (Fig. 2A).

The sample area 2, located around 120 km southwest of area 1, covers the transition region between the Araçuaí and Ribeira orogenic domains (Fig. 1). It encompasses a portion of the southern Rio Doce magmatic arc, including related basins and basement. The Rhyacian Juiz de Fora (granulite facies) and Quirino (amphibolite facies) complexes make up the basement, respectively in the northern and southern parts of area 2. The Juiz de Fora complex mostly consists of enderbitic to charnockitic orthogneisses, while the Quirino complex mainly consists of tonalitic to granitic orthogneisses (Heilbron et al., 2003; Tupinambá et al., 2012). The granitic and mafic rocks of the Rio Doce arc occur in the eastern and southern portions of area 2.

All analysed paragneiss samples of areas 1 and 2 were collected in different outcrops of the Andrelândia Group. They show very similar mineralogical compositions, including quartz, alkali feldspar, plagioclase, garnet, biotite and sillimanite. Biotite mostly occurs as reddish brown flakes, indicating enrichment in titanium. Garnet porphyroblasts and porphyroclasts show inclusions of plagioclase, biotite, quartz, sillimanite and monazite (Fig. 3). Sillimanite generally shows fibrous habitus. Alkali (K-Na) feldspars frequently display perthitic intergrowths and sericitisation. Usually, the plagioclase shows antiperthitic intergrowths and incipient alteration processes. Typical accessory minerals are apatite, monazite, zircon, and opaque minerals (sulphide, magnetite and ilmenite).

The sampled paragneisses of the Andrelândia Group probably represent pelitic wacke sediments. They are mostly migmatites with stromatic, folded and ptygmatic structures. Variable amounts of garnet-bearing granitic leucosomes in the paragneisses (e.g., RC-02 and RC-03; Fig. 3) attest distinct partial melting rates related to one or more migmatisation processes. The leucosomes can be concordant or discordant to the gneissic banding and locally they form small bodies of S-type leucogranites. Mylonitic textures are very common in the studied paragneisses (e.g. RC-30; Fig. 3). Porphyroclasts of garnet, feldspar and quartz, stretched along the regional foliation, show pressure shadows with biotite and quartz. In both study areas, the Andrelândia metasedimentary rocks are characterised by two main ductile deformational fabrics (D_1 and D_2). Although these two fabrics can be recognised in outcrops, they were not identified with certainty by microstructural analyses on the sampled paragneisses. In general, the foliation S_2 related to D_2 tends to obliterate the D_1 fabrics in the selected samples. In regional scale, D_1 indicates tectonic transport to the north, which was followed by the tectonic vergence to the west related to D_2 (Heilbron et al., 2003; Noce et al., 2003; Peres et al., 2004; Alkmim et al., 2006). Stretched minerals, such as biotite, quartz and sillimanite materialise the S_2 foliation, which can form a mylonitic banding sub-parallel to the former S_1

foliation (Fig. 3). According to field measurements, the S_2 foliation average strike/dip is 120°/50°, for sample area 1, and 135°/65°, for sample area 2 (Fig. 2).

The last deformational fabrics D_3 and D_4 can be observed in certain outcrops of the study region (Heilbron et al., 2003; Noce et al., 2003, 2007; Gradim et al., 2012; Queiroga et al., 2012a, 2012b), but are very hard to identify throughout the studied samples. The S_3 foliation, superimposed on D_1 and D_2 fabrics, characterises the dextral NNE-SSW-trending shear zones related to the lateral escape of masses from the southern Araçuaí to the Ribeira orogenic sectors (Costa, 1998; Peres et al., 2004; Alkmim et al., 2006). These zones, probably generated around 550–535 Ma, preceded the mainly brittle D_4 deformation related to the gravitational collapse (c. 535–490 Ma) of the Araçuaí orogen (Alkmim et al., 2006). In the region encompassing the study areas 1 and 2, Heilbron et al. (2003) and Noce et al. (2003) describe a significant change from amphibolite to granulite facies towards east. Regionally, the pelitic gneisses reached peak temperatures between 750 °C and 900 °C, at pressures from 8 kbar to 10 kbar (Schultz-Kuhnt, 1985; Duarte et al., 2004; Bento dos Santos et al., 2010, 2011; Gradim et al., 2012; Trouw et al., 2013). It is important to mention that, from the Brasília belt to the southern Araçuaí orogen, passing through the Ribeira belt, the Andrelândia Group includes sediments deposited in continental rift, passive margin and orogenic basins (Paciullo et al., 2000; Ribeiro et al., 2003; Heilbron et al., 2004; Belém et al., 2011; Trouw et al., 2013).

4. Analytical methods and samples

After detailed field and microscopic studies on samples from a number of paragneiss outcrops, we selected seven fresh samples from different exposures ascribed to the Andrelândia Group, covering the two studied areas (Fig. 2 and Table 1). All selected samples are free of weathering and hydrothermal alteration. Our sampling also paid special attention to the mineralogical similarity of the selected paragneisses, even though the rocks locally show small differences in grain size, banding and deformational features. Furthermore, we separated as much palaeosome as possible in order to reduce the influence of leucosomes in zircon and monazite concentrates. The samples were prepared for analyses in laboratories of the Federal University of Minas Gerais (CPMTC-UFMG) and University of Rio de Janeiro State (MULTILAB-UERJ). Zircon and monazite concentrates were extracted from rock samples using conventional gravimetric and magnetic (Frantz isodynamic separator) techniques. Final separation was achieved by hand picking. Monazite and zircon grains were mounted and polished in distinct epoxy disks. Optical and secondary electron images were taken from all mounted samples, and complemented by cathodoluminescence (CL) images to reveal morphological features and internal structures of zircon grains. The in situ monazites analyses were performed in thin sections on the EMP.

4.1. LA-MC-ICP-MS U-Pb in zircon

All selected zircon grains were mounted and then photographed for cathodoluminescence (CL) images under the scanning electron microscope (SEM, Quanta-250-FEI). Further, the zircon grains were analysed with Laser microprobe (Excimer Laser 193 µm by Photon – Machines Inc. Model ATLEX SI), pulsed with ArF, and attached to the MC-ICP-MS (Neptune-Plus) equipment in the multi-use isotopic laboratory (MULTILAB) at the University of Rio de Janeiro State (UERJ). Isotopic data were acquired by static mode under a laser beam spot of 25 µm and operating conditions presented in Supplementary File 2. Element

Fig. 3. Photographs of selected paragneiss samples from areas 1 and 2 (Fig. 2), illustrating outcrop (left), macroscopic (middle), and non-polarised and polarised microscopic (right) features. Quartz, plagioclase, garnet, biotite, alkali feldspar and sillimanite materialise the regional foliation S_2. Quartz-feldspar-rich leucosomes parallel to the S_2 foliation are most abundant in samples RC-34 and RC-38. Mylonitic features are shown by samples RC-30, RC-34, RC-38 and RC-46. Biotite occurs as reddish-brown flakes, and porphyroclasts and porphyroblasts of feldspars and garnets stretched and enveloped by the S_2 foliation are common in all samples. Mineral inclusions in garnet may represent relics of a former D_1 fabric. (For interpretation of the references to colour in this figure legend, the reader is referred to the web version of this article.)
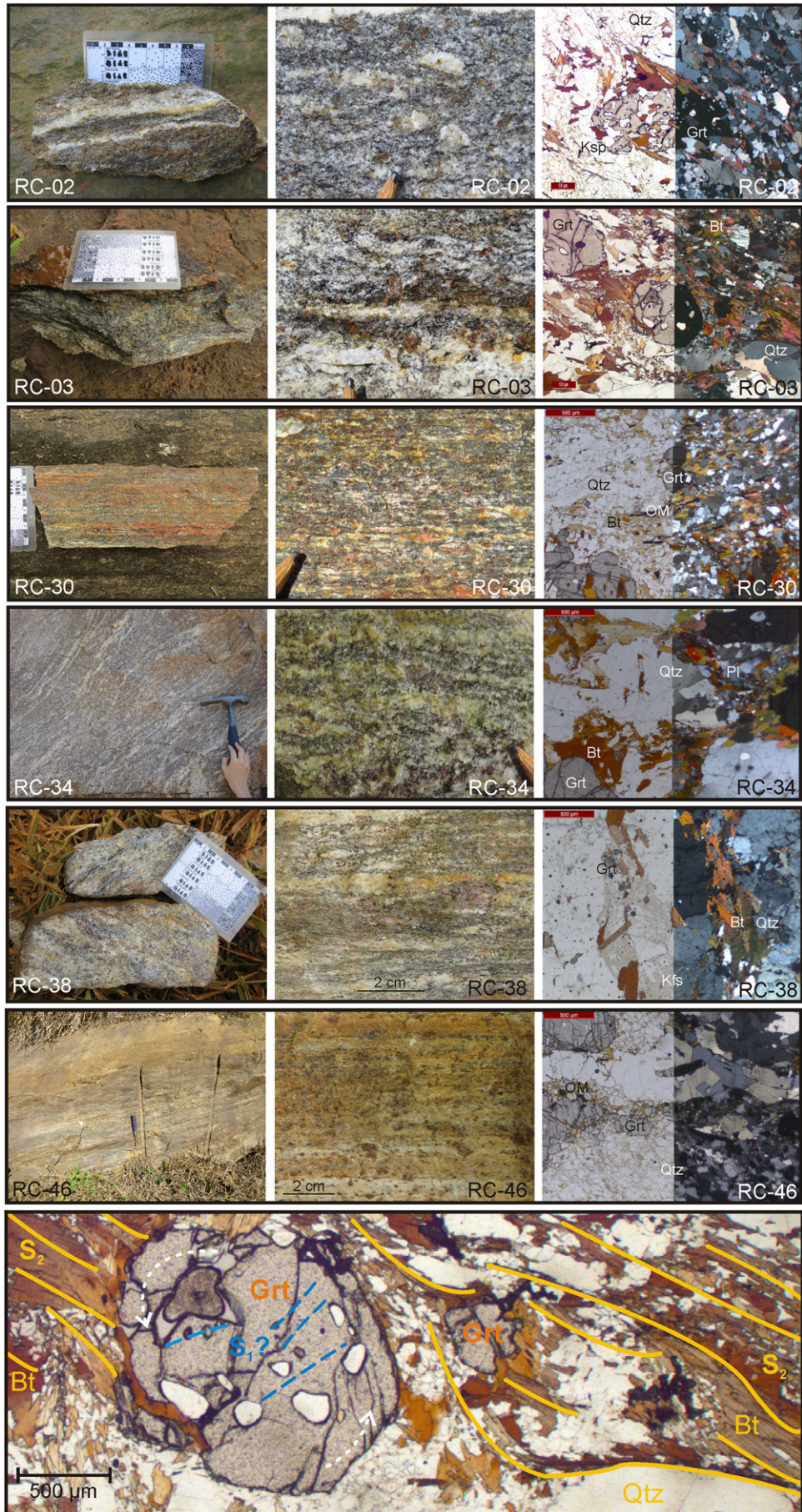
fractionation by induction of the Laser and essential mass discrimination were monitored by analyses of external zircon standard (GJ-1; Jackson et al., 2004). External uncertainties were propagated by quadratic addition of individual measurements of the external standard GJ-1 and individual measures of every sampled zircon (or spot). Detailed methodological conditions are described in Chemale et al. (2012). For data quality control of the sample sets and the GJ-1 standard, grains of 91500 standard with an age of 1065 ± 0.3 Ma (Wiedenbeck et al., 1995) were analysed. Concordia ages and weighted average ages are reported with 2σ errors using Isoplot 3.0 (Ludwig, 2003). Detailed measurement conditions are given in Supplementary File 2.

4.2. LA-ICP-MS U-Pb in monazite

The monazite grains were analysed by Thermo-Finnigan Neptune MC-ICP-MS, coupled with a 193 nm HelEx Photon-Machine laser ablation system in the Isotope Laboratory of Federal University of Ouro Preto, Brazil. As external standards, we used the Bananeira (G.O. Gonçalves et al., 2016; L. Gonçalves et al., 2016) and Steenkampscraal (Liu et al., 2012) monazites. Concordia ages and weighted average ages are reported with 2σ errors, using Isoplot 3.0 (Ludwig, 2003). Detailed measurement conditions can be found in Supplementary File 2.

4.3. LA-ICP-MS Lu-Hf in zircon

The isotopic analyses for Lu-Hf in zircon were carried out by using the LA-MC-ICP-MS equipment of the MULTILAB-UERJ, Rio de Janeiro, Brazil. In total, 148 Lu-Hf isotopic analyses were conducted for samples RC-02, RC-03, RC-38 and RC-46. It was attempted, to spot the same zircon grain domains as already analysed for U-Pb dating. The laser was operated with a spot of 40 μm in diameter (65% power), fluence of 1.61 J/cm 250 s, and a pulse rate of 9 Hz. Helium was used as carrier gas to minimize oxide formation and increase Hf sensitivity (Bahlburg et al., 2011). For $\varepsilon_{Hf(t)}$ values calculation we adopted a decay constant of ^{176}Lu of 1.867×10^{-11} (Söderlund et al., 2004) and present-day chondritic ratios of ^{176}Hf/^{177}Hf = 0.282785 plus ^{176}Lu/^{177}Hf = 0.0336 (Bouvier et al., 2008). The Hf evolution curve of the depleted mantle was determined from present-day depleted mantle values with ^{176}Hf/^{177}Hf ratio of 0.28325 and ^{176}Lu/^{177}Hf ratio of 0.0388 (Griffin et al., 2000; updated by Andersen et al., 2009). Following Pietranik et al. (2008), the continental model of felsic crust was calculated using the initial ^{176}Hf/^{177}Hf ratio of zircon and the ^{176}Lu/^{177}Hf = 0.022 ratio.

4.4. EMP Th-U-Pb monazite

After microscopic studies under polarised light, selected thin sections were investigated under a scanning electron microscope (SEM) Quanta 650 FEG MLA by FEI Company, at the Department of Economic Geology and Petrology of the Technical University of Freiberg, Germany. Automated mineralogical methods were performed with the mineral liberation analysis software MLA 2.9 version by FEI Company, steering a Bruker EDS system. Analysis of Th, U and Pb for calculation of monazite model ages, as well as for Ca, Si, LREE and Y for corrections and evaluation of the mineral chemistry were carried out on a microprobe JEOL JXA8900 RL at the Institut für Werkstoffwissenschaft at Freiberg. First, for each single analysis, an age was calculated using the equations given by Montel et al. (1996). The error resulting from counting statistics was typically on the order of ±20 to ±40 Ma (1σ) for Early Palaeozoic ages. This error is reduced in Palaeoproterozoic monazites due to their increased Pb contents. Using these apparent age data, weighted average ages for monazite populations in the samples were then calculated using Isoplot 3.0 (Ludwig, 2003). The determined ages are interpreted as closure time for the Th–U–Pb system of monazite during growth or recrystallisation in the course of metamorphism. Second, the ages were ascertained using the ThO$_2$*-PbO isochrones method

(CHIME) of Montel et al. (1996) and Suzuki et al. (1994), where ThO^{2*} is the sum of the measured ThO^2 plus ThO^2 equivalent to the measured UO^2. The age is calculated from the slope of the regression line in ThO^{2*} vs. PbO coordinates forced through zero. In all analysed samples, the model ages obtained by the two different methods agree exceptionally well. Detailed measurement conditions are described in Supplementary File 2.

4.5. Geothermobarometry

Samples were first investigated as polished thin sections under the SEM (Quanta 650 FEG). For RC-02, RC-03 and RC-34 the method of Garnet X-ray Mapping (GXMAP) was applied. In samples RC-38, RC-43 and RC-46 the rock-forming minerals were identified microscopically under polarised light. All samples were further investigated using the JEOL JXA 8900RL electron microprobe at the Institut für Werkstoffwissenschaft/ Freiberg and at the Electron Microscopy Center of the Federal University of Minas Gerais (CM-UFMG), Brazil. To illustrate zonation trends of the garnets in the profiles, the data are plotted in the grossular-pyrope-spessartine ternary diagram as proposed by Schulz (1993) and in the revised X_{Ca}–X_{Mg} diagram by Martignole and Nantel (1982).

Supplementary File 2 shows the arrangements of single spot measurement points for garnet (Grt), plagioclase (Pl) and biotite (Bt), which are used to calculate temperature and pressure conditions (Holdaway, 2001; Wu et al., 2004).

5. Results

As different analytical methods and techniques were applied on the same samples, the results are summarised for each performed technique and analysed mineral (compare Table 1). Detailed data tables are given in Supplementary Files 3A–3E.

5.1. Geothermobarometry of metamorphic conditions

The paragneiss samples show only one type of garnet chemical zonation trend. On average, they consist of 15–30% pyrope, 1–3% spessartine, 4–5% grossular and 60–75% almandine. For each sample, distinct and representative single analyses out of the garnet zonation trend were selected and used together with coexisting biotite and plagioclase for the garnet–biotite Fe–Mg exchange geothermometer and the garnet-plagioclase Ca-net-transfer geobarometer. Common sillimanite was only observed in sample RC-38. Taking all five samples into account, the results are in range of 614–733 °C at 4.22–6.43 kbar (Table 2) and correspond to high amphibolite facies (Fig. 4). The T$_{max}$ and P$_{max}$ for RC-03 and RC-34 (sample area 1; Fig. 2) are quite identical and reach 733 °C (RC-03) and 6.15 kbar (RC-34). In sample area 2, the values for RC-38 and RC-46 are in the same range, with T$_{max}$ of 680 °C and P$_{max}$ of 6.43 kbar (RC-38). Detailed measured and calculated data are given in Supplementary File 3E.

5.2. EMP Th-U-Pb and LA-ICP-MS metamorphic monazite ages

For a meaningful data comparison, we summarise the results from both geochronological methods applied on monazite crystals of the studied samples. U-Pb (LA-ICP-MS) age Concordia diagrams for the analysed monazites, and a detailed database of all analyses is presented in Fig. 9A and Supplementary Files 3A, 3B and 3C.

5.2.1. Sample RC-02 (quartz-plagioclase-K-feldspar-biotite-garnet paragneiss)

In a RC-02 sample thin section, 128 EMP measurements were distributed over 24 monazites. Among those 128 measurements, 25 are from monazites included in garnets. The maximal grain size is 200 μm (mz10) but the diameter also decreases for some grains down to 20 μm, mz11 (Fig. 5A). The Pb data ranges from 0.08 (mz22-10) to 0.35

Table 1
Compilation of studied samples and applied analytical methods for AROS metasedimentary rocks (Andrelândia Group). UTM coordinates are in WGS24, Zone 23 K.

Sample	UTM coordinates	Mineralogy	Methods
RC-02	755214/7747628	Qtz-Pl-Kfs-Bt-Grt	LA-ICP-MS U-Pb zircon
			LA-ICP-MS U-Pb monazite
			EMP Th-U-Pb monazite
			LA-ICP-MS Lu-Hf magmatic zircon
RC-03	755935/7734053	Qtz-Pl-Grt-Bt-Kfs	LA-ICP–MS U–Pb zircon
			LA-ICP-MS U-Pb monazite
			EMP Th-U-Pb monazite
			LA-ICP-MS Lu-Hf magmatic zircon
			Geothermobarometry (Grt-Bt-Pl)
RC-34	753654/7710340	Qtz-Pl-Bt-Grt	LA-ICP-MS U-Pb zircon
			EMP Th-U-Pb monazite
			Geothermobarometry (Grt-Bt-Pl)
RC-30	777133/7714568	Qtz-Pl-Bt-Grt-Sil	LA-ICP-MS U-Pb zircon
RC-38	742122/7636281	Qtz-Bt-Pl-Grt-Sil	LA-ICP-MS U-Pb zircon
RC-46	719626/7605780	Qtz-Bt-Grt-Kfs	Geothermobarometry (Grt-Bt-Pl)

(mz17ng-1). The Th* results lie between 4.19 (mz22-10) and 14.0 (mz19ng-2). The calculated ages vary between 601 ± 47 Ma (mz19ng-3) and 534 ± 109 (mz18ng-6) for analyses of enclosed monazites, and go down to 482 ± 140 Ma (mz16-2) for matrix monazites. Fifty-two monazite grains analysed by LA-ICP-MS yielded U-Pb ages between 612 ± 13 and 531 ± 14 Ma, and show two Concordia ages: 596 ± 4 Ma and 548 ± 3 Ma (Fig. 9A and Supplementary File 3A).

5.2.2. Sample RC-03 (quartz-plagioclase-garnet-biotite-K-feldspar paragneiss)
For RC-03 thin section, 63 EMP single spot analyses, 16 of them from enclosed monazites in garnet, were performed on 18 monazites (detailed analytical data in Supplementary Files 3B and 3C). The average size of the grains is between 70 and 100 μm in diameter. The Pb data range between 0.13 (mz1-1) and 0.18 (mz11-1). The Th* values lie between 6.07 (mz1-1) and 7.92 (mz4iG-29) (Fig. 5B). The maximal calculated age is 613 ± 98 Ma (mz12ig-2, Fig. 5B). The youngest monazite age is 480 ± 98 Ma (mz17-1). With regard to 49 monazite grains analysed by LA-ICP-MS, the U-Pb ages range between 585 ± 9 and 493 ± 13 Ma and show two well-constrained Concordia ages: 564 ± 1 Ma and 504 ± 4 Ma (Fig. 9A and Supplementary File 3A).

5.2.3. Sample RC-34 (quartz-plagioclase-biotite-garnet paragneiss)
The EMP dating results of this sample includes 86 single analyses in 19 large monazite grains. Fourteen spot analyses refer to monazites enclosed in garnet. RC-34-mz2 (Fig. 5C) with a diameter of 220 μm represents the biggest grain, while smaller ones reach 50 μm (e.g., RC-34-mz15). The Pb content varies between 0.1 (mz10-2) and 0.23 (mz1-4). The Th* values range between 5.82 (mz18-2) and 11.02 (mz4-3). The determined maximal metamorphic age for RC-34 is 609 ± 91 Ma (mz5ig-4) and the minimum is 509 ± 122 Ma (mz10-2).

5.3. U-Pb detrital and metamorphic zircon ages

Despite the peraluminous nature of the studied gneisses, implying derivation from sediments rich in mud fraction, a significant number of detrital zircon grains was recovered and analysed for each sample. We describe the obtained zircon ages and their clusters based on respective Th/U ratios, as well as on grain morphological and internal textural features revealed by CL images (Fig. 6). The age values from detrital grains of magmatic zircons are represented in a relative probability diagram (Fig. 8).

5.3.1. Sample RC-02 (quartz-plagioclase-K-feldspar-biotite-garnet paragneiss)
The 59 zircon grains from RC-02 sample show large variations in size and morphology. Elongated oscillatory-zoned zircons, classified as detrital grains of magmatic origin, reach lengths up to 400 μm and show evidences of fracturing and alteration (Fig. 6). Smaller (up to 200 μm) zircons show CL features of convoluted zoning and clear rim overgrowth. The zircon grains of metamorphic origin are characterised by a homogenous internal structure in CL images. The ages for detrital grains of magmatic origin range between 2803 ± 21 Ma (spot 42.1) and 1803 ± 30 Ma (spot 68.1). In consideration of CL images, Th/U (>0.2) and determined ages, the data from sample RC-02 can be grouped into two main clusters (Fig. 6). The Archaean ages between 2803 ± 21 Ma (spot 42.1, Th/U = 0.71) and 2701 ± 20 Ma (spot 41.1, Th/U = 2.64) make up 8% of the data. The Palaeoproterozoic ages range from 2158 ± 32 Ma (spot 60.1, Th/U = 1.09) to 1803 ± 30 Ma (68.1, Th/U = 0.26), representing 80% of the data (Figs. 6 and 7A). The remaining 12% spots from five zircons yielded metamorphic data with Th/U ratios <0.2, and ages between 591 ± 9 Ma (spot 32.1, Th/U = 0.15) and 584 ± 35 Ma (spot 34.1, Th/U = 0.07, Fig. 9).

5.3.2. Sample RC-03 (quartz-plagioclase-garnet-biotite-K-feldspar paragneiss)
This sample shows elongated zircon grains, varying from 80 to 200 μm in length. The grains characterised by oscillatory zoning and Th/U ratios <0.2 are of magmatic origin (Fig. 6). The ages from detrital grains of magmatic zircons distribute in the following main clusters (Fig. 7B): 87%, Neoproterozoic ages from 987 ± 28 Ma (spot 60.1, Th/U = 0.43) to 614 ± 12 Ma (spot 46.1, Th/U = 0.34); 7%, Palaeoproterozoic ages

Table 2
Summarised results for the metasedimentary samples of the western AROS, n = number of spots.

Sample	Metamorphic conditions		Magmatic zircon ages Ma (n)	Metamorpiczircon age Ma (n)	Monazite age Ma (n)	Hf isotope model ages Ma (n)	ε_{Hf}
	T (C°)	P (kbar)					
RC-02	–	–	2803 ± 21–1803 ± 30 (54)	591 ± 9–584 ± 35 (5)	612 ± 13–482 ± 140 (180)	3530–2440 (22)	−2.2–(−22.7)
RC-03	640–733	6.02–4.22	2632 ± 16–614 ± 11 (104)	618 ± 9–543 ± 6 (12)	613 ± 98–493 ± 13 (112)	3040–740 (39)	+14.9–(−6.7)
RC-30	–	–	–	605 ± 10–546 ± 9 (43)	–	–	–
RC-34	658–625	6.15–4.63	2052 ± 20–1359 ± 16 (31)	621 ± 18–573 ± 27 (17)	609 ± 91–509 ± 122 (83)	–	–
RC-38	680–646	6.43–4.77	1988 ± 46–579 ± 11 (41)	618 ± 8–573 ± 8 (28)	–	2650–2210 (38)	−16.5–(−25.3)
RC-46	655–614	5.67–4.87	1937 ± 29 Ma–592 ± 11 (52)	610 ± 10–581 ± 7 (13)	–	3169–1424 (49)	+17.0–(−23.0)
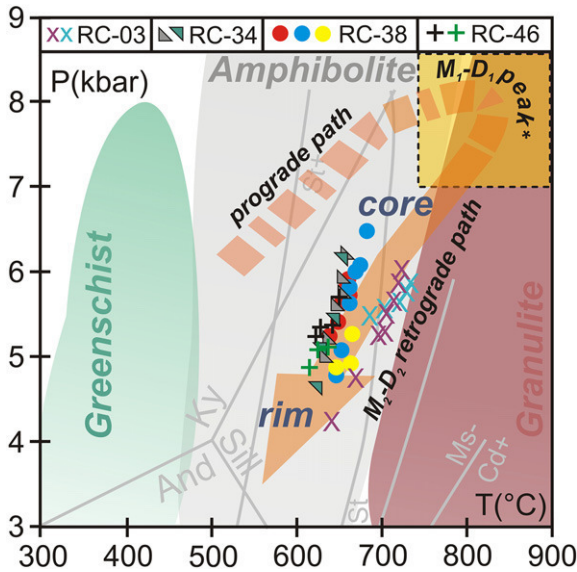
Fig. 4. Metamorphic P-T conditions (calculated after Holdaway, 2001; Wu et al., 2004; Table 2) for the studied paragneisses and referenced data. *Field of M_1-D_1 peak shows metamorphic conditions (850 °C ± 50 °C and 8 kbar ± 1 kbar) presented by Bento dos Santos et al. (2010, 2011). Garnet-biotite thermometer and GASP barometer P-T results enclose an error of ± 50 °C and ± 1 kbar (see text, Table 2 and Supplementary File 3E). Stability fields for kyanite (Ky), andalusite (And), sillimanite (Sil) and staurolite-in (St+); staurolite-out (St−), cordierite-in (Cd+) and muscovite-out (Ms−) are outlined for general orientation by invariant reaction lines (after Spear, 1993). Distinct mineral chemical zonation trends observed in garnet porphyroblasts correspond to segmental trends during garnet crystallisation in limited assemblage with biotite, plagioclase and quartz.

from 2401 ± 33 Ma (spot 10.1, Th/U = 0.54) to 1783 ± 28 Ma (spot 122.1, Th/U = 0.52); 5%, Mesoproterozoic ages from 1051 ± 26 Ma (spot 80.1, Th/U = 0.60) and 1003 ± 28 Ma (spot 16.1, Th/U = 1.21); and only one Archaean grain (spot 66.1, 2632 ± 16 Ma, Th/U = 0.63; Fig. 8).

Several grains show evidence of metamorphic overgrowth at the rims (e.g., 96.1 and 92.1; Fig. 6). A smaller number of rounded grains of metamorphic origin have homogeneous internal structure and low Th/U ratios. Only 13 among 116 analysed grains can be certainly classified as metamorphic (e.g., spot 19.1). The U-Pb ages of the neoformed metamorphic zircons (Fig. 6) range between 611 ± 16 Ma (spot 20.1, Th/U = 0.01) and 543 ± 6 Ma (spot 26.1, Th/U = 0.04) (Fig. 9).

5.3.3. Sample RC-30 (quartz-plagioclase-biotite-garnet-sillimanite paragneiss)

This sample only yielded U-Pb data from metamorphic-anatectic zircon grains. The ages from 43 analytical spots show an almost continuous age range from 605 ± 10 Ma to 546 ± 9 Ma, suggesting Pb loss during metamorphic-anatectic episodes. However, the best calculation gives a metamorphic Concordia age at 576 ± 13 Ma (Fig. 9A and Supplementary File 3B), in good agreement with the climax of the collisional metamorphism in the Araçuaí orogen (Fig. 9).

5.3.4. Sample RC-34 (quartz-plagioclase-biotite-garnet paragneiss)

The 48 zircon grains from sample RC-34 can be subdivided into two main populations. The elongated grains up to 350 μm in length with rounded edges and high Th/U ratios make up the predominant group, and are considered to be detrital grains of magmatic origin (Fig. 6). Overgrowth as metamorphic rims are common and frequently observed (e.g., Zr-02-C-l-08; Fig. 6). In fact, the RC-34 detrital zircon grains with magmatic ages form one main cluster (82%) from 2052 ± 20 Ma (Zr-02-CII-23, Th/U = 0.46) to 1609 ± 30 Ma (Zr-02-CII-31a, Th/U = 0.37; Figs. 7C and 8). Only one grain of Mesoproterozoic age (Zr-02-CII-21, 1359 ± 16 Ma, Th/U 0.41) complete the obtained magmatic ages.

The second population shows smaller grain diameters and indistinct zoned internal structures, representing metamorphic zircons dated between 621 ± 25 Ma (Zr-02-CIII-2, Th/U = 0.03) and 573 ± 27 Ma (Zr-02-CIII-08, Th/U = 0.10; Fig. 9).

5.3.5. Sample RC-38 (quartz-plagioclase-biotite-garnet-sillimanite paragneiss)

According to features from CL images and Th/U ratios of 72 analysed zircon grains, 44 represent detrital grains of magmatic origin. The shape of these grains varies from zoned elongated (44.1; Fig. 6) to smaller rounded grains (60.1; Fig. 6). The maximal length is up to 250 μm. The detrital grains of magmatic origin represent 61% of all grains, and range in age between 1988 ± 46 Ma (spot 68.1, Th/U = 0.10; Fig. 6) and 583 ± 8 Ma (spot 30.1, Th/U = 1.14; Figs. 7D and 8). Most of them are Neoproterozoic grains with ages between 650 ± 13 Ma (spot 65.1, Th/U = 0.65; Fig. 6) and 583 ± 8 Ma (spot 30.1 Th/U = 1.14). A striking feature of sample RC-38 is that no zircon shows metamorphic overgrowth rims, although 30 grains (42%) are characterised by typical features of metamorphic zircon, like low Th/U ratios and homogenous recrystallisation (e.g., spot 6.1). The ages for metamorphic zircon grains vary between 618 ± 8 Ma (spot 10.1, Th/U = 0.05) and 573 ± 8 Ma (spot 52.1, Th/U = 0.01; Fig. 9).

5.3.6. Sample RC-46 (quartz-garnet-K-feldspar-biotite-sillimanite paragneiss)

Among 72 analysed zircon grains, 52 can be considered of magmatic origin, while 20 are metamorphic. The grains generally show lengths up to 200 μm and zoned fragments. Most of the magmatic zircons are characterised by rounded shapes, being interpreted as detrital grains. The metamorphic grains show homogenous soccer ball morphology, typical of high-grade metamorphic rocks (Fig. 6). The detrital grains of magmatic origin range in age from 1937 ± 29 Ma to 592 ± 11 Ma (Figs. 7E and 8), with the following population distribution: 39%, Neoproterozoic ages from 983 ± 17 Ma (spot 27.1, Th/U = 1.11) to 592 ± 11 Ma (spot 21.1, Th/U = 1.34); 25%, Mesoproterozoic ages from 1525 ± 39 Ma (spot 54.1, Th/U = 1.75) to 1027 ± 22 Ma (spot 18.1, Th/U = 0.45); and 7%, Palaeoproterozoic ages from 1937 ± 29 Ma (spot 57.1, Th/U = 0.64) to 1749 ± 36 Ma (spot 59.1, Th/U = 0.69). Metamorphic zircons grains (29%) yielded ages between 610 ± 10 Ma (spot 26.1, Th/U = 0.07) and 581 ± 7 Ma (spot 65.1, Th/U = 0.27, Fig. 9).

5.4. LA-ICP-MS Lu-Hf isotope analysis

The Lu-Hf isotope analyses were performed on detrital zircon grains of magmatic origin in order to obtain robust data to discriminate between crustal and juvenile sources for the paragneiss sedimentary protoliths (Fig. 10). These data can be useful to correlate with possible sources located in distinct magmatic arcs found in the AROS, as well as in other geotectonic sectors of Western Gondwana (Figs. 1 and 11).

5.4.1. Sample RC-02

Among the 22 analysed grains, the Archaean zircons dated at c. 2803 and c. 2751 Ma yielded positive $\varepsilon_{Hf(t)}$ values of + 13.6 and + 7.4, with Hf T_{DM} model ages at 2440 Ma and 2720 Ma, respectively. These $\varepsilon_{Hf(t)}$ values correlate with the depleted mantle value, representing juvenile zircons extracted from mantle sources (Fig. 10). For the remaining 20 detrital grains with magmatic ages between 2124 Ma and 1847 Ma, all $\varepsilon_{Hf(t)}$ values are negative and range from − 2.2 to − 22.7, with Hf T_{DM} model ages from 3530 Ma to 2440 Ma, suggesting sources in a recycled Archaean continental crust.

5.4.2. Sample RC-03

The 39 analysed detrital zircon grains of magmatic origin from sample RC-03 group in three different clusters. Four zircon grains with crystallisation ages of 2632 Ma to 1971 Ma show negative $\varepsilon_{Hf(t)}$ values
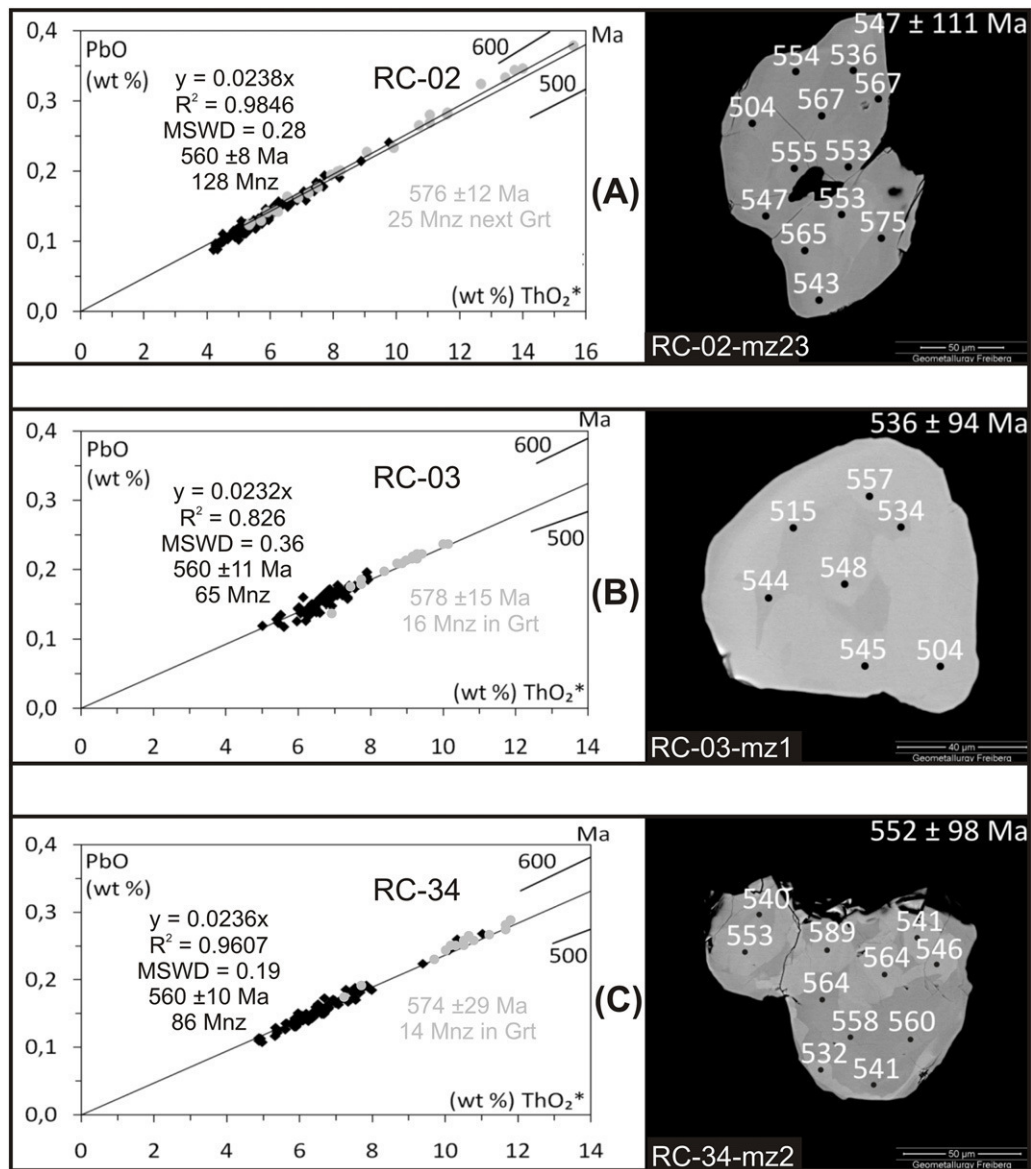
Fig. 5. On the right side of the figure the backscattered electron image (BSE) of dated monazite show grains with zoning, partial alteration and surrounded by biotite. Numbers are single Th-U-Pb ages in Ma (see Supplementary File 3C). Average ages of each grain are given in the up right corner. The left side shows Th-U-Pb chemical model ages of monazite in total PbO vs. ThO_2^* (wt%) isochron diagrams; ThO_2^* is $ThO_2 + UO_2$ equivalents expressed as ThO_2 after (Suzuki et al., 1994). Grey points symbolise analysed monazites next or enclosed to garnet (ages range shown in Fig. 9). Isochrones and errors are calculated from regression forced through zero (Montel et al., 1996; Ludwig, 2003). All monazite mineral data are listed in Supplementary File 3C.

between −0.4 to −4.2, projecting back to moderately juvenile sources of 3040 Ma to 2601 Ma. The three grains of zircons crystallised between 1153 Ma and 1034 Ma show $\varepsilon_{Hf(t)}$ values from positive to negative (+7.7 to −6.7) and Hf model ages from 2050 Ma to 1350 Ma (Fig. 10). The remaining 31 grains with magmatic crystallisation ages between 891 Ma and 614 Ma yielded almost only positive $\varepsilon_{Hf(t)}$ values, ranging between +14.9 to −2.9. They outline a common crustal evolution path projecting back to Hf T_{DM} model ages from 2220 Ma to 700 Ma, indicating mostly juvenile to moderately juvenile sources.

5.4.3. Sample RC-38

The Lu-Hf analyses on 39 age concordant detrital zircons of magmatic origin show distinctive negative $\varepsilon_{Hf(t)}$ values between −16.5 and −25.3, with Hf T_{DM} model ages from 2810 Ma to 2100 Ma, representing sediment sources formed by evolved crustal material (Fig. 10). Two zircons of Palaeoproterozoic crystallisation ages are the

exceptions and show a positive $\varepsilon_{Hf(t)}$ value of +6.5 (juvenile material), as well as a negative one of −6.3, indicating evolved material.

5.4.4. Sample RC-46

The $\varepsilon_{Hf(t)}$ values of the 49 analysed detrital zircon grains of magmatic origin range between +17.3 to −23.0, including contributions from juvenile rocks to evolved crustal sources (Fig. 10). The Hf T_{DM} model ages spread from 2550 Ma to 1690 Ma. The $\varepsilon_{Hf(t)}$ values decrease from positive, in Mesoproterozoic zircons, to strikingly negative $\varepsilon_{Hf(t)}$ values (−8.5 to −23.0) in Ediacaran zircons (Fig. 10). The change of Hf isotopic signatures reflects an evolution from older juvenile to younger evolved sources.

6. Discussions and correlations

Aiming to disclose sediment provenances of paragneisses ascribed to the Andrelândia Group in the AROS, we selected the samples in areas

Fig. 6. Selected CL images of analysed zircon grains arranged in age groups: Archaean, Palaeoproterozoic, Mesoproterozoic and Neoproterozoic (following ICS version 2015). RC-02: Palaeoproterozoic grains show thin metamorphic overgrowth. Metamorphic zircons are characterised by broad sector zoning. RC-03: Rounded magmatic zircons have scattered faint metamorphic overgrowth. Metamorphic zircon (detrital and neoformed) grains have a ball-shaped nature and well-developed sector zoning. RC-34: Magmatic zircons exhibit typical oscillatory zonation and thin chaotic metamorphic rims. The oldest metamorphic zircons are interpreted as high P-T related (see text). RC-38: Most magmatic zircons are elongated and zoned with lengths up to 250 μm. Metamorphic zircon grains show high P-T features and weak zonation. RC-46: Palaeoproterozoic grains have metamorphic rims and are weakly zoned. Metamorphic grains are ball-shaped with high P-T features.

covering a large region from the eastern border of the Araçuaí belt domain to the boundary between the Rio Doce and Rio Negro domains (Figs. 1 and 2). From west to east, the study region covers the basement (Mantiqueira complex) of the lower plate (i.e., the São Francisco basement reworked within the Araçuaí belt domain), the c. 600 Ma Santo Antônio do Grama ophiolitic suite, the Abre Campo suture zone, and the fore-arc to intra-arc zones of the Rio Doce magmatic arc and related (Juiz de Fora and Quirino) basement complexes (Figs. 1 and 2). In the following sections, we first discuss the results on the metamorphism, as a basis to the provenance study approach on the paragneisses.

6.1. Metamorphism

Our results point out very similar metamorphic paths for the studied paragneisses. The new data clearly suggest that all samples underwent the same metamorphic events, constrained by the age distributions for metamorphic zircons and monazites (Figs. 4 and 9; Table 2). According to preceding geological descriptions, the main regional ductile structure recorded by the studied samples is the S_2 foliation, related to the D_2-M_2 fabrics. Unequivocal D_1-M_1 fabrics and mineral assemblages seem to be absent in the studied samples and may be only preserved as trails of mineral inclusions within rotated garnets (Fig. 3). Although, several authors have described a prograde metamorphism (M_1) with P-T conditions of granulite facies (Schultz-Kuhnt, 1985; Trouw et al., 2000, 2013; Noce et al., 2003; Duarte et al., 2004; Heilbron et al., 2003, 2008; Karniol et al., 2009; Bento dos Santos et al., 2010, 2011), our samples

only show a retrograde metamorphic path in amphibolite facies (Fig. 4). Therefore, the mineral assemblages *syn*-kinematic to the S_2 foliation (Fig. 3), like biotite + garnet + feldspars ± sillimanite, provide important evaluations to quantify the P-T conditions of the related M_2 metamorphism. The total absence of muscovite, orthopyroxene and hercynite, as well as the presence of fibrous sillimanite in the studied garnet-biotite paragneisses, are indicators of upper amphibolite facies (Yardley, 2004). According to macroscopic and microscopic features (Fig. 3), the garnets are mostly syn-kinematic to the regional foliation S_2. Therefore, chemical composition variations from garnet cores to rims outline a M_2 P-T path (Fig. 4). The temperatures and pressures recorded by garnet porphyroblasts and porphyroclasts syn-kinematic to the S_2 foliation, with P-T conditions of $T_{max} = 733$ °C and $P_{max} = 6.43$ kbar, are of high-amphibolite facies (Fig. 4; Table 2 and Supplementary File 3E). In addition, our calculated geothermobarometric data clearly support a retrograde P-T path, with garnets starting recrystallisation around 730 °C at 6.4 kbar, along a regular decreasing P-T path down to 610 °C at 4.2 kbar (Fig. 4 and Table 2). Accordingly, the indistinct zonation in the analysed garnets explains the relatively narrow range of calculated temperatures and pressures.

The determined P-T path together with compiled data (quoted in Fig. 4) outline a clockwise decrease of pressure and temperature after peak metamorphic conditions, which is typical of continental collision belts (e.g., Wakabayashi, 2004). There are no significant difference of temperature and pressure given by samples from areas 1 and 2, regarding their locations in relation to the Rio Doce arc (Fig. 2). This suggests
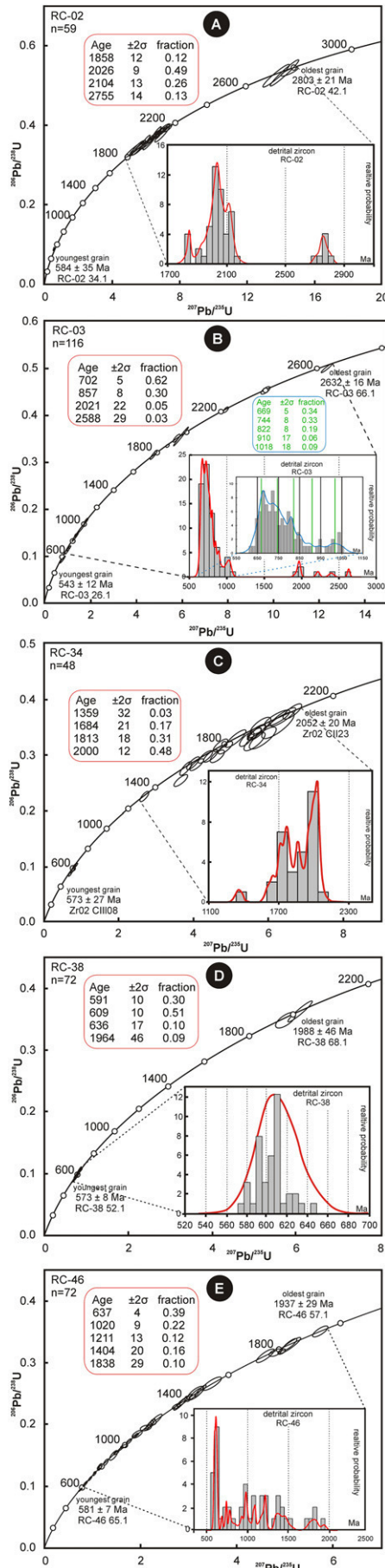
that M_2 metamorphism accompanied the collisional deformation D_2, overprinting previous fabrics and mineral assemblages. Actually, the S_2 foliation completely overprinted the oldest foliation S_1 in our samples, except for some probable S_1 relicts, like the inclusion trails in a rotated garnet found in sample RC-03 (Fig. 3).

In fact, our samples lack sufficient textural evidence to support tectono-metamorphic correlations with precise time intervals within the wide age range shown by our studies. Therefore, it is important to consider the tectonic stages recognised in the Araçuaí belt and Rio Doce arc domains, in order to correlate the obtained metamorphic ages with the regional scenario. These tectonic stages include the pre-collisional (630–585 Ma), collisional (585–535 Ma), and post-collisional (535–480 Ma) time periods (Pedrosa-Soares et al., 2011a; updated with U-Pb ages from Heilbron et al., 2013; Gradim et al., 2014; De Campos et al., 2016; G.O. Gonçalves et al., 2016; L. Gonçalves et al., 2016; Melo et al., 2016; Richter et al., 2016; and Tedeschi et al., 2016). They cover a long-lasting orogenic period (c. 150 Ma) from the earliest pre-collisional to the last post-collisional intrusions, involving different tectonic regimes and requiring distinct heat sources (Pedrosa-Soares et al., 2001, 2011a; Alkmim et al., 2006; Gradim et al., 2014; Tedeschi et al., 2016). Certainly, there are transitions in time and space from one stage to another. Nevertheless, it is very unlikely that the long time span shown by our metamorphic ages represents only one continuous tectono-thermal event.

In fact, the metamorphic zircon and monazite ages for the studied paragneisses also record a long-lasting (c. 621 Ma to c. 480 Ma) orogenic event in the Rio Doce arc domain (Fig. 9). The U-Pb (LA-ICP-MS) ages of metamorphic zircons from area 1 (samples RC-02, RC-03, RC-30 and RC-34; Fig. 2) range between c. 621 Ma to c. 543 Ma, and for area 2 (samples RC-38 and RC-46) from c. 618 Ma to c. 573 Ma (Fig. 9). Although, the wide range of metamorphic zircon ages apparently suggest a continuous time interval (Fig. 9A and B), the data tend to concentrate around two main peaks at 603 ± 2 Ma (49% of the ages values) and 580 ± 1 Ma (51%). This, together with the monazite age distribution and peaks (21%, 584 ± 3 Ma; 57%, 559 ± 2 Ma, 22%, 516 ± 4 Ma; Fig. 9A and B) probably reflects the distinct tectonic stages of the Rio Doce arc domain.

The metamorphic zircon and monazite ages overlap in a wide interval (from c. 613 Ma to c. 543 Ma; Fig. 9), suggesting that they were originated during the same metamorphic events. The oldest metamorphic zircons crystallised around 621–618 Ma, while the oldest monazites included in garnets grew around 613–601 Ma (Fig. 9). The data from monazites found as inclusions in rotated garnets could constrain an age for the M_1 metamorphism around 613–601 Ma (samples RC-03 and RC-34; Figs. 3 and 9). Furthermore, the oldest zircons (c. 621–605 Ma; Fig. 6; sample RC-34) could record the M_1 P-T peak in granulite facies (Fig. 4), because they show soccer ball morphology and high P-T rims with chaotic internal textures (cf. Corfu et al., 2003; Rubatto and Hermann, 2007).

Garnets syn-kinematic to S_2 foliation host the oldest monazites (c. 613–601 Ma) and probably represent M_1. Controversially, these S_2 garnets also contain monazites of the same ages as those found in the rock matrix, ranging from c. 598 Ma to c. 480 Ma (Fig. 9). In such a long time interval it would be hard to constrain the age limits for the M_2 P-T path. However, the sample RC-02 located within the Abre Campo shear zone, at the eastern limit of the lower plate and far from the Rio Doce arc (Fig. 2), shows a narrow age interval (591–584 Ma) for metamorphic zircons. These ages suggest the onset of the M_2 retrograde path around 590 Ma. The youngest metamorphic zircon age constrains the lower boundary of the M_2 retrograde path around 546 Ma (sample RC-30;

Fig. 7. Concordia age diagram for zircons of all samples (A–E), except RC-30. Zoomed is the relative probability age distribution of magmatic zircons and red framed their fraction. Two Palaeoproterozoic grains are not included for sample RC-38. (For interpretation of the references to colour in this figure legend, the reader is referred to the web version of this article.)

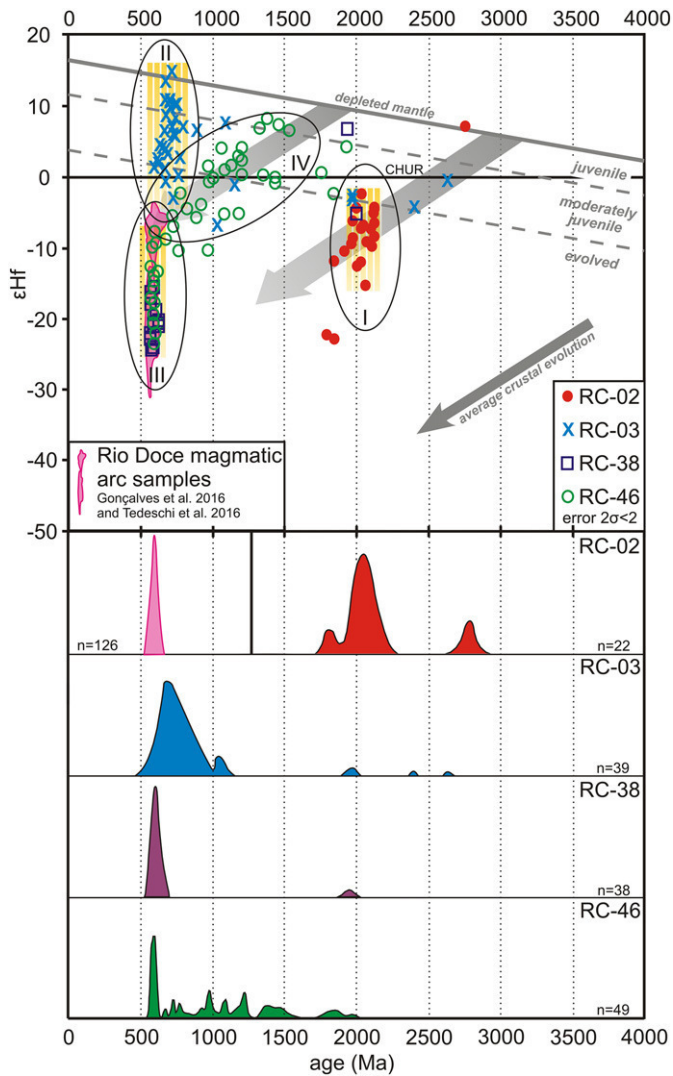Fig. 8. Synopsis of detrital zircon age data for paragneisses from the Andrelândia Group. In the lower part, bar diagrams show distribution of protolith ages in relation to potential source areas, according to the following references: 1, G.O. Gonçalves et al., 2016; L. Gonçalves et al., 2016; 2, Tedeschi et al., 2016; 3, Heilbron, 2012; 4, Heilbron et al., 2013; 5, Tupinambá et al., 2012 (*including data from the Serra da Prata); 6, Queiroga et al., 2007; Queiroga, 2010; 7, Pedrosa-Soares et al., 1998; 8, Tassinari et al., 2001; 9, Schmitt et al., 2008; 10, Tupinambá et al., 2007; 11, Menezes et al., 2012; 12, Tack et al., 2001; 13, Chaves and Correia-Neves, 2005; 14, Chaves et al., 2005; 15, Silva et al., 2008; 16, Tack et al., 2010; 17, Konopásek et al., 2014; 18, Luft et al., 2011; 19, Heilbron et al., 2010; 20, Noce et al., 2007; 21, Silva et al., 2015; 22, André et al., 2009; 23, Albert et al., 2016; 24, Fischel et al., 1998.

Fig. 9), in agreement with the monazite Concordia age for sample RC-02 (547 ± 3 Ma; Fig. 9).

The youngest monazite ages (c. 539 Ma to c. 480 Ma) were obtained from samples RC-02, RC-03 and RC-34, located within or close to the Abre Campo shear zone, and show no correlation with the metamorphic zircon data (Figs. 2 and 9). Although this shear zone is related to the D_3 strike-slip deformation (c. 550–535 Ma; Alkmim et al., 2006), our samples do not show any microscopic evidence that can be related to this fabrics. Therefore, it is possible that the youngest monazites record the D_3 deformation and/or the thermal episode related to the post-collisional collapse of the Araçuaí orogen (Alkmim et al., 2006; Gradim et al., 2014; De Campos et al., 2016).

The presented metamorphic conditions and ages for the studied paragneisses, compared with the compiled literature (cited along the text), allows us to suggest three tectono-thermal phases, as follows (Figs. 4 and 9):

— Phase 1 (c. 621–590 Ma) characterised by the prograde metamorphism that reached the M_1 P-T peak in granulite facies, related to the S_1 foliation. The phase 1 can be correlated with the pre-collisional (subduction-related) to early collisional stages (630–585 Ma) of the Rio Doce arc domain.
— Phase 2 (c. 590–540 Ma) characterised by the M_2 retrograde metamorphism in amphibolite facies, related to the S_2 foliation. The phase 2 seems to cover the late pre-collisional to late collisional stages (585–535 Ma) of the Rio Doce arc domain.
— Phase 3 (c. 540–480 Ma) includes the recrystallisation processes and isotopic resettings related to the D_3 deformation and post-collisional thermal events; both occurring in amphibolite facies, with monazite growth in the rock matrix, and no more zircon recrystallisation and resetting. The phase 3 seems to cover the late collisional escape along regional strike-slip shear zones (e.g., ACsz, Figs. 1 and 2), as well as the post-collisional thermal processes related to the gravitational collapse of the Araçuaí orogen.

6.2. Sediment provenance study

The detailed characterisation of sediment sources is based on U-Pb and Lu-Hf data obtained from detrital zircon grains (Figs. 8, 10 and Supplementary File 3D). The main candidates of sediment sources are the basement complexes and related supracrustal units older than 1 Ga, found in the AROS and São Francisco craton, as well as the Neoproterozoic rocks from AROS precursor basins and magmatic arcs. Indeed, the chrono-correlated units located in Africa should be considered as potential sediment sources as well (Fig. 11; Table 3 and Supplementary File 1).

For provenance studies, we use data from samples the RC-02, RC-03, RC-34, RC-38 and RC-46 (Fig. 8). As all grains from sample RC-30 are interpreted as neoformed metamorphic-anatectic zircons they are not considered here (Supplementary File 3A). Samples RC-02 and RC-34 show the same geochronological pattern, both lacking Neoproterozoic detrital grains and with most grains with Palaeoproterozoic ages (Fig. 8). For samples RC-03, RC-38, RC-46 most detrital grains yield Neoproterozoic ages (Table 2), although their Lu-Hf signatures are surprisingly contrasting in relation to the most probable sources (Fig. 10).

Fig. 9. Comparison of metamorphic timing and deformation in the studied paragneisses. A, Concordia ages for metamorphic zircons and monazites (2σ applied for all calculations and include decay constant error): 1, MSWD = 0.00029, Probability = 0.99; 2, MSWD = 0.03, Probability = 0.86; 3, MSWD = 0.116, Probability = 0.73; 4, MSWD = 0.0048, Probability = 0.94; 5, MSWD = 0.082, Probability = 0.78; 6, MSWD = 0.0072, Probability = 0.93; 7, MSWD = 0.091, Probability = 0.76; 8, MSWD = 0.0077, Probability = 0.93; 9, MSWD = 0.74, Probability = 0.39; 10, MSWD = 0.80, Probability = 0.37; 11, MSWD = 0.49, Probability = 0.48. B, U-Pb age histogram distribution and outlined peaks of metamorphic zircons (orange) and monazites (grey). C, Breakdown of age distribution for single samples and applied analytical method. Vertical bars represent calculated age distributions; limited values above them are ages in Ma. Tectono-thermal phases: 1, c. 621–590 Ma; 2, c. 590–540 Ma; 3, c. 540–480 Ma. (For interpretation of the references to colour in this figure legend, the reader is referred to the web version of this article.)

Generally, the four investigated samples show different sets of Hf data (Fig. 10). In fact, we did not expected all those contrasting spectra of detrital zircon ages and Lu-Hf signatures because all samples were collected from the same regional lithostratigraphic unit, the Andrelândia Group.

The age spectra for samples RC-02 and RC-34 (Figs. 8 and 10) show great influence of Rhyacian-Orosirian sediment sources, with ages comparable to those found in the surrounding basement domains (Figs. 8 and 11). This, together with the absence of Neoproterozoic grains, suggest that the samples represent a precursor basin formed before the Rio Negro and Rio Doce magmatic arcs burst upon the scene (Figs. 1 and 12A). The Hf data for sample RC-02 point out a remelting process of a crust originated in the Archaean, with most zircon grains showing very negative $\varepsilon_{Hf(t)}$ values (−5 to −25; Fig. 10-I). The two Archaean detrital grains from sample RC-02 show $\varepsilon_{Hf(t)}$ values of depleted mantle. Grains in the striped field around 2200–1900 Ga (Fig. 10) indicate a combination of materials with the same age but from different sources, i.e., one source of evolved material originated from reworked Archaean crust and the other source of moderately juvenile rocks (Fig. 10). The best candidate to be a source largely formed by reworked Archaean crust is the Mantiqueira complex (2.14–2.04 Ga; $\varepsilon_{Nd(t)} = -9$ to −13; Table 3; Fischel et al., 1998; Noce et al., 2007; Heilbron et al., 2010), representing a continental magmatic arc formed on the eastern margin of the São Francisco palaeocontinental block. Sources for the grains with less negative $\varepsilon_{Hf(t)}$ values (zero to −5) are the Juiz de Fora and Pocrane complexes, formed in an essentially juvenile arc system (2.2–1.9 Ga; $\varepsilon_{Nd(t)} = +7.70$ to −3.5; $\varepsilon_{Hf(t)} = +2.5$ to −4.3; Table 3; Fischel et al., 1998; Noce et al., 2007; André et al., 2009; Heilbron et al., 2010; Novo, 2013; Albert et al., 2016).

In this scenario, samples RC-02 and RC-34 would represent a basin related to the passive margin located in the eastern border of the São Francisco palaeocontinental block (Fig. 11). The youngest concordant zircon from sample RC-34 (1359 ± 16 Ma) suggest the maximum depositional age for that AROS precursor basin.

The sample RC-03 records a completely different U-Pb and Lu-Hf dataset in relation to the above described samples. Neoproterozoic ages between c. 1000 Ma and 614 Ma represent 92% of the detrital zircon grains (Figs. 7B and 8). The youngest detrital grains dated around 614 Ma constrain the maximum sedimentation age for this paragneiss protolith. Nearly all Neoproterozoic detrital grains younger than 1 Ga show positive $\varepsilon_{Hf(t)}$ values (+14.9 to +0.3), including the youngest ones with ages of c. 614 Ma ($\varepsilon_{Hf(t)} = +2.0$; Figs. 6 and 10-II). This implies that even the youngest grains require Neoproterozoic juvenile sources. The best AROS candidate to be a Neoproterozoic juvenile source rich in zircon is the Rio Negro-Serra da Prata magmatic arc system (Figs. 8 and 11). It is considered as an arc system related to intra-oceanic subduction between c. 900 and c. 630 Ma (Fig. 12A), with granitic rocks showing whole-rock $\varepsilon_{Nd(t)}$ values of +5 to −3 (Table 3; Heilbron, 2012; Tupinambá et al., 2012). Indeed, the AROS ophiolite complexes (e.g., RF-SJS-DS and SAG; Figs. 1, 2, 8 and 11) are also possible sources for juvenile zircons aging c. 660 to c. 600 Ma ($\varepsilon_{Nd(t)} = +6.50$ to +1.08; Table 3; Pedrosa-Soares et al., 1992, 1998; Tassinari et al., 2001; Queiroga et al., 2007; Schmitt et al., 2008; Queiroga, 2010). Although

Fig. 10. Hf isotope data for magmatic zircons from AROS paragneisses. Reference lines on Hf plot are as followed: CHUR chondritic uniform reservoir (Bouvier et al., 2008). Grey dashed lines classify fields of juvenile (0–5 ε-units below DM), moderately juvenile (5–12 ε-units below DM) and evolved (>12 ε-units below DM; Bahlburg et al., 2011). Vertical striped fields characterise interpreted mixing of material with different Hf isotope composition. Encircling fields I–IV: RC-02 (I) is mostly composed of reworked Archaean basement crust with negative $\varepsilon_{Hf(t)}$ values. RC-03 (II) shows moderate juvenile to juvenile sources with positive $\varepsilon_{Hf(t)}$ interfused of minor material of non-juvenile origin. RC-38 (III) and RC-46 (III and IV) contain material of mainly evolved crust composition with strong negative $\varepsilon_{Hf(t)}$ values. For further interpretation see text.

the youngest detrital zircons (c. 630–614 Ma) from sample RC-03 remember ages of the Rio Doce arc, no positive $\varepsilon_{Hf(t)}$ nor $\varepsilon_{Nd(t)}$ value was yet reported for this arc ($\varepsilon_{Hf(t)}$ = −4.31 to −30.15; Table 3; Figs. 10 and 11; G.O. Gonçalves et al., 2016; L. Gonçalves et al., 2016; Tedeschi et al., 2016). In fact, the sample RC-03 requests a more complex palaeogeographic-palaeotectonic explanation, because it is the first evidence of an important sediment contribution from the Rio Negro-Serra da Prata arc system to a basin related to the Rio Doce arc domain (Figs. 2, 11 and 12). This requires that the juvenile Rio Negro-Serra da Prata arc system (an intra-oceanic island arc) was relatively close, if not completely amalgamated, to the Rio Doce arc domain before c. 614 Ma (age of the youngest detrital zircon grains with positive $\varepsilon_{Hf(t)}$). Actually, this is a realistic possibility in view of the available data, since Tupinambá et al. (2012) demonstrated that the stage strictly related to ocean-ocean subduction in the Rio Negro arc lasted until c. 630 Ma. In this scenario, it is possible that the Rio Negro arc started to collide with the Rio Doce arc domain between 630 Ma and 614 Ma and

supplied sediments to a basin related to the Rio Doce arc domain (Fig. 12). This was probably an orogenic arc-related basin, because the Rio Doce magmatic arc was already rising during that time. However, it would have been a short-lived basin with the sedimentation timing bracketed by the youngest detrital grains (c. 614 Ma) and the oldest neoformed metamorphic zircons (c. 611 Ma; Figs. 6, 7, 8, 9 and Supplemental File 3A).

In contrast to the scenario suggested by sample RC-03, the sample RC-38 shows 82% detrital grains within the time interval (c. 630–590; Fig. 8) of the Rio Doce arc ages for magmatic crystallisation, all of them with negative $\varepsilon_{Hf(t)}$ values (−15 to −25; Fig. 10-III). It implies that the RC-38 protolith was sediment of the far most important source in the Rio Doce arc domain, representing a probable intra-arc basin.

Sample RC-46 brought a further surprise, as it shows a very wide spectrum of ages (Fig. 8) and a distribution of positive and negative $\varepsilon_{Hf(t)}$ values very distinct relation to the other studied samples, implying a rather complex provenance interpretation (Fig. 10). All detrital grains with ages around 610 Ma and $\varepsilon_{Hf(t)}$ negative (−5 to −25) have significant overlaps with grains of sample RC-38 (Figs. 8 and 10-III) and can be related to sources located in the Rio Doce arc (Table 3). The grains with ages from c. 900 Ma to c. 630 Ma and positive to moderately negative $\varepsilon_{Hf(t)}$ values suggest sources located in the Rio Negro – Serra da Prata arc system. Most intriguing is the significant number (30%) of Mesoproterozoic to Early Tonian detrital grains with $\varepsilon_{Hf(t)}$ values from significantly positive (+10; Fig. 10-IV) to around zero. There is no yet known possible juvenile source of this age in the studied region, excluding some small metamafic and meta-ultramafic bodies (Angeli et al., 2001; Novo, 2013). Other possible sources to explain those $\varepsilon_{Hf(t)}$ values are the Mesoproterozoic-Tonian mafic dyke swarms ($\varepsilon_{Nd(t)}$ = −0.3 to −1; Chaves and Correia-Neves, 2005) and the Early Tonian rift-related bimodal magmatism ($\varepsilon_{Nd(t)}$ = −0.53 to −14; Tack et al., 2001; Tupinambá et al., 2007; Silva et al., 2008; Gradim et al., 2012; Menezes et al., 2012; Chaves et al., 2014) found in the São Francisco-Congo craton and Araçuaí-West Congo orogen (Figs. 8 and 10-IV). Despite the long distance in relation to AROS, the Karagwe-Ankole-Kibaran belt in the Congo-Burundi region show positive $\varepsilon_{Hf(t)}$ values (+6.2 to +0.2) for Mesoproterozoic granitic rocks (Table 3; Tack et al., 2010) suggesting another possible source for sample RC-46 (Figs.8 and 11). In this regard, Porada (1989) and Ernst et al. (2013) suggested the transport of detrital sediments from the Karagwe-Ankole-Kibaran belt to the western border of the Angola block, which is an AROS basement counterpart located in Africa. A further less distant, essentially juvenile sources of Late Orosirian ages with $\varepsilon_{Nd(t)}$ from +4.3 to −2.05 are found in the Kaoko belt (Luft et al., 2011; Konopásek et al., 2014; Table 3; Fig. 11). The other way round, sample RC-46 could display the whole overlapping evolution from juvenile to evolved signatures of the magmatic arc domains. This would correspond to published data of the Rio Negro arc by Tupinambá et al. (2012) that describes Nd isotopic signatures from $\varepsilon_{Nd(t)}$ = +5 to −3, for the less evolved c. 790–620 Ma diorites to granodiorites, changing down to $\varepsilon_{Nd(t)}$ = −3 to −14, for the c. 610–605 Ma shoshonitic granites.

6.3. Conclusions

The presented datasets and correlations, complemented by a thorough data compilation from the literature, encourage the authors to discuss some hints to disclose palaeogeographic-palaeotectonic scenarios before and during the Western Gondwana amalgamation (Figs. 11 and 12). For the sake of simplicity, we avoid to repeat references frequently quoted in the previous items.

The studied paragneisses disclose a broad scenario of sediment sources (Figs. 8 and 11), all of them situated in crustal pieces that formed the central-eastern region of Western Gondwana after the Brasiliano – Pan-African collisional event (Cordani et al., 2003; Tohver et al., 2006; Frimmel et al., 2011). Many of those pieces represent basement domains already bounded within the São Francisco – Congo
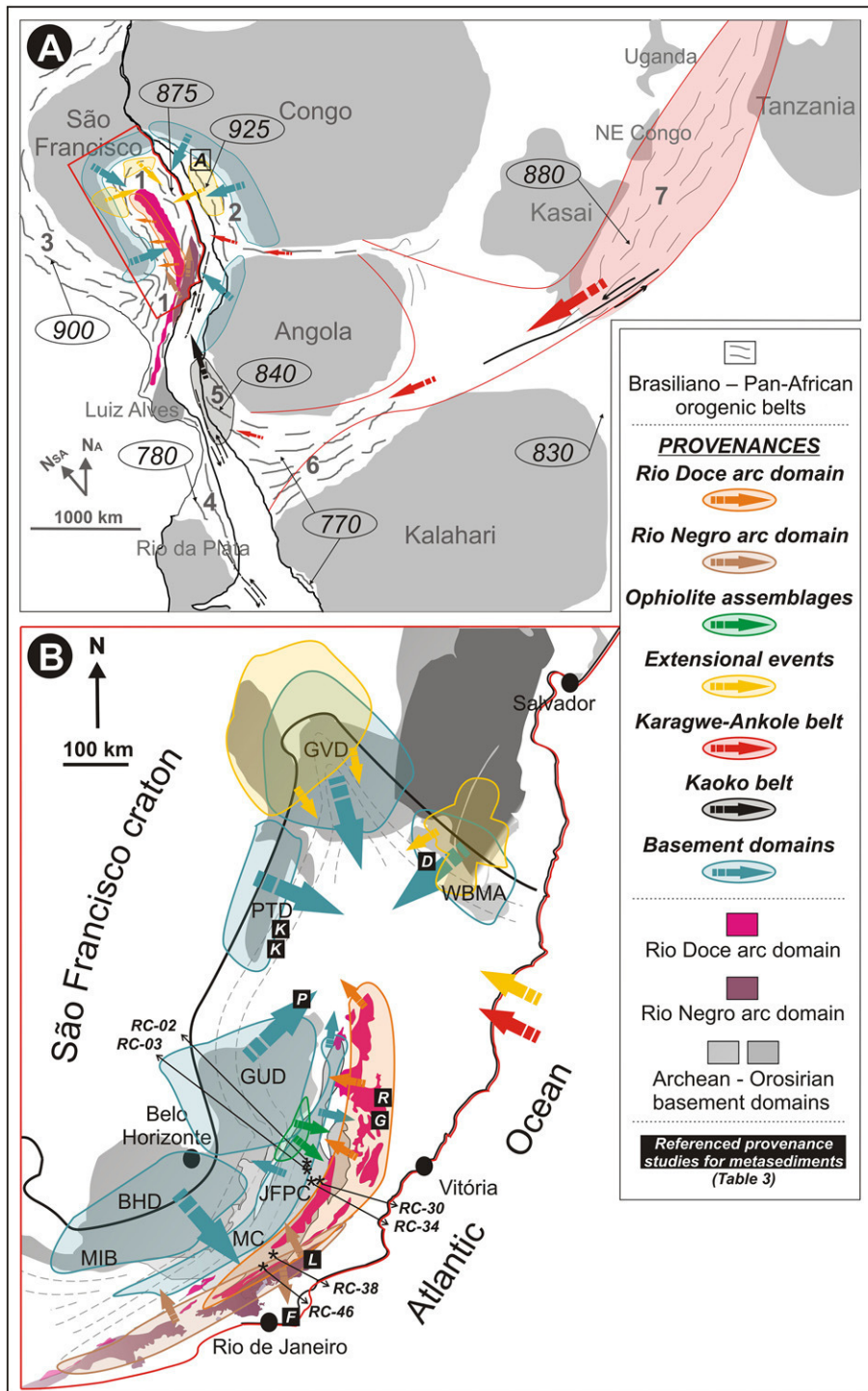
Fig. 11. Simplified maps showing possible provenances for the studied paragneisses in the AROS. Arrows and shapes represent probable primary sources and their sediment transport towards the accumulation basins in the AROS. Maps are compiled from Porada, 1989; Heilbron et al., 2010; Ernst et al., 2013; Silva et al., 2015. A – Integrated map of SE Brazil and central western Africa. Legend: Brasiliano – Pan-African orogenic belts: 1 AROS, 2 West Congo and Kimezian, 3 Brasília, 4 Dom Feliciano, 5 Kaoko, 6 Damara, 7 Karagwe-Ankole (Mesoproterozoic). Circled numbers represent rift events (Ma) after Gaucher et al., 2009; Frimmel et al., 2011. B – Zoomed AROS region surrounded by the São Francisco craton and Archaean to Orosirian basement domains/complexes, after Silva et al., 2015: WBMA - Western Bahia magmatic arc, GVD - Gavião domain, PTD - Porteirinha domain, GUD - Guanhães domain, BHD - Belo Horizonte domain, MIB - Mineiro belt, MC - Mantiqueira complex, JFPC - Juiz de Fora-Pocrane complex. Data references for each primary sediment source are presented in Table 3.

palaeocontinent around 2 Ga, and acted as sediment suppliers for the AROS precursor basins (Fig. 12). In this scenario, samples RC-02 and RC-34 (area 1), even with far more sediment contributions from the Rhyacian-Orosirian basement complexes, suggest a mixed sediment provenance for an AROS precursor basin (Figs. 11 and 12). Their age

spectra and Hf isotopic signatures (Figs. 8 and 10) indicate massive sediment contribution of the Mantiqueira continental arc, located to the west of the Abre Campo suture (Fig. 1), and of the juvenile Juiz de Fora – Pocrane magmatic arc, placed to the east of the suture (Fig. 11). This mixed provenance suggests a basin fill before the Late Cryogenian

Table 3

Sediment provenances characteristics compilation for AROS metasedimentary rocks (regarded to Fig. 11). U-Pb ages in Ma are the time intervals of possible detrital zircons and their main lithology. Age data and geochemical signatures ($\varepsilon_{Hf(t)}$ and $\varepsilon_{Nd(t)}$) are cited from references 1–24 (Fig. 8). The referenced provenance studies are those located in Fig. 11 with recognition of pointed out sources (framed letters: L – Lobato et al., 2015; F – Fernandes et al., 2015; A – Affaton et al., 2015; R – Richter et al., 2016; G – Gradim et al., 2014; P – Peixoto et al., 2015; D – Gonçalves-Dias et al., 2011; K – Kuchenbecker et al., 2015. Last column allocates analysed samples to described provenances (see text).

Provenance	Ages (Ma)	Lithologies	Geochemical signature	Reference	Zircon ages in study (Fig. 11)	Sample
Rio Doce arc domain	c. 630–556	Tonalitic to granodioritic batholiths	$\varepsilon_{Hf(t)}$ −4.31–(−30.15)[1,2] $\varepsilon_{Nd(t)}$ −5.5–(−11.1)[3,4]	1, 2, 3, 4	F, R, G, P	RC-38, RC-46
Rio Negro arc domain	c. 860–600	Granitoids	$\varepsilon_{Nd(t)}$ +5–(−3)[5]	5	L, F, R, G, P	RC-03, RC-46
Ophiolite assemblages	c. 660–630	Meta-ultramafic and metamafic	$\varepsilon_{Nd(t)}$ +6.50–+1.08[6,7]	6, 7, 8, 9	F, R, G, P	RC-38, RC-46
Extensional events	c. 1780–680	Granitoids, dykes, mafic-ultra mafic	$\varepsilon_{Nd(t)}$ −0.53–(−14)[12]	10, 11, 12, 13, 14, 15	A, D, K	RC-03, RC-46
Karagwe-Ankole belt	c. 1380–1370	Granitoids, gneisses	$\varepsilon_{Nd(t)}$ +6.2–+0.2[16]	16	A, D, K	RC-46
Kaoko belt	c. 1700–1800	Amphibolites, metasediments	$\varepsilon_{Nd(t)}$ +4.3–(−2.05)[17]	17, 18	L, F, A, R, G, P, D	RC-02, RC-03, RC-34
Archaean–Orosirian basement	c. 3500–1800	Orthogneisses	$\varepsilon_{Nd(t)}$ +7.70[22] $\varepsilon_{Nd(t)}$ −0.78–(−10.88)[21] $\varepsilon_{Nd(t)}$ −0.4–(−13.0)[20] $\varepsilon_{Hf(t)}$ +2.5–(−4.3)[23]	19, 20, 21, 22, 23, 24	L, F, A, G, P, D, K	RC-02, RC-03, RC-34, RC-38

oceanic opening in the precursor basin system of the Araçuaí-West Congo rift 2 (Fig. 12B).

The Neoproterozoic magmatic arcs point to very distinct palaeotectonic and palaeogeographic scenarios. According to the literature, the Rio Negro – Serra da Prata arc system represents a long-lived (c. 860–605 Ma), essentially juvenile orogenic system (an island arc), and implying intra-oceanic subduction in a relatively large ocean (Figs. 11 and 12A–B). Its youngest juvenile rocks (c. 630 Ma) suggest an end for the ocean-ocean subduction stage in Early Ediacaran time. This arc system is the most probable source for the abundant juvenile zircon grains of Tonian to Ediacaran ages, together with the minor contribution from AROS ophiolitic complexes. Our sample RC-03 provides an outstanding example of such a juvenile contribution of the Rio Negro-Serra da Prata arc system to a sedimentary basin located in the Rio Doce arc domain (Figs. 8 and 10). Despite some Late Cryogenian to Early Ediacaran zircon grains with positive $\varepsilon_{Hf(t)}$ values that can be supplied from ophiolitic rocks, the RC-03 zircon age spectrum represents sediments of widespread juvenile Hf signature in a time span reaching the Early Tonian. It implies that a long-lived source rich in juvenile granitic rocks, like the Rio Negro – Serra da Prata arc system, supplied most sediments for the RC-03 protolith. If this is correct, it strongly suggests that the Rio Negro – Serra da Prata arc system was close to, if not completely amalgamated with the Rio Doce arc domain just before c. 614 Ma, the age of the youngest juvenile zircon grains (Fig. 12). The ages from these grains compared to the oldest neoformed metamorphic zircons suggest a very short-lived basin, limited in time between c. 614 Ma and c. 611 Ma, and located in the western region of the Rio Doce arc domain (Figs. 1, 2 and 12). Therefore, the metamorphic zircons aging around 611–600 Ma (RC-03; Figs. 6 and 9) also suggest that sediments underwent the pre-collisional metamorphism in the fore-arc (subduction wedge?) region of the growing Rio Doce arc (see Peixoto et al., 2015, and Tedeschi et al., 2016). According to Schmitt et al. (2008, 2016) and Fernandes et al. (2015), the Cabo Frio domain includes the back-arc Palmital basin and a c. 608 Ma ophiolite, which would have been formed during the convergence and amalgamation of the Rio Negro and Rio Doce arc domains (Figs. 1 and 12).

The Rio Doce magmatic arc developed between c. 630 Ma and c. 580 Ma, on an active continental margin located to the west of the Rio Negro arc system (Figs. 1 and 12). That active continental margin represented the western border of the upper plate located to the east of the AROS ophiolitic belt (e.g., RF-SJS-DS and SAG; Fig. 1). Samples RC-38 and RC-46 recorded very significant contributions of the Rio Doce arc, but they seem to represent very distinct palaeogeographic scenarios. With >90% of zircon grains in the time span of the Rio Doce arc, most of them with strongly negative $\varepsilon_{Hf(t)}$ values, sample RC-38 suggests an intra-arc sedimentation (Fig. 11).

Conversely, the wide age spectrum of RC-46, linked to the mostly positive $\varepsilon_{Hf(t)}$ values for Mesoproterozoic zircons (c. 1.5 to 1 Ga) shifting to only negative $\varepsilon_{Hf(t)}$ values for Neoproterozoic zircon grains, indicate a complex provenance picture (Figs. 10 and 11). A possible source for all those positive $\varepsilon_{Hf(t)}$ Mesoproterozoic zircons is the Karagwe-Ankole-Kibaran belt and related sedimentary deposits. That source suggests a long distance transport of sediments in Western Gondwana (Fig. 11). The best sediment source candidates for the negative $\varepsilon_{Hf(t)}$ zircon grains of Tonian and Cryogenian ages are the anorogenic igneous rocks related to the Araçuaí-West Congo precursor rifts (i.e., Macaúbas rift 1 and 2; Pedrosa-Soares and Alkmim, 2011; Kuchenbecker et al., 2015) (Fig. 12). Finally, the detrital zircon grains with ages in the range of 630–592 Ma, all of them with negative $\varepsilon_{Hf(t)}$ values, outline a track similar to the Hf signature of the Rio Doce arc, but can also include contributions from the late shoshonitic granites of the Rio Negro arc (Fig. 10). The youngest detrital grains constrain the maximum sedimentation age around 592 Ma (RC-46; Supplementary File 3A). This basin, located in the southeastern Rio Doce arc region, close to the central tectonic boundary (CTB, Fig. 1) and the Rio Negro arc domain, records a complex mixture of sediments with a wide age spectrum (c. 592–1937 Ma). It involves materials of Palaeoproterozoic and Mesoproterozoic sources located in Africa, of Tonian-Cryogenian precursor rifts, and of the Rio Negro and Rio Doce arcs. This suggests a shift from passive to active margin settings, followed by land connections promoted by convergence and collision. These conditions would allow a complex sediment transport and mixture, during the late amalgamation of Western Gondwana.

According to some authors (e.g., Heilbron et al., 2008; Tupinambá et al., 2012) and our data, the Neoproterozoic pre-collisional palaeogeographic scenario requires a large space separating the palaeocontinental blocks represented in the AROS region and its counterparts located in Africa, allowing to the development of an intra-oceanic arc system. All those crustal pieces were involved in a complex system of sediment transportation and distribution, during Western Gondwana amalgamation. The age data for the collisional event indicate that Western Gondwana amalgamation was virtually synchronous and accomplished by the Ediacaran-Cambrian boundary, in the study region.

Supplementary data to this article can be found online at http://dx.doi.org/10.1016/j.gr.2017.07.004.
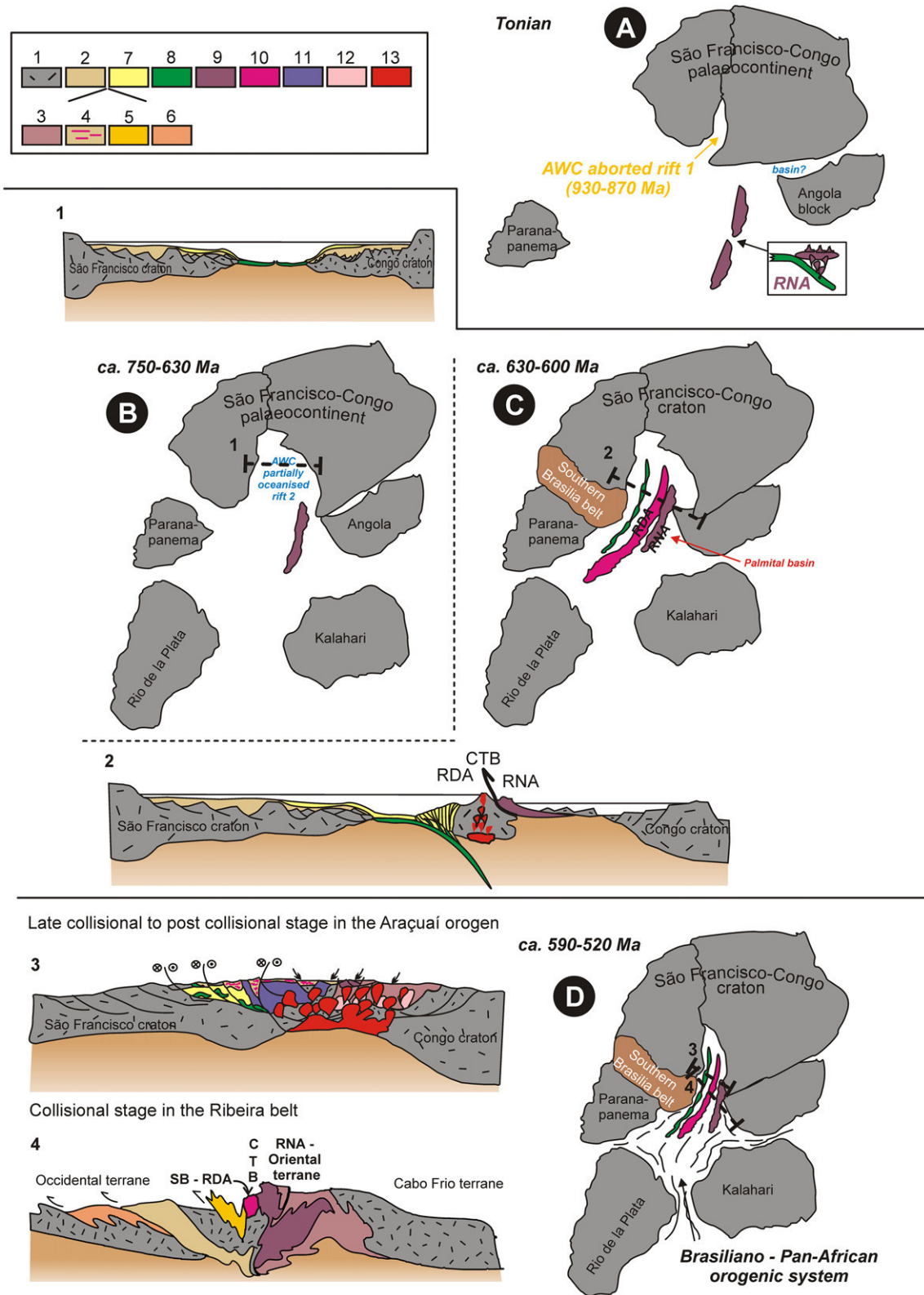
Fig. 12. Cartoon illustrating an evolutionary scenario for the Western Gondwana landmasses during the development of the precursor basins, magmatic arcs and final closure of the AROS (based on our and in Trompette, 1994; Pedrosa-Soares et al., 2001, 2008, 2011a; Tack et al., 2001; Cordani et al., 2003; Alkmim et al., 2006; Heilbron et al., 2008, 2013; Schmitt et al., 2008; Pedrosa-Soares and Alkmim, 2011; Frimmel et al., 2013). A, Tonian scenario: the palaeocontinental blocks, the Rio Negro - Serra da Prata intra-oceanic arc system in a large Adamastor Ocean, and the first Araçuaí-West Congo aborted rift (Macaúbas rift 1). B, Late Tonian-Cryogenian scenario: oceanic opening following the Araçuaí-West Congo (Macaúbas) rift 2, while the Rio Negro - Serra da Prata arc keeps evolving and the large Adamastor Ocean starts to close further to the south. C, Early Ediacaran scenario: formation of the Rio Doce magmatic arc and ophiolite emplacement followed by convergence and collision of the Rio Negro - Serra da Prata arc and the Rio Doce arc domains. D, Ediacaran-Cambrian scenario: Western Gondwana amalgamation in the late collisional stage (ca. 540 Ma) followed by post-collisional processes. 1, continental basement; 2, precursor basin sediments; 3, Rio Negro arc related rocks; 4, Rio Doce arc related metasediments; 5, metasediments of the Paraíba do Sul group; 6, Neoproterozoic metasedimentary rocks; 7, deep-sea sediments; 8, oceanic crust (ophiolites); 9, Rio Negro magmatic arc (including Serra da Prata magmatic arc); 10, Rio Doce magmatic arc; 11, G1 supersuite; 12, G2 and G3 supersuites; 14, G5 supersuite.

Heilbron, M., Tupinambá, M., Duarte, B., Eirado, L., Nogueira, J., Prado, J., Sucena, M., 2003. Geologia da Folha Leopoldina (SF.23-X-D-V). Belo Horizonte, COMIG/UFMG/UFRJ/UERJ - Projeto Sul de Minas, escala 1:100.000.

Heilbron, M.L., Pedrosa-Soares, A.C., Campos Neto, M.C., Silva, L.C., Trouw, R., Janasi, V.A., 2004. Brasiliano orogens in southeast and south Brazil. Journal of the Virtual Explorer 17 (Paper 4).

Heilbron, M., Valeriano, C., Tassinari, C., Almeida, J.C.H., Tupinamba, M., Siga Junior, O., Trouw, R., 2008. Correlation of Neoproterozoic terranes between the Ribeira Belt, SE Brazil and its African counterpart: comparative tectonic evolution and open questions. In: Pankhurst, R.J., Trouw, R.A.J., Brito Neves, B.B., DeWit, M.J. (Eds.), West Gondwana Pre-cenozoic Correlations across the South Atlantic Region. Geological Society London Special Publications 294, pp. 211–237.

Heilbron, M., Duarte, B., Valeriano, C., Simonetti, A., Machado, N., Nogueira, J., 2010. Evolution of reworked Paleoproterozoic basement rocks within the Ribeira belt (Neoproterozoic), SE-Brazil, based on U Pb geochronology: implications for paleogeographic reconstructions of the Sao Francisco-Congo paleocontinent. Precambrian Research 178, 136–148.

Heilbron, M., Tupinambá, M., Valeriano, C.M., Armstrong, R., Do Eirado Silva, L.G., Melo, R.S., Simonetti, A., Pedrosa-Soares, A.C., Machado, N., 2013. The Serra da Bolívia complex: the record of a new Neoproterozoic arc-related unit at Ribeira belt. Precambrian Research 238, 158–175.

Holdaway, M.J., 2001. Recalibration of the GASP geobarometer in light of recent garnet and plagioclase activity models and versions of the garnet-biotite geothermometer. American Mineralogist 86, 1117–1129.

Jackson, S.E., Pearson, N.J., Griffin, W.L., Belousova, E.A., 2004. The application of laser ablation-inductively coupled plasma-mass spectrometry to in situ U-Pb zircon geochronology. Chemical Geology 211, 47–69.

Juliani, C., Hackspacher, P., Dantas, E.L., Fetter, A.H., 2000. The Mesoproterozoic volcano-sedimentary Serra do Itaberaba Group of the Central Ribeira Belt, Sao Paulo State, Brazil: implications for the age of the overlying São Roque Group. Revista Brasileira de Geociencias 30, 82–86.

Karniol, T.R., Machado, R., Bilal, E., Moutteet, J., 2009. Geothermobarometry of granulites and aluminous gneisses in the Italva - Patrocínio do Muriaé section, northern Rio de Janeiro. Revista Brasileira de Geociencias 39, 519–532.

Konopásek, J., Košler, J., Sláma, J., Janoušek, V., 2014. Timing and sources of pre collisional Neoproterozoic sedimentation along the SW margin of the Congo Craton (Kaoko Belt, NW Namibia). Gondwana Research 26, 386–401.

Kuchenbecker, M., Pedrosa-Soares, A.C., Babinski, M., Fanning, M., 2015. Detrital zircon age patterns and provenance assessment for pre-glacial to post-glacial successions of the Neoproterozoic Macaúbas Group, Araçuaí orogen, Brazil. Precambrian Research 266, 12–26.

Liu, Z.C., Wu, F.Y., Yang, Y.H., Yang, J.H., Wilde, S.A., 2012. Neodymium isotopic compositions of the standard monazites used in U-Th-Pb geochronology. Chemical Geology 334, 221–239.

Lobato, M., Heilbron, M., Torós, B., Ragatky, D., Dantas, E., 2015. Provenance of the Neoproterozoic high-grade metasedimentary rocks of the arc-related oriental terrane of the Ribeira belt: implications for Gondwana amalgamation. Journal of South American Earth Sciences 63, 260–278.

Ludwig, K.R., 2003. User's Manual for Isoplot 3.00 A Geochronological Toolkit for Excel. Special Publication Number 4Berkeley Geochronological Center, p. 71.

Luft Jr., J.L., Chemale Jr., F., Armstrong, R., 2011. Evidence of 1.7- to 1.8-Ga collisional arc in the Kaoko Belt, NW Namibia. International Journal of Earth Sciences 100, 305–321.

Martignole, J., Nantel, S., 1982. Geothermobarometry of cordierite-bearing metapelites near the Morin anorthosite complex, Grenville province, Quebec. The Canadian Mineralogist 20, 307–318.

Meira, V.T., Garcia-Casco, A., Juliani, C., Almeida, R.P., Schorscher, J.H.D., 2015. The role of intracontinental deformation in supercontinente assembly: insights from the Ribeira Belt, southeastern Brazil (Neoproterozoic West Gondwana). Terra Nova 27, 206–217.

Melo, M.G., Stevens, G., Lana, C., Pedrosa-Soares, A.C., Frei, D., Alkmim, F.F., Alkmin, L.A., 2016. Two cryptic anatectic events within a syn-collisional granitoid from the Araçuaí orogen (southeastern Brazil): evidence from the polymetamorphic Carlos Chagas batholith. Lithos 277, 51–71.

Menezes, R.C.L., Conceição, H., Rosa, M.L.S., Macambira, M.J.B., Galarza, M.A., Rios, D.C., 2012. Geoquímica e Geocronoligia de granitos anorogênicos Tonian (ca. 914–899 Ma) da Faixa Araçuaí no Sul do estado da Bahia. Geonomos 30, 1–13.

Montel, J.M., Foret, S., Veschambre, M., Nicollet, C., Provost, A., 1996. Electron microprobe dating of monazite. Chemical Geology 131, 37–53.

Noce, C.M., Romano, A.W., Pinheiro, C.M., Mol, V.S., Pedrosa-Soares, A.C., 2003. Geologia das Folhas Ubá e Muriaé. In: Pedrosa-Soares, A.C., Noce, C.M., Trouw, R., Heilbron, M. (Eds.), Projeto Sul de Minas – Etapa I: Geologia e Recursos Minerais do Sudeste Mineiro. 12. COMIG/UFMG/UFRJ/UERJ, Belo Horizonte, pp. 623–659.

Noce, C.M., Pedrosa-Soares, A.C., Piuzana, D., Armstrong, R., Laux, J.H., Campos, C.M., Medeiros, S.R., 2004. Ages of sedimentation of the kinzigitic complex of a late orogenic thermal episode in the Araçuaí orogen, northern Espírito Santo State, Brazil: zircon and monazite U-Pb SHIRIMP and ID-TIMS data. Revista Brasileira de Geociencias 349, 587–592.

Noce, C.M., Novo, T., Figueiredo, C., Pedrosa-Soares, A. C., 2006. Mapa geológico da Folha Manhuaçu (SF.23-X-B-III). Rio de Janeiro, CPRM/UFMG - Programa Geologia do Brasil, escala 1:100.000.

Noce, C.M., Pedrosa-Soares, A.C., Silva, L.C., Armstrong, R., Piuzana, D., 2007. Evolution of polyciclic basement complexes in the Araçuaí orogen based on U-Pb SHRIMP data: implications for Brazil-Africa links in Paleoproterozoic time. Precambrian Research 159, 60–78.

Novo, T.A., 2013. Caracterização do Complexo Pocrane, Magmatismo Básico Mesoproterozóico e Unidades Neoproterozóicas do Sistema Araçuaí–Ribeira, com Ênfase em Geocronologia U-Pb (SHRIMP e LA–ICP–MS). 193. Universidade Federal de Minas Gerais, Belo Horizonte.

Paciullo, F.V.P., Ribeiro, A., Andreis, R.R., Trouw, R.A.J., 2000. The Andrelândia Basin, a Neoproterozoic intraplate continental margin, southern Brasília belt, Brazil. Revista Brasileira de Geociencias 30, 200–202.

Pedrosa-Soares, A.C., Alkmim, F.F., 2011. How many rifting events preceded the development of the Araçuaí-West Congo orogen? Geonomos 19, 244–251.

Pedrosa-Soares, A.C., Noce, C.M., Vidal, P.H., Monteiro, R.L.B.P., Leonardos, O.H., 1992. Toward a new tectonic model for the Late Proterozoic Araçuaí (SE-Brazil) – West Congolian (SW Africa) Belt. Journal of South American Earth Sciences 6, 33–47.

Pedrosa-Soares, A.C., Vidal, P., Leonardos, O.H., Brito-Neves, B.B., 1998. Neoproterozoic oceanic remnants in eastern Brazil: further evidence and refutation of an exclusively ensialic evolution for the Araçuaí–West Congo Orogen. Geology 26, 519–522.

Pedrosa-Soares, A.C., Cordani, U., Nutman, A., 2000. Constraining the age of Neoproterozoic glaciation in eastern Brazil: first U–Pb SHRIMP data from detrital zircons. Revista Brasileira de Geociencias 30, 58–61.

Pedrosa-Soares, A.C., Noce, C.M., Wiedemann, C.M., Pinto, C.P., 2001. The Araçuaí–West Congo orogen in Brazil: an overview of a confined orogen formed during Gondwanaland assembly. Precambrian Research 110, 307–323.

Pedrosa-Soares, A.C., Alkmim, F.F., Tack, L., Noce, C.M., Babinski, M., Silva, L.C., Martins-Neto, M.A., 2008. Similarities and differences between the Brazilian and African counterparts of the Neoproterozoic Araçuaí-West-Congo orogen. Geological Society, London, Special Publications 294, 153–172.

Pedrosa-Soares, A.C., Babinski, M., Noce, C.M., Martins, M., Queiroga, G., Vilela, F., 2011a. The Neoproterozoic Macaúbas Group, Araçuaí orogen, SE Brazil. Geological Society, London, Memoirs 36, 523–534.

Pedrosa-Soares, A.C., De Campos, C., Noce, C.M., Silva, L.C., Novo, T., Roncato, J., Medeiros, S., Castañeda, C., Queiroga, G., Dantas, E., Dussin, I., Alkmim, F.F., 2011b. Late Neoproterozoic–Cambrian granitic magmatism in the Araçuaí orogen (Brazil), the eastern Brazilian Pegmatite Province and related mineral resources. Geological Society, London, Special Publications 350, 25–51.

Peixoto, E., Pedrosa-Soares, A.C., Alkmim, F.F., Dussin, I.A., 2015. A suture-related accretionary wedge formed in the Neoproterozoic Araçuaí orogen (SE Brazil) during western Gondwanaland assembly. Gondwana Research 27, 878–896.

Peres, G.G., Alkmim, F.F., Jordt-Evagalista, H., 2004. The southern Araçuaí belt and the Dom Silvério Group: geologic architecture and tectonic significance. Anais Academia Brasileira de Ciências 180.

Pietranik, A.B., Hawkesworth, C.J., Storey, C.D., Kemp, A.I.S., Sircombe, K.N., Whitehouse, M.J., Bleeker, W., 2008. Episodic, mafic crust formation from 4.5 to 2.8 Ga: new evidence from detrital zircons, Slave craton, Canada. Geology 36, 875–878.

Porada, H., 1989. Pan-African rifting and orogenesis in southern and equatorial Africa and eastern Brazil. Precambrian Research 44, 103–136.

Queiroga, G.N., 2010. Caracterização de restos de litosfera oceânica do Orógeno Araçuaí entre os paralelos 17° e 21° S. (PhD thesis). Universidade Federal de Minas Gerais, Brazil.

Queiroga, G.N., Pedrosa-Soares, A.C., Noce, C.M., Alkmim, F.F., Pimentel, M.M., Dantas, E., Martins, M., Castañeda, C., Suita, M.T.F., Prichard, F., 2007. Age of the Ribeirão da Folha ophiolite, Araçuaí Orogen: the U–Pb zircon dating of a plagiogranite. Geonomos 15, 61–65.

Queiroga, G.N., Gradim, D.T., Pedrosa-Soares, A.C., Pinho, R.R., Vilela, F., Noce, C.M., Nola, T., Novo, T.A., Suleimam, M.A., Basto, C.F., 2012a. Folha Jequeri SF-23-X-B-II-4, escala 1: 50.000.

Queiroga, G.N., Novo, T., Pedrosa-Soares, A.C., 2012b. Mapeamento Geológico da região da Serra dos Turvos, Caratinga (MG), Setor Sul do Orógeno Araçuaí. Geonomos 20, 23–31.

Ribeiro, A., Ávila, C.A., Valença, J.G., Paciullo, F.V.P., Trouw, R.A.J., 2003. Geologia da Folha São João del Rei (1:100.000). Relatório Final. In: Pedrosa Soares, A.C., Noce, C.M., Trouw, R.A.J., Heilbron, M. (Eds.), Geologia e recursos minerais do Sudeste mineiro, Projeto Sul de Minas-Etapa I (COMIG, UFMG, UFRJ). Companhia Mineradora de Minas e COMIG, Belo Horizonte MG, pp. 521–659.

Richter, F., Lana, C., Stevens, G., Buick, I., Pedrosa-Soares, A.C., Alkmim, F.F., Cutts, K., 2016. Sedimentation, metamorphism and granite generation in a back-arc region: records from Ediacaran Nova Venécia Complex (Araçuaí Orogen, southeastern Brazil). Precambrian Research 272, 78–100.

Rolim, V.K., Rosière, C.A., Santos, J.O.S., McNaughton, N.J., 2016. The Orosirian-Statherian banded iron formation-bearing sequences of the southern border of the Espinhaço Range, Southeast Brazil. Journal of South American Earth Sciences 65, 43–66.

Rubatto, D., Hermann, J., 2007. Experimental zircon/melt and zircon/garnet trace element partitioning and implications for the geochronology of crustal rocks. Chemical Geology 241, 38–61.

Schmitt, R.S., Trouw, R.A.J., Van Schmus, W.R., Passchier, C.W., 2008. Cambrian orogeny in the Ribeira Belt (SE Brazil) and correlations within West Gondwana: ties that bind underwater. Geological Society, London, Special Publications 294, 279–296.

Schmitt, R.S., Trouw, R.A.J., Van Schmus, W.R., Armstrong, R., Stanton, N.S.G., 2016. The tectonic significance of the Cabo Frio Tectonic Domain in the SE Brazilian margin: a Paleoproterozoic through Cretaceous saga of a reworked continental margin. Brazilian Journal of Geology 46, 37–66.

Schultz-Kuhnt, D., 1985. Petrographische Untersuchungen einer Zone Amphibolit und granulitfazieller Gesteine im Raum Jequeri, östliches Minas Gerais, Brasilien Clausthal. 167.

Schulz, B., 1993. P-T-deformation paths of Variscan metamorphism in the Austroalpine basement: controls on geothermobarometry from microstructures in progressively deformed metapelites. Swiss Bulletin 73, 257–274.

Silva, L.C., McNaughton, N.J., Armstrong, R., Hartmann, L., Fletcher, I., 2005. The Neoproterozoic Mantiqueira Province and its African connections. Precambrian Research 136, 203–240.

Silva, L.C., Pedrosa-Soares, A.C., Teixeira, L.R., 2008. Tonian rift-related, A-type continental plutonism in the Araçuaí orogen, eastern Brazil: new evidences for the breakup stage of the São Francisco–Congo Paleocontinent. Gondwana Research 13, 527–537.

Silva, L.C., Pedrosa-Soares, A.C., Armstrong, R., Pinto, C.P., Magalhães, J.T.R., Pinheiro, M.A.P., Santos, G.G., 2015. Disclosing the Paleoarchean to Ediacaran history of the São Francisco craton basement: the Porteirinha domain (northern Araçuaí orogen, Brazil). Journal of South American Earth Sciences 68, 50–67.

Söderlund, U., Patchett, J.P., Vervoort, J.D., Isachsen, C.E., 2004. The 176 Lu decay constant determined by Lu–Hf and U–Pb isotope systematics of Precambrian mafic intrusions. Earth and Planetary Science Letters 219, 311–324.

Spear, F.S., 1993. Metamorphic phase equilibria and pressure temperature-time paths. Monographs 1. Mineralogical Society of America, p. 799.

Suita, M.T.F., Pedrosa-Soares, A.C., Leite, C., Nilson, A.A., Prichard, H., 2004. Complexos Ofiolíticos do Brasil e a Metalogenia Comparada das Faixas Araçuaí e Brasília. In: Pereira, E., Castroviejo, R., Ortiz, F. (Eds.), Complejos Ofiolíticos en Iberoamérica: guías de prospección para metales preciosos. Ciencia y Tecnología para el Desarrollo-CYTED, pp. 101–132.

Suzuki, K., Adachi, M., Kajizuka, I., 1994. Electron microprobe observations of Pb diffusion in metamorphosed detrital monazites. Earth and Planetary Science Letters 128, 391–405.

Tack, L., Wingate, M.T.D., Liégeois, J.P., Fernandez-Alonso, M., Deblond, A., 2001. Early Neoproterozoic magmatism (1000–910 Ma) of the Zadinian and Mayumbian Groups (Bas-Congo): onset of Rodinian rifting at the western edge of the Congo Craton. Precambrian Research 110, 277–306.

Tack, L., Wingate, M.T.D., De Waele, B., Meert, J., Belousova, E., Griffin, B., Tahon, A., Fernandez-Alonso, M., 2010. The 1375 Ma Kibaran Event in Central Africa: prominent emplacement of bimodal magmatism under extensional regime. Precambrian Research 180, 63–84.

Tassinari, C., Munhá, J., Ribeiro, A., Correia, C., 2001. Neoproterozoic oceans in the Ribeira Belt (southeastern Brazil): the Pirapora do Bom Jesus ophiolitic complex. Episodes 24, 245–251.

Tedeschi, M., Novo, T., Pedrosa-Soares, A.C., Dussin, I., Tassinari, T., Silva, L.C., Gonçalves, L., Alkmim, F.F., Lana, C., Figueiredo, C., Dantas, E., Medeiros, S., De Campos, C., Corrales, F., Heilbron, M., 2016. The Ediacaran Rio Doce magmatic arc revisited (Araçuaí-Ribeira orogenic system, SE Brazil). Journal of South American Earth Sciences 68, 167–186.

Tohver, E., D'Agrella Filho, M., Trindade, R.I.F., 2006. Paleomagnetic record of Africa and South America for the 1200–500 Ma interval, and evaluation of Rodinia and Gondwana assemblies. Precambrian Research 147, 193–222.

Trompette, R., 1994. Geology of western Gondwana (2000–500 Ma). Pan-African-Brasiliano aggregation of South America and Africa. Precambrian Research 78, 301–302.

Trouw, C.C., 2008. Mapeamento da Folha Virgínia, MG: geocronologia U-Pb (SHRIMP) em zircões e interpretação geotectônica. (Tese de Doutorado). 140. Programa de Pós-graduação em Geologia, Instituto de Geociências, Universidade Federal do Rio de Janeiro, Rio de Janeiro.

Trouw, R.A.J., Heilbron, M., Ribeiro, A., Paciullo, F.V.P., Valeriano, C.M., Almeida, J.C.H., Tupinambá, M., Andreis, R.R., 2000. The Central segment of the Ribeira Belt. In: Cordani, U.G., Milani, E.J., Thomaz-Filho, A., Campos, D.A. (Eds.), Tectonic Evolution of South America, Rio de Janeiro, 31st International Geological Congress, pp. 287–310.

Trouw, R.A.J., Peternel, R., Ribeiro, A., Heilbron, M., Vinagre, R., Duffles, P., Trouw, C.C., Fontainha, M., Kussama, H.H., 2013. A new interpretation for the interference zone between the southern Brasília belt and the central Ribeira belt, SE Brazil. Journal of South American Earth Sciences 48, 43–57.

Tupinambá, M., Machado, N., Heilbron, M., Ragatky, D., 2007. Meso-neoproterozoic litho-spheric extensional events in the São Francisco Craton and its surrounding south American and African metamorphic belts: a compilation of U-Pb ages. Revista Brasileira de Geociencias 37, 87–91.

Tupinambá, M., Heilbron, M., Valeriano, C.M., Porto Jr., R., Blanco de Dios, F., Machado, N., Silva, L.G.E., Almeida, J.C.H., 2012. Juvenile contribution of the Neoproterozoic Rio Negro magmatic arc (Ribeira Belt, Brazil): implications for western Gondwana amal-gamation. Gondwana Research 21, 422–438.

Valeriano, C.M., Tupinambá, M., Simonetti, A., Heilbron, M., Almeida, J.C.H., do Eirado, L.G., 2011. U-Pb LA-MC-ICPMS geochronology of Cambro-Ordovician post-collisional granites of the Ribeira belt, southeast Brazil: terminal Brasiliano magmatism in cen-tral Gondwana supercontinent. Journal of South American Earth Sciences 32, 416–428.

Valeriano, C., Mendes, J.C., Tupinambá, M., Bongiolo, E., Heilbron, M., Junho, M.C.B., 2016. Cambro-Ordovician post-collisional granites of the Ribeira belt, SE-Brazil: a case of terminal magmatism of a hot orogen. Journal of South American Earth Sciences 68, 269–281.

Valladares, C.S., Machado, N., Heilbron, M., Duarte, B.P., Gauthier, G., 2008. Sedimentary provenance in the central Ribeira belt based on laser-ablation ICPMS 207Pb/206Pb zircon ages. Gondwana Research 13, 516–526.

Vieira, V.S., 2007. Significado do Grupo Rio Doce no contexto do Orógeno Araçuaí. (PhD Thesis). Universidade Federal de Minas Gerais, Belo Horizonte.

Wakabayashi, H., 2004. Tectonic mechanisms associated with P-T paths of regional meta-morphism: alternatives to single-cycle thrusting and heating. Tectonophysics 392, 193–218.

Wiedenbeck, M., Alle, P., Corfu, F., Griffin, W.L., Meier, M., Oberli, F., von Quadt, A., Roddick, J.C., Spiegel, W., 1995. 3 natural zircon standards for U-Th-Pb, Lu-Hf, trace-element and REE analyses. Geostandards Newsletter 19, 1–23.

Wu, C.M., Zhang, J., Ren, L.D., 2004. The GBPQ Garometer: empirical garnet - biotite - pla-gioclase - quartz (GBPQ) geobarometry in medium- to high-grade metapelites. Jour-nal of Petrology 45, 1907–1921.

Yardley, B.W.D., 2004. An Introduction to Metamophic Petrology. Longman Earth Sciences Series.

4. Discussion

The two focused lithological units of this study represent distinct geological settings in the geotectonic evolution of the AROS region since the Precambrian. The ortho-derived gneisses of the Juiz de Fora, Pocrane and Quirino complexes inter alia make up the basement of this orogenic system and have their origin in magmatic arc activity during the Rhyacian-Orosirian (ROOS, Publication 1). The stratigraphically younger para-derived rocks represent the cover of this Palaeoproterozoic basement unit (Publication 2).

A certain relation in between these two lithologies is that the rocks of the ROOS can be considered as a possible source for the covering paragneisses. Another commonality is the fact that both units underwent the same regional metamorphism in the Neoproterozoic (Publication 2).

As described in the introduction, the partial petrographical and mineralogical similarity of the sampled lithologies influenced the course of the recent study. The mafic composited enderbitic and tonalitic gneisses of the three ROOS complexes allowed mostly a clear lithological allocation. But in some cases (e.g. RC-15, RC-17, RC-43), rocks sampled as paragneisses turned out to be ortho-derived and, for example, showed no detrital zircon grains. The problematic classification of the sampled gneisses is illustrated in Figure 4. In case of samples RC-15, RC-17 and RC-43, the distinction between ortho- or para-derived gneisses was only possible after zircon separation, CL photography and U-Pb age determination. Detrital zircon grains (as fragments and/or rounded shapes) were interpreted as clear indications for grain transport and associated to para-derived gneisses. Contrastingly, zircon grains showing igneous features (e.g. prismatic shape, oscillatory zonation) and only one concordant U-Pb age were associated to be separated from ortho-derived gneisses (Fig. 4).

Another parameter for lithological classification was the identification of typical mineral assemblages for metamorphic amphibolite and granulite facies (amphibolite -> pyroxene and biotite -> K-feldspar + garnet + orthopyroxene). Unfortunately, here as well, the samples of paragneisses and orthogneisses show distinct overlaps. For example, unusual garnets porphyroblasts were also identified in ortho-derived rock samples from the Juiz de Fora complex (Fig. 4). Summarising it should be noted that in several cases, a clear lithological allocation was only possible after detailed studies and U-Pb age determination.
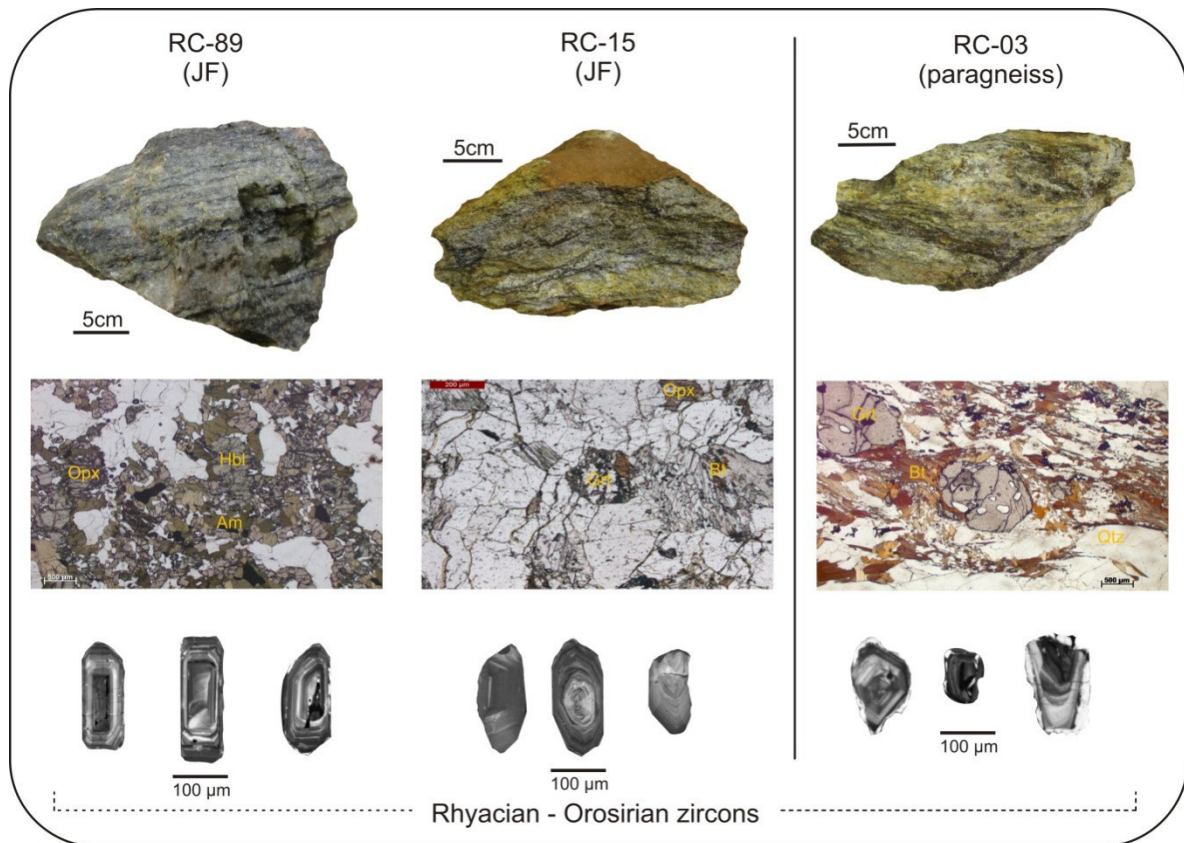
Fig. 4: Representative analysed samples and their difficult classification as ortho- (Publication 1) or para-derived gneiss (Publication 2). RC-89, a classic greenish enderbitic to charnockitic rock from the ROOS including mafic mineral (Hbl+Opx+Bt). RC-03, layered paragneiss of felsic composition (Qtz+Pl) and large garnet porphyroblasts. RC-15, difficult to define sample allocated to the ROOS (includes garnet porphyroblasts but few mafic minerals). A major criticism for classification was the zircon grain shape in CL images (detrital or not).

4.1 Reflection on U-Pb ages and Lu-Hf isotope systems

These two analytical methods and the associated chronometers zircon and monazite are a main component of the recent study. At best, the separated grains represent parameters of the whole sampled rock and allow general interpretations and conclusions. The analysed 620 zircons and 357 monazites describe a time interval of almost ~2.3 Ga for the AROS region and its geotectonic evolution. 309 Lu-Hf isotope system analyses of detrital and igneous zircons complement this data set. As illustrated in Figure 5 the zircon data gather in two mains age peaks (ROOS and BPAO), which are the main focus of each Publication.
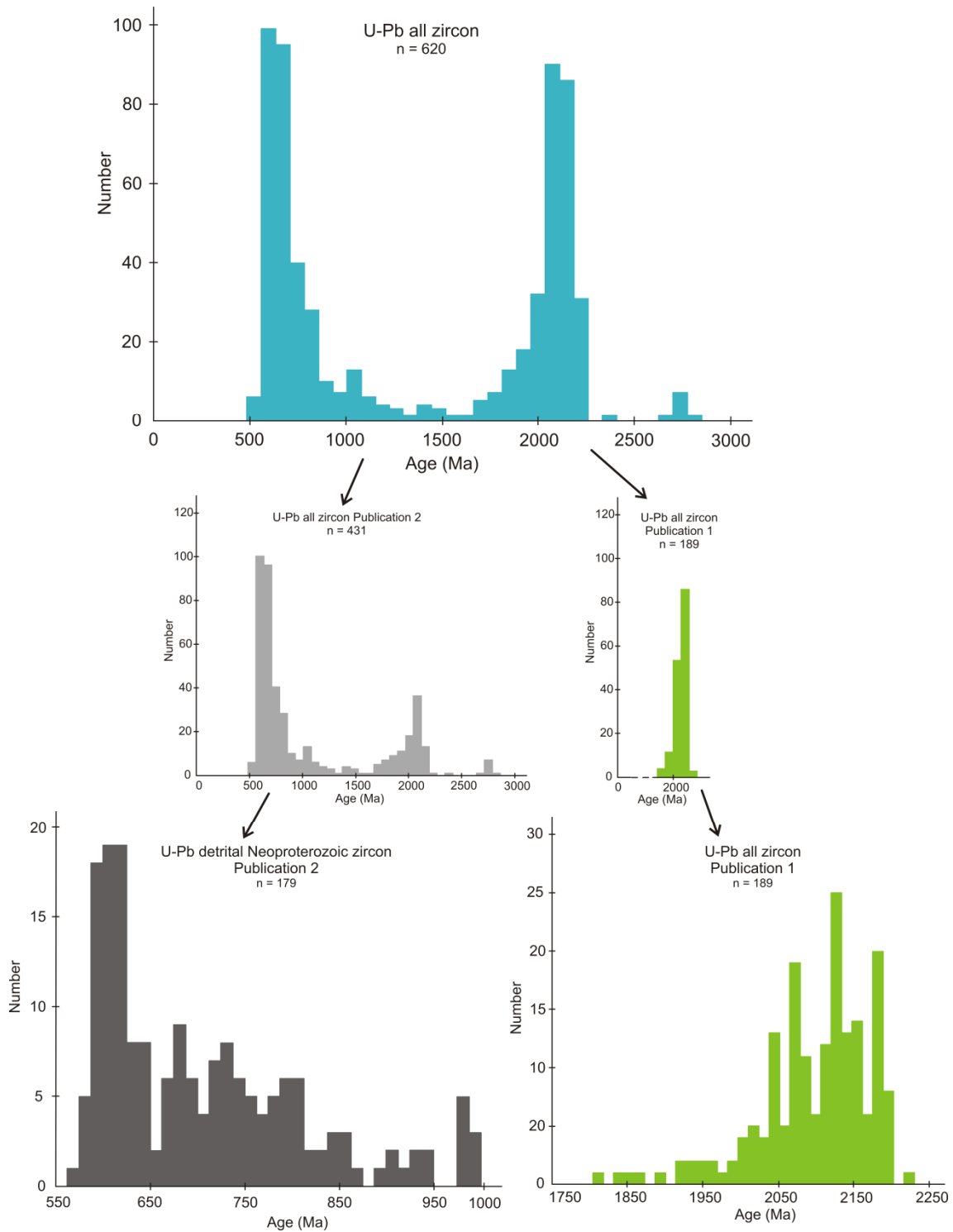
Fig. 5: U-Pb age histograms for all concordant analysed zircon grains and their allocation to Publications 1 and 2. The 620 separated grains include detrital, metamorphic and magmatic zircons. Lower part left illustrates the detrital Neoproterozoic zircons subjected in Publication 2. The additional 357 metamorphic monazite analyses by EMP and LA-ICP-MS are not included, see Publication 2.

The ROOS complexes outlined by U-Pb ages and complex Lu-Hf isotopic distribution represents one sediment provenance for the further analysed paragneisses. The geochronological older ROOS

zircons can be found as detrital grains among the studied paragneisses (Fig. 5). Restrictively, it is apparent that the JU-ROOS represents a minor important sediment source (Figs. 6 and 7, allocation of $\varepsilon Hf_{(t)}$ values). However, the original remelted material (independent from kind of crystallisation) was still generated from evolved felsic crust (Mantiqueira arc). As several paragneisses were sampled in the western most portion of the AROS it is much more likely that the Mantiqueira basement served as main Palaeoproterozoic sediment supplier (Fig. 7).

By association between source (ROOS) and product (paragneisses), ages of maximum deposition have a key function for the geotectonic model. The two samples RC-02 and RC-34 (Publication 2) are concluded as strong basement influenced paragneisses (Table 2 of Publication 2) showing maximum deposition ages of 1803 ± 30 Ma (RC-02) and 1359 ± 16 Ma (RC-34), which allow sediment influence from the JU-ROOS (youngest zircon grain 1864 Ma). In relation to their geographical location (west), sediment generated from the JU-ROOS seems highly unlikely (far). Samples of paragneisses that could have had sediment input from the JU-ROOS are RC-38 and RC-46 (Fig. 7). It is conspicuous that detrital zircons of sample RC-02, interpreted having their provenance in the Mantiqueira arc, reach the age of 1803 Ma, in turn, igneous zircons of samples RC-15, RC-43 and RC-101 show the youngest age of zircon crystallisation by ~2066/2067 Ma. This age discrepancy suggests regional different magmatic arc activity and supports the idea for lasting migmatisation and mylonitisation. Further, in RC-15, RC-43, RC-94 and RC-101 inherited Archaean zircons are completely absent (RC-02 includes inherited Archaean grains). In conclusion, it should be noted that zircon grains (detrital and igneous) aging 2224-1803 of negative $\varepsilon Hf_{(t)}$ (Fig. 7) might have a different crystallisation history and/or a product of further partial meting events.

One of the main interesting results and conclusion of Publication 2 is the description of Neoproterozoic juvenile material (RC-03), interpreted as evidence for Rio Negro arc influence on the AROS, a detailed U-Pb-Hf breakdown for this special sample is applied (Fig. 6).

The Neoproterozoic zircon grains display different internal textures in relation to their $\varepsilon Hf_{(t)}$ signal. On one hand this could imply different provenances (Rio Negro and/or Serra da Prata arc?, Tupinambá et al., 2012; Heilbron et al., 2013) or different crystallisation features for the protolith. In addition, Figure 6 also illustrates a detailed breakdown of detrital Neoproterozoic and Mesoproterozoic zircon grains for sample RC-46. The designation of a juvenile Mesoproterozoic provenance led to extensive source interpretations (see Publication 2).

The obtained results of U-Pb and Lu-Hf isotopy for the ortho-derived as well as for the para-derived samples highly suggest a joint application of both methods. This should be taken into account for future studies.
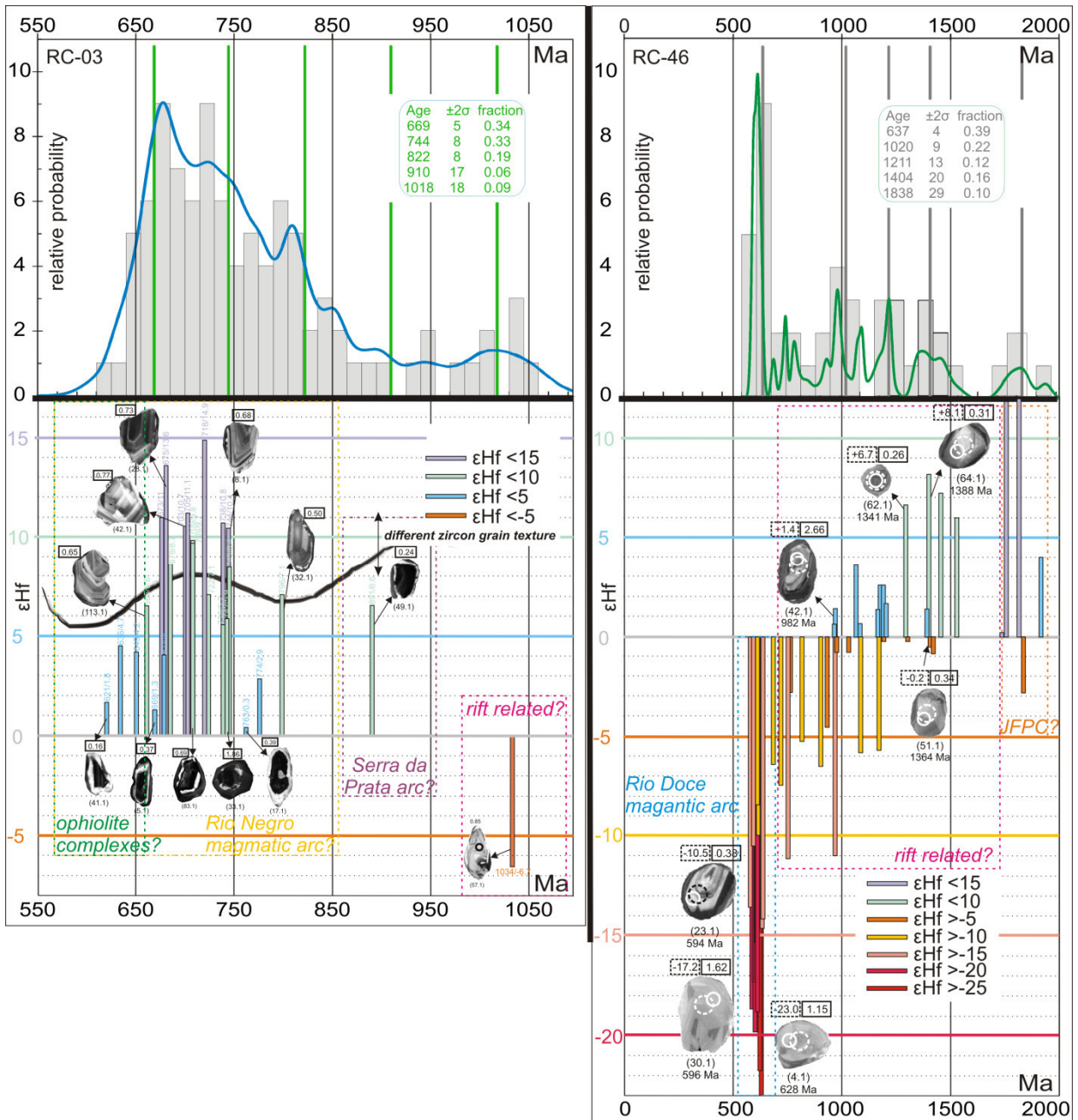
Fig. 6: Detailed relative probability diagram for detrital Neoproterozoic U-Pb zircon ages and associated $\varepsilon_{Hf(t)}$ values of sample RC-03 and RC-46. Possible discussed sources are framed and in italic.

The summary of all Lu-Hf analytical data from Publications 1 and 2 allows the outline of an Hf evolutional diagram for the geotectonic development of the AROS (Fig. 7). It involves at least two Rhyacian-Orosirian magmatic arcs: the evolved Mantiqueira arc, demonstrably active since c. 2224 and the juvenile to moderately juvenile Juiz de Fora-Pocrane arc with magmatism starting c. 2196. A regional separation by space but almost simultaneous in time for the ROOS arcs is very likely. Further, a not yet identified long lasting Meso- to Neoproterozoic arc evolving from juvenile to evolved signature has to be considered (Fig. 7, RC-46). Perhaps it is evolving basement of the

evolved Rio Doce magmatic arc. A so far not considered geotectonic setting for the AROS would be the Rio Negro magmatic arc (Fig. 7).
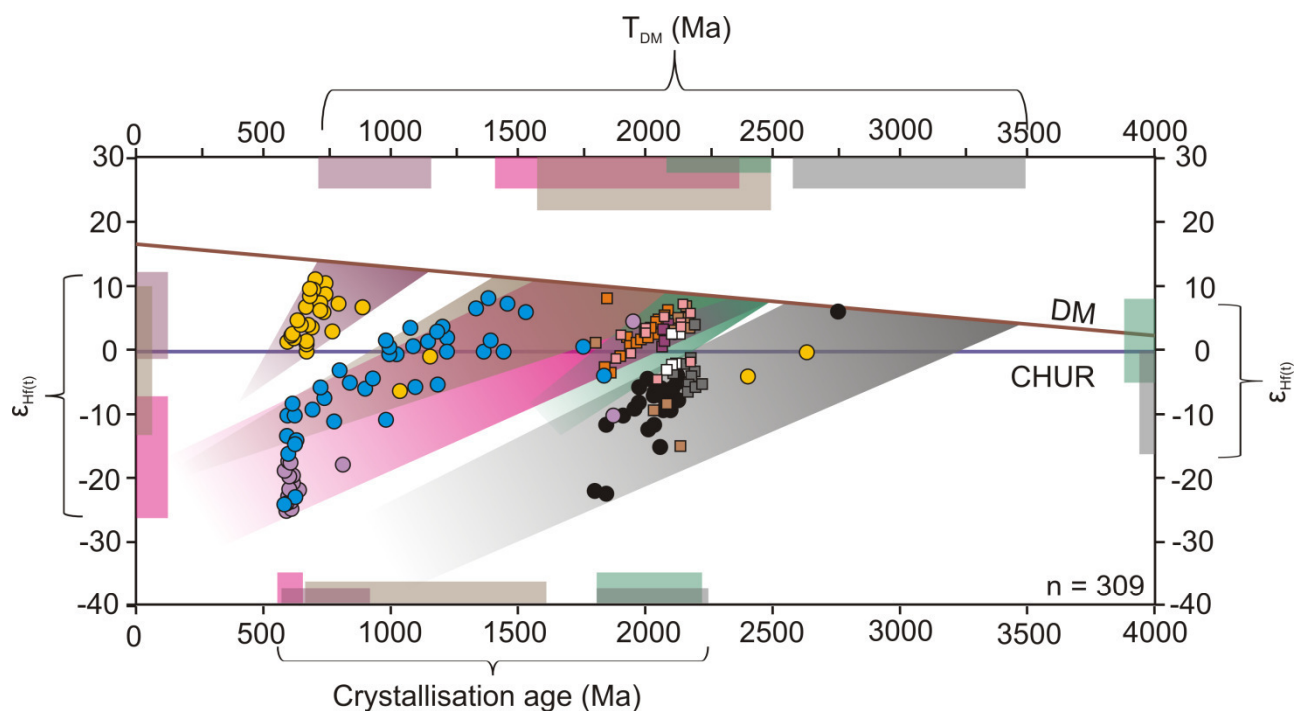
	RC-02 ●	RC-03 ○	RC-15 ■	RC-17 ■	RC-38 ●	RC-43 ■	RC-46 ●	RC-93 ■	RC-94 □	RC-101 ■
$\varepsilon_{Hf(t)}$	-2.2 - (-22.7)	+14.9 - (-6.7)	+6.9 - (-7.4)	+6.3 - (-3.5)	-16.5 - (-25.3)	+3.7 - (-7.3)	+17.0 - (-23.0)	+4.4 - (+0.6)	+6.4 - (-3.0)	+8.2 - (-2.5)
T_{DM} (Ga)	3.5-2.4	3.0-0.7	2.8-2.1	2.4-2.0	2.7-2.2	2.8-2.5	3.2-1.4	2.3-2.1	2.5-2.1	2.6-2.1

	Crystallisation ages (Ma)	$\varepsilon_{Hf(t)}$
Mantiqueira magamtic arc (MCA)	~2224 - 1803	-1.4 - (-22.7)
Juiz de Fora-Pocrane magmatic arc (JFP)	~2196 - 1864	+8.2 - (-3.5)
Mesoproterozoic - Neoproterozoic	~1850 - 690	+8.1 - (-11.1)
Rio Negro magmatic arc (RNA)	~796 - 598	+14.9 - (-0.6)
Rio Doce magmatic arc (RDA)	~638 - 590	-8.4 - (-25.3)

Fig. 7: Hf-evolution diagram for geological settings involved in the AROS development. Table shows $\varepsilon_{Hf(t)}$ and Hf T_{DM} data for every single analysed sample. Lower part summarises U-Pb and Lu-Hf data.

5. Conclusions

5.1 Integration in the evolutional model of the AROS region

The best way to illustrate conclusions of geotectonic studies is a summarising evolutional model. From the AROS point of view such model extends over a long time period (demonstrably at least c. 2.3) and involves different geotectonic settings (cratons, rift basins, magmatic arcs).

The initial evolutional stage can be set at around c. 2.0 Ga. According to publications of Ledru et al. (1994); Roger and Santosh (2002); Zhao et al. (2002); De Weale et al. (2008); Meert and Santosh (2017); D'Agrella-Filho and Cordani.(2017) global landmasses in the Mid-Palaeoproterozoic (Rhyacian – Orosirian) were principally represented by Archaean cratons. For the AROS region evolution the most important involved cratons were the São Francisco and the Congo + West Africa cratons (Fig. 8).

A result of former craton collision (São Francisco and Congo megacraton) was the formation of a Palaeoproterozoic belt, which extended along the eastern side of the São Francisco craton. In parts this belt is preserved in the Eastern Bahia belt and by Palaeoproterozoic domains more south (e.g. Gavião, Porterinhas). Its fragments are now the basement of the AROS and WCB and consist of the following rock assemblages associated to distinct tectonic settings:

In consideration that the São Francisco and the Congo palaeocontinents used to be separated by a precursor basin, an intense magmatic arc activity within and at the margins of this basin is presumed (Fig. 8). In this scenario the Juiz de Fora-Pocrane arc (Publication 1) is a remnant of an island arc and requires an intra-oceanic subduction zone for this precursor basin. In relation to the determined U-Pb data it can be suggested that this juvenile magmatic event lasted at least from c. 2224 to c. 1864 Ma. Almost simultaneous, the Mantiqueira magmatic arc developed on the eastern active margin of the São Francisco palaeocontinent. Evidences from zircon U-Pb and Lu-Hf data suggest a collision between the Juiz de Fora-Pocrane arc and the São Francisco palaeocontinent (Mantiqueira arc) and mark a Palaeoproterozoic metamorphism(amalgamation of JU-ROOS and W-CO-ROOS).

Continental magmatic arc activity also affected the western margin of the Congo palaeocontinent, forming the Kimezian arc (c. 2088-2014 Ma). This extended Rhyacian-Orosirian intrusive events and the involved basin closure can be seen as an initial stage for the Columbia supercontinent assembly (c. 1.45 Ga; Meert and Santosh, 2017) OR as part of global Rhyacian-Orosirian events (Zhao et al., 2002) for the isolated São Francisco-Congo palaeocontinent (D'Agrella-Filho and Cordani, 2017). The illustrated tectonic setting in Fig. 8 (left) would reflect a situation between the

end of magmatic arc activity (c. 1864 – JF-Po and c. 1803 - MA) and the assembly of the Columbia supercontinent.

The time period between c. 1.8 Ga and c. 1.0 Ga was probably characterised by plate tectonism (Columbia and Rondinia supercontinents? – with or without CSFP). The next following demonstrable change for the AROS geotectonic setting is recorded by several rifting events starting around c. 1.0 Ga (Publication 2). The finally result of these extensional rifts were the development of a last AROS precursor basin. Like demonstrated in Publication 1, a series of Neoproterozoic magmatic arcs formed within this ocean (Rio Negro-Serra da Prata arc) and at its margins (Rio Doce arc). The suggested nutcracker evolutional model for the Araçuaí belt by Alkmim et al., (2006) seems most likely and is assumed here for ongoing geotectonism. The Neoproterozoic magmatic arcs represent the main AROS orogenic stage and undoubtable are most likely sediment sources for AROS paragneisses (Publication 2). The new data suggest an arc-arc collision between the Rio Negro and the Rio Doce arc before c. 614 Ma in the AROS. The geotectonic evolution was completed by series of intrusions and arc-continent collision. The associated metamorphism was widely recorded in the analysed paragneisses. In larger scale this Neoproterozoic orogenic stages mark another supercontinent assembly of Gondwana, Fig. 8.
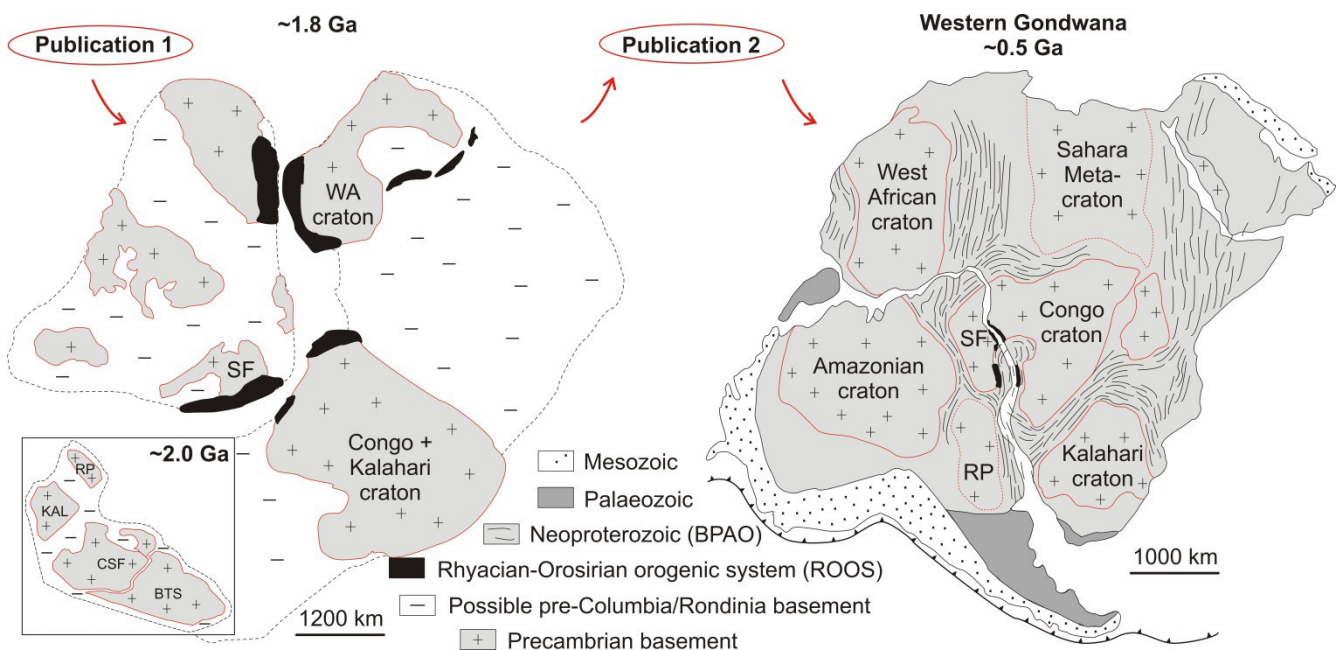

Fig. 8: Adaption of Publications 1 and 2 to geotectonic reconstructions. The geotectonic processes concluded for the respective Publication influenced and constrained the tectonic model demonstrably in regional scale. SF, São Francisco; WA, West Africa; CSF, Congo/São Francisco; BTS, Borborema/Trans-Sahara; KAL, Kalahari; RP, Rio de la Plata. Palaeotectonic maps are adopted from; Zhao et al., 2002; Gray et al., 2008; D'Agrella-Filho and Cordani, 2017; Meert and Santosh, 2017.

6. Error evaluation

There is no scientific work without any discussion and consideration of possible errors influencing the carried out data. The evaluation of errors is derived from different working stages of this study and corresponds to decreasing scale:

1. As the study area is really large, the basic map material of the sampling- and field work were already existing geological maps. The accuracy of these maps is assumed but can not 100% be guaranteed.

2. Every sample point (outcrop) underwent a detailed and intensive personal study and interpretation. The samples were always taken under fair conditions and kept free from contaminations.

3. Field work and geological interpretation is always subjectively. Field trips and sample discussions were applied to stay most objectively as possible.

4. The same applies for thin section analyses. Here, a repetition of analyses and comparison to existing samples was performed.

5. All isotopic analyses were performed in well-established laboratories with machines of high quality. A certain correctness of the carried out data is prerequisite and expected.

6. The detailed data calculation and error correction follows established and common international references (U-Pb analyses: *Mud Tank* - Black and Gulson, 1978; Compston et al., 1984, 1992; Suzuki et al., 1994; *91500* - Wiedenbeck et al., 1995; Montel et al., 1996; Smith et al., 1998; Ludwig, 2003; *GJ1* - Jackson et al., 2004; *Temora* – Black et al., 2003; *Plešovice* - Slama et al., 2008; Chemale et al., 2012; *Steenkampscraal* - Liu et al., 2012; *Bananeira* - Gonçalves et al., 2016; *BB* - Santos et al., 2016; Lu-Hf analyses: Griffin et al., 2000; Söderlund et al., 2004; Bouvier et al., 2008; Pietranik et al., 2008; Andersen et al., 2009; Bahlburg et al., 2011; Dhuime et al., 2011; and geothermobarometry analyses: Martignole and Nantel, 1982; Schulz, 1993; Holdaway, 2001; Wu et al., 2004.

7. The interpretation and following conclusions are also subjectively, but consider all known and published information.

7. References (those not cited in Publications)

Almeida, F.F.M., Hasui, Y., Brito Neves, B.B., 1976. The Upper Precambrian of South America. Geo-Sciences Institute Belletin 7, 45-80.

Barbosa, O., 1954. Evolution du geossinclinal Espinhaço.In: International Geological Congress, Comptes. Rendus, section XIII 19, 1-37.

Black, L. P. and Gulson, B. L., 1978.The Age of the Mud Tank carbonatite, Strangways Range, Northern Territory. BMR Journal of Australian Geology and Geophysics 3, 227-232.

Black, L.P., Kamo, S.L., Allen, C.M., Aleinikoff, J.N., Davis, D.W., Korsch, R.J., Foudoulis, C., 2003. TEMORA 1: a new Zircon standard for phanerozoic U-Pb geochronology. Chemical Geology 200, 155-170.

Brandalise, L. A., Pinto, C. P., Viana, H. S., Bruno, E. M.,Zucchetti, M., 1992. Província Alcalina da Mantiqueira, Serra da Mantiqueira-MG. Revista da Escola de Minas, 45.

Carvalho J.B., Pereira L.M.M., 2000. Projeto Leste: Petrografia, relatório integrado. Etapa II. Belo Horizonte: SEME/CPRM/CODEMIG, CD-ROM.

Ebert, H. 1956. Pesquisas geológicas na parte sudeste do Estado de Minas Gerais. Rio de Janeiro, DGM, p. 79-89 (Relatório Anual do Diretor). In: Noce, C.M., Pedrosa-Soares, A.C., Silva, L.C. and Alkmim, F.F., 2007. O Embasamento Arqueano e Paleoproterozóico do Orógeno Araçuaí. Geonomos 15, 17-23.

Ebert, H., 1957. Relat6rio de Atividades. In: Relatório Anual do Diretor da Div. Geol. Min.,DNPM, Rio de Janeiro, Ano 1956, 97-107.

Ebert, H., 1968. Ocorrência de fácies graulíticas no sul de Minas Gerais e em áreas adjacentes, em dependência da estrutura orogênica – hipótese sobre a sua origem. An. Acad. Brasil. Ci. 40, 215-229.

Féboli and Paes, 2000. Projeto Leste-MG. Folha Itanhomi (SE.24-Y-C-I), Belo Horizonte, SEME/COMIG/CPRM, escala 1:100.000.

Gradim D.T., Noce, C.M., Novo T., Queiroga G.N., Pedrosa-Soares A.C., Suleimam M.A., Martins M., 2012. Mapa geológico da Folha Viçosa (SF.23-X-B-V), Belo Horizonte, CPRM/UFMG, escala 1:100.000.

Heilbron, M. D. C. P. L., 1993. Evolução tectono-metamórfica da seção Bom Jardim de Minas (MG)-Barra do Pirai (RJ): setor central da faixa Ribeira (Doctoraldissertation, Universidade de São Paulo).

Heilbron, M., Mohriak, W. U., Valeriano, C. M., Milani, E. J., Almeida, J., Tupinambá, M. 2000. From collision to extension: the roots of the southeastern continental margin of Brazil. Atlanticriftsand continental margins, 1-32.

Heilbron, M., 2012. Geologia e recursos minerais da folha Santo Antônio de Pádua, SF. 26-X-D-VI, Estado do Rio de Janeiro escala 1:100.000. Programa Geologia do Brasil, CPRM-UERJ.

Horn, A., Faria, B., Gardini, G., Vasconcellos, L., Oliveira, M., 2006. Geologia da Folha Espera Feliz. Rio de Janeiro, CPRM-Serviço Geológico do Brasil, UFMG-Programa Geologia do Brasil, escala 1:100.000.

Machado, N., Valladres, C.S., Heilbron, M. and Valeriano, C. M., 1996.U-Pb geochronology of the central Ribeira belt (Brazil) and implications for the evolution of the Brazilian Orogeny.Precambrian Research 79, 347-36.Martignole, J. and Nantel, S., 1982. Geothermobarometry of cordierite-bearing metapelites near the Morin anorthosite complex, Grenville province, Quebec. The Canadian Mineralogist 20, 307-318.
349, 587-592.

Noce, C.M., Novo, T., Figueiredo, C., Pedrosa-Soares, A. C., 2006. Mapa geológico da Folha Manhuaçu (SF.23-X-B-III). Rio de Janeiro, CPRM/UFMG - Programa Geologia do Brasil, escala 1:100.000.

Novo, T., Noce, C.M., Batista, G., Quéméneur, J., Martins, B., Santos, S., Carneiro, G., Horn, A., 2012. Mapa geológico da Folha Manhumirim, (SF.24-V-A-I). Belo Horizonte, CPRM/UFMG, escala 1:100.000.

Oliveira M.J.R. 2000. Projeto Leste-MG. Folha Conselheiro Pena (SE.24-Y-C-II), Belo Horizonte, SEME/COMIG/CPRM, escala 1:100.000

Pedrosa-Soares, A. C., Noce, C.M., Vidal, P.H., Monteiro, R.L.B.P., Leonardos, O.H., 1992. Toward a new tectonic model for the Late Proterozoic Araçuaí (SE-Brazil) – West Congolian (SW Africa) Belt. Journal of South American Earth Sciences 6, 33-47.

Pereira, L. M. M. andZucchetti, M., 2000. Projeto Leste: Petrografia, relatório integrado. Etapa II. Belo Horizonte: SEME/CPRM/CODEMIG, CD-ROM.

Queiroga, G.N., Gradim, D.T., Pedrosa-Soares, A.C., Pinho, R.R., Vilela, F., Noce, C.M., Nola, T., Novo, T.A., Suleimam, M.A., Basto, C.F., 2012. Folha Jequeri SF-23-X-B-II-4, escala 1:50.000.

Romano, A.W. and Noce, C.M., 2003. Geologia da Folha Muriaé (SF.23-X-D-III). Belo Horizonte, COMIG/UFMG/UFRJ/UERJ - Projeto Sul de Minas, escala 1:100.000.

Signorelli, N., 2003. Carta geológica – folha Caratinga (1:100.000). Projeto Leste CPRM/ CODEMIG. 2ª. Ed. CD-ROM.

Tuller, M., 2000.ProjetoLeste-MG. Folha Ipanema (SE.24-Y-C-IV), Belo Horizonte, SEME/COMIG/CPRM, escala 1:100.000.

Tupinambá, M., Almeida, C., Eirado, E., Duarte, B., Heilbron, M., 2003. Geologia da Folha Pirapetinga (SF.23-X-D-VI). Belo Horizonte, COMIG/UFMG/UFRJ/UERJ - Projeto Sul de Minas, escala 1:100.000.

Tupinambá, M., Heilbron, M., Duarte, B. P., Nogueira, J. R., Valladares, C., Almeida, J.,Ragatky, C. D., 2013. Geologia da Faixa Ribeira Setentrional: estado da arte e conexões com a Faixa Araçuaí. Revista Geonomos, 15.

Vieira, V., 1993. Baixo Guandu, Folha SE.24-Y-C-V-Estado de Minas Gerais e Espirito Santo. Brasilia: DNPM/CPRM, escala 1:100.000.